Alternative alkali resistant deNOx technologies

PSO Project 7318

Kristensen, Steffen Buus; Due-Hansen, Johannes; Putluru, Siva Sankar Reddy; Kunov-Kruse, Andreas Jonas; Fehrmann, Rasmus; Jensen, Anker Degn

Publication date:
2011

Document Version
Publisher's PDF, also known as Version of record

Technical University of Denmark

2007-2010

PSO Project 7318

Alternative alkali resistant $deNO_x$ technologies

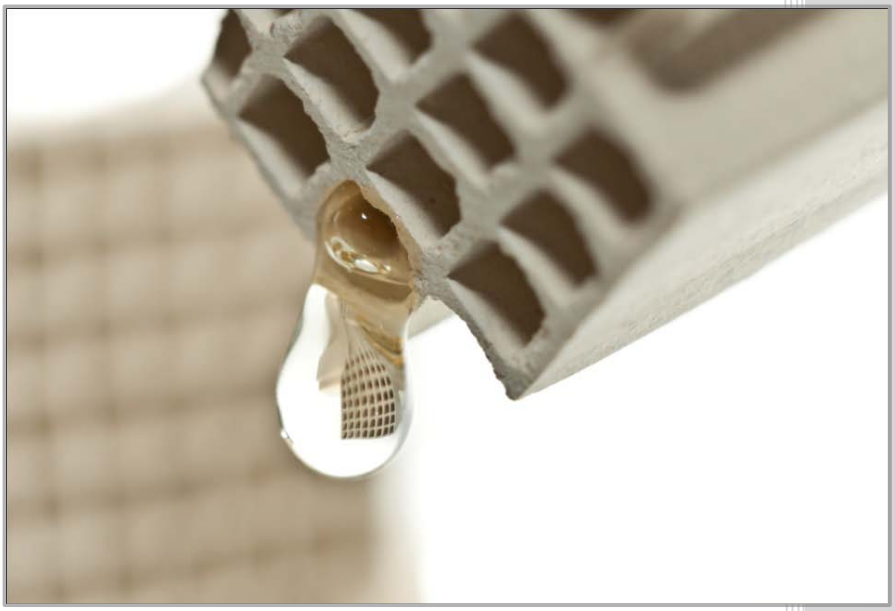

Steffen Buus Kristensen

Johannes Due-Hansen

Siva Sankar Reddy Putluru

Andreas Kunov-Kruse

Rasmus Fehrmann

Anker Degn Jensen

Technical University of Denmark

DTU Chemistry and

DTU Chemical Engineering

April 2011

DTU Chemistry
Department of Chemistry

Centre for Catalysis and Sustainable Chemistry

Preface

The following work is the final report for the PSO project 7318 entitled "Alternative deNO$_x$ catalysts and technologies" funded by energinet.dk, 2007-2010. The project is a joint effort of Danish organizations and companies who share experience and interest in sustainable energy production especially within the use of biomass and waste without compromising the emission of NOx to the atmosphere.

Dansk resumé

Projektets formål er at indkredse, fremstille og afprøve mulige alkaliresistente deNOx katalysatorer til brug i biomasse-, affalds- eller fossilt-brændsel-samfyrede installationer som kraftværker og affaldsforbrændingsanlæg, hvor røggassen typisk har et højt indhold af specielt kaliumforbindelser, der deaktiverer den traditionelle V_2O_5/TiO_2 katalysator hurtigt. Desuden undersøges nye teknologier som baserer sig på en beskyttende coating af katalysatorelementerne samt selektiv reversibel absorption af NO_x med ioniske væsker. Flere lovende alternative deNOx katalysatortyper er blevet fremstillet i dette projekt:

1) V, Fe, Cu baserede nano-TiO2 og nano-TiO_2-SO_4^{2-} katalysatorer,
2) V/ ZrO_2-SO_4^{2-} og V/ ZrO_2-CeO_2 katalysatorer,
3) V, Fe, Cu baserede Zeolitkatalysatorer samt
4) V, Fe, Cu baserede Heteropolysyre katalysatorer.

Disse katalysatorer har ved laboratorietests udvist væsentlig bedre alkaliresistens end den katalysatortype der anvendes industrielt i dag. Desuden udviser to af de alternative katalysatorer nemlig 20 wt.% V_2O_5-TiO_2-SO_4^{2-} nano-katalysatoren og 4wt% CuO-Mordenit zeolitkatalysatoren også væsentlig højere aktivitet uden alkaliforgiftning end den industrielt anvendte katalysator. Disse katalysatorer synes derfor også attraktive selv under brug af "normale" brændsler og er derfor særligt stærke kandidater til videre udvikling til kommercielle katalysatorer. Resultaterne af coating undersøgelserne har også udmøntet sig lovende, især ved brug af Mg-forbindelser, der kan fange alkalisaltene før de når de katalytisk aktive centre.

Denne teknologi er netop nu under afprøvning hos Haldor Topsøe A/S. Endelig har to ioniske væsker BMIM-acetat og BMIM-triflat udvist stor reversibel affinitet for NO selv i våde modelrøggasser. De er derfor kandidater til videreudvikling bl.a. i porøse bærermaterialer til såkaldte SILP-absorbermaterialer, sandsynligvis velegnede til installation end-of-pipe i røggaskanaler. De udviklede katalysatorer og teknologier har udmøntet sig i 7 patentansøgninger i projektperioden ligesom resultaterne er beskrevet i 36 tidsskriftartikler og konferencebidrag. En PhD-afhandling er også resultat af projektet: Johannes-Due Hansen "Alternative deNO$_x$ Catalysts and Technologies", DTU Kemi, DTU, Juni 2010.

Endelig videreføres de mest værdifulde fund og nye ideer i et netop bevilget 1-årigt Proof of Concept (PoC) projekt fra Forskningsstyrelsen, det igangværende erhvervsforskerprojekt "DeNOx-katalysatorer til biomassefyring" med det tiknyttede såkaldte "Turbo-projekt" "DeNOx Catalysts for Biomass Fired Power Plants and Waste Inceneration" finansieret direkte af DONG Energy og Vattenfall A/S samt det pr. 1/11-2010 igangsatte energinet.dk projekt "Hydrocarbon Selective Catalytic Reduction" med de samme samarbejdspartnere som i nærværende PSO-projekt.

26/4-2011

Rasmus Fehrmann **Date**

Project partners

Table of Contents

1. DeNO$_x$ Technologies

1.1 Introduction

The simplest way to remove NO is in principle by its decomposition reaction outlined in reaction (1-1):

$$2NO \leftrightarrow N_2 + O_2 \qquad \Delta H^o_{298K} = 183 \text{ kJ/mol} \qquad (1\text{-}1)$$

The simple NO decomposition is thermodynamically favoured at lower temperatures, as outlined in Figure 1.1, but the reaction does not occur spontaneously due to slow kinetics. Many efforts have been attempted to catalyze the reaction, and several materials have been found (e.g. iron or copper oxides supported on ZSM-5), but a suitable catalyst which is active and resistant enough are yet to be found [1-5]. Consequently, to reduce NO to N_2 selectively at sufficiently low temperatures, a catalyst must be applied.

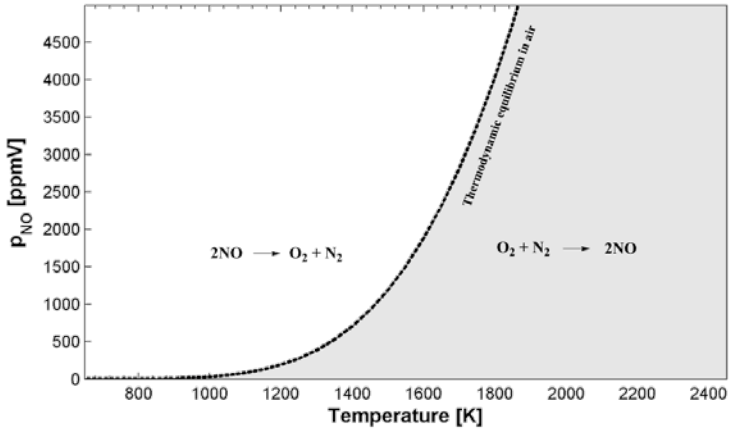

Figure 1.1 Theoretical equilibrium concentration of NO in air under the assumption that ΔH^o and ΔS^o are temperature-independent.

Although the specific type of catalyst may vary, the reduction of NO can efficiently be accomplished by a range of different reductants, e.g. CO, hydrocarbons, H_2, or NH_3. Ammonia is unique in its ability to selectively react with NO_x to form N_2 instead of being oxidized by oxygen to from N_2, N_2O or NO. This feature is however not shared by other simple reductants such as CO or hydrocarbons, and is as such unique of ammonia [6]. In the selective catalytic reduction, NO and NO_2 is eliminated by a reaction with NH_3 and O_2 to the harmless N_2 and H_2O. The dominating reactions for these nitrous species are outlined in reaction (1-2) to (1-6):

$$4NO + 4NH_3 + O_2 \rightarrow 4N_2 + 6H_2O \qquad \Delta H^o_{298K} = -1632 \text{ kJ/mol} \qquad (1\text{-}2)$$
$$6NO + 4NH_3 \rightarrow 5N_2 + 6H_2O \qquad \Delta H^o_{298K} = -1815 \text{ kJ/mol} \qquad (1\text{-}3)$$
$$2NO + 2NO_2 + 4NH_3 \rightarrow 4N_2 + 6H_2O \qquad \Delta H^o_{298K} = -1458 \text{ kJ/mol} \qquad (1\text{-}4)$$
$$2NO_2 + 4NH_3 + O_2 \rightarrow 3N_2 + 6H_2O \qquad \Delta H^o_{298K} = -1334 \text{ kJ/mol} \qquad (1\text{-}5)$$
$$6NO_2 + 8NH_3 \rightarrow 7N_2 + 12H_2O \qquad \Delta H^o_{298K} = -2734 \text{ kJ/mol} \qquad (1\text{-}6)$$

All of the above deNO$_x$ reactions are strongly exothermic in character and also exhibits a substantial decrease in the Gibbs free energy (all lower than -1250 kJ/mol). This means that all of the reactions (1-2) to (1-6) can be considered to occur only from the left to right.

Of the many catalyst combinations investigated, those based on vanadia supported on titania promoted with tungsta (WO_3) or molybdena (MoO_3) were found to possess genuine advantages in NO reduction and SO_2 oxidation [6]. Today, after three decades of studies and industrial application, the most widespread commercial SCR catalyst is based on V_2O_5/TiO_2 formulations, such as V_2O_5-WO_3/TiO_2 and V_2O_5-MoO_3/TiO_2. The present catalysts are constituted of TiO_2 anatase supports with a submonolayer surface coverage of V_2O_5 and WO_3 (or MoO_3). The surface area of the catalysts is around 50-100 m^2/g, with a V_2O_5 content of 0.5-3 wt% and WO_3 or MoO_3 loading of 5-10 wt%. Vanadia, especially as bulk, is responsible for the undesired oxidation of SO_2, and the vanadia content is thus generally kept low in the presence of high SO_2 concentrations [6]. Monolayer catalysts are more efficient than bulk V_2O_5 and utilizing TiO_2 anatase as support material relies on the fact that TiO_2 is only weakly and reversibly sulfated in presence of SO_2 and oxygen [7].

Due to the high catalytic activity of this catalyst, the mechanical structure of catalyst has been optimized to exhibit lowest possible pressure drop over the catalytic bed. This is done by the so-called honeycomb technology, where the catalysts are shaped in form of honeycomb monoliths with parallel channels, to some extent allowing dust particles to pass though the monolith. By altering the channel size, the honeycomb structure can be designed to meet high dust (~10 mm channels) or low dust (~3 mm channels) conditions, thereby minimizing the risk of a huge pressure drop over the catalytic bed.

The SCR process of vanadium-based catalysts are most efficient around 350-400ºC. This is important to consider, since the gas is gradually cooled during the post-treatment system, and why both high and low dust position can be considered (cf. Figure 1.2). High dust configuration is the most widely used SCR configuration in coal-fired plants. The main advantage is that the temperature right after the boiler economizer is in the range suitable for the SCR reaction. In this configuration, the catalyst is thus exposed to fly ash and chemical compounds present in the flue gas that can both plug the catalyst and degrade it mechanically and chemically. However, appropriate design of a high-dust SCR system can mitigate the impacts on the catalyst. If this was not the case, the cost of a high temperature electrostatic precipitator (H-ESP) placed in between the boiler and the SCR reactor could still be a convenient investment. This solution is known as low dust configuration. In a tail end configuration, the SCR reactor is placed between the Flue Gas Desulphurization plant (FGD) and the stack. In this case the absence of SO_2 in the flue gas allows the use of more reactive catalyst formulations, mainly because the oxidation of SO_2 to SO_3 is not a problem. At the same time, the life of the catalyst is also increased because of the low dust loading.

The traditional SCR catalyst is operating at temperatures around 300-400° C. Because of this high operating temperature, the catalyst bed must be located upstream of the desulfurizer and/or of particulate control device to avoid reheating of the flue gas. This makes the catalyst to deactivate from high concentrations of sulfur dioxide and dust. Therefore, there is a great interest in developing active SCR catalysts that work at low temperature ranges 80-280° C [9-15],which

would render placement of the SCR unit possible in the tail end after the desulfurizer and particulate control installations.

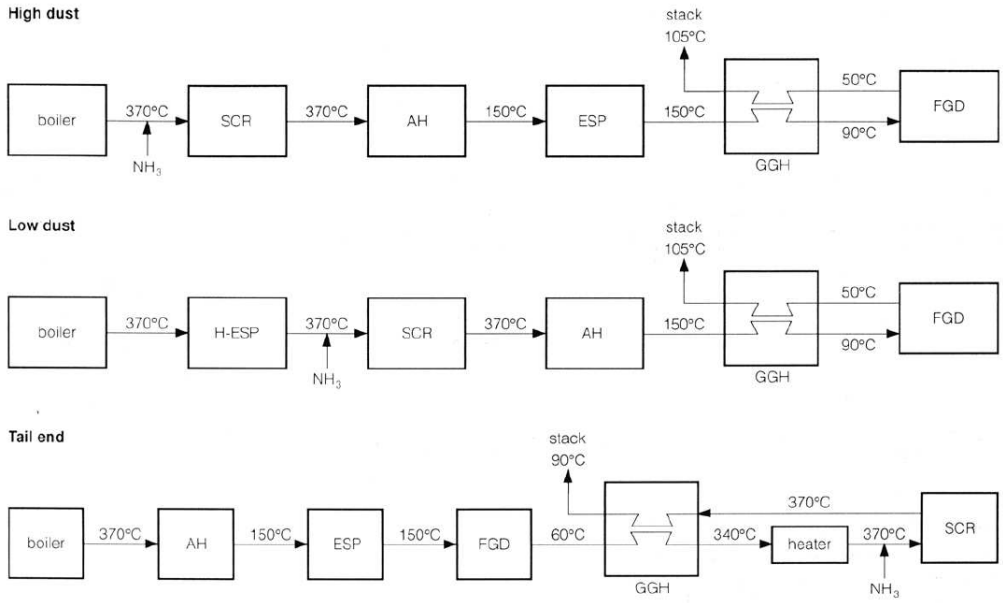

Figure 1.2 SCR process arrangements. SCR: selective catalytic reduction, AH: air preheater, ESP: electrostatic precipitator, H-ESP: high temperature ESP, GGH: gas-gas heater, FGD: flue gas desulfurization. Adapted from [8].

1.2 Vanadium surface chemistry and mechanistic considerations

1.2.1 Vanadium surface species

The catalytic properties of the supported vanadium catalysts are strongly affected by the vanadia loading, preparation method, and type of support and promoter. The type of metal oxide species present on the support surface is determined by the content of vanadium. At low loadings the isolated and monomeric VO_x species predominate, which, with increasing loading, will react to form dimeric and polymeric species until monolayer coverage is reached, illustrated in Figure 1.3. The crystalline phase of V_2O_5 will dominate on the surface above monolayer coverage. In the case of titania as the support material, the monolayer is achieved at 7.9 VO_x/nm^2, whereas on zirconia the limit is already reached at 6.8 VO_x/nm^2 [16].

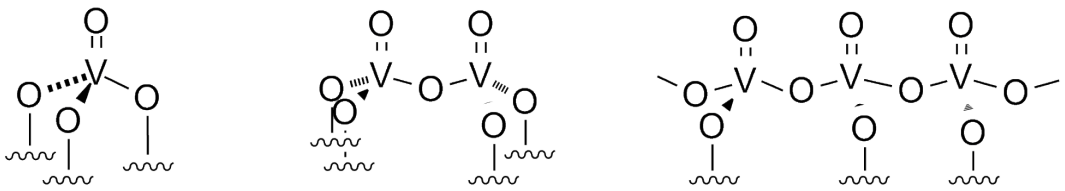

Figure 1.3 Structural configurations of dispersed vanadates on e.g. TiO_2 in their dehydrated form. Vanadium loading increases from left to right.

By impregnation of TiO_2 with V_2O_5, the number of surface Lewis acid sites decrease, since the TiO_2 surface consists only of this type of acid sites. Simultaneously an increase in the number of Brønsted acid sites is observed, because the vanadia species consist of both types. These Brønsted acid sites are V-OH groups. With a vanadia content of around a monolayer of VO_x species, approximately 5-10% of the vanadium atoms will have V-OH Brønsted sites [18].

1.2.2 Vanadium-based catalytic cycle

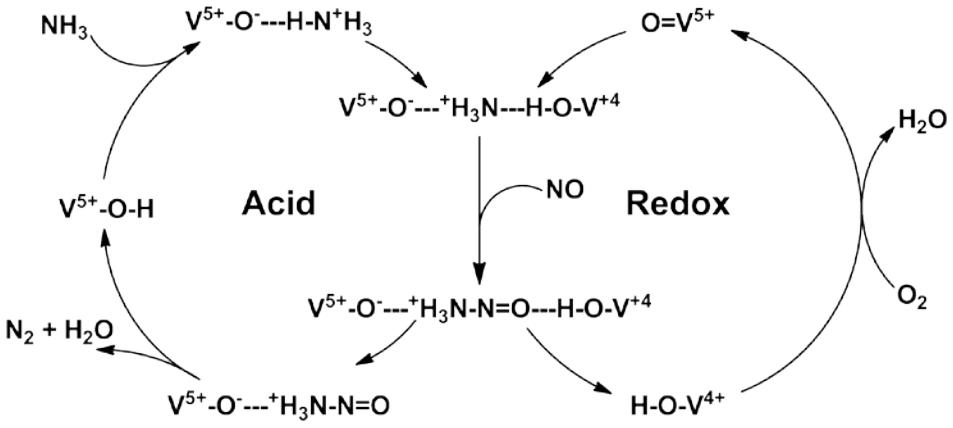

Figure 1.4 Proposed catalytic cycle, illustrating the acid and redox cycles of the SCR reaction over a V_2O_5/TiO_2. Adapted from [17]

Even though one of the first reaction schemes proposed for the SCR reaction was based on a Langmuir-Hinshelwood mechanism [19], there is a today general consensus that the SCR reaction occurs via an Eley-Rideal type mechanism [1]. The mechanism presented by Topsøe in Figure 1.4 is a perfected version of that proposed by Inomata et al. in 1980 [9]. As outlined in Figure 1.4, ammonia is first adsorbed on the Brønsted site of surface V^V-OH, forming an activated intermediate. The intermediate is very reactive towards gaseous NO, causing a reaction whereby the V^V-OH is regenerated under the liberation of N_2 and H_2O from the catalyst surface. In the redox side of the reaction scheme, a reoxidation step is occurring, where O_2 is indicated to react (not stoichometrically, though) with V^{IV} to form V^V and thus complete the catalytic cycle.

1.3 Catalyst deactivation

The catalyst should in principle never lose activity since it is not consumed by the reaction. Unfortunately this is not the case since they deactivate with time. Catalyst deactivation can be subdivided into physical and chemical deactivation. Physical deactivation occurs when the pores or structure of the catalyst is blocked, causing a reduction of the active surface area. This can be caused by dust in the off-gas or deposition of salts formed during or after the combustion. The chemical form of deactivation is caused by a reaction between a chemical compound and the active site, thereby rendering the site inactive resulting is catalyst activity. Both forms of deactivation result in loss of overall catalyst activity.

1.3.1 Deactivation by bio fuels

Bio Fuels – or biomass, includes organic matter including threes, agricultural energy crops, crop and timber waste, aquatic plants, animal waste, household, municipal & industrial waste. Contrary to fossil fuels they are regarded as environmentally sustainable energy sources, since they are part of the carbon eco-cycle on earth, and therefore regarded as an energy source with zero– or at least "neutral" CO_2 emissions. Even though they politically are considered very "clean" fuels, it has turned out that the reactions occurring inside the boilers during combustion of biomass tend to be more "dirty". Natural gas comprise a relatively clean combustion gas, whereas combustion of e.g. municipal waste or bio-fuel often contain species that can lead to possible deactivating of traditional vanadia-titania-based SCR catalysts. The composition of various species of both fuel and ash associated with commercial or pilot plants currently combusting or co-combusting biomass have recently been reported [20-22]. All studies show a significant increase in the quantity of alkali and alkaline-earth elements (K, Na, Mg, Ca), phosphorous and chlorine in the biomass-based fuels compared to coal (cf. Table 1.1). The quantity of potassium and chlorine in the straw can be more than an order of magnitude higher than that of coal. Especially the high content of potassium in e.g. wood and straw is of concern. Alkali metals were identified early as poisons for vanadia-titania-based SCR catalysts by Chen and Yang [23], where they found that the strength of the poison is related to the increase of basicity. Potassium is thus a stronger poison the vanadium-based catalyst than sodium and lithium.

Table 1.1 Fuel compositions of three coal types and Danish straw. All numbers are given in wt%. Adapted from [21]

	COPRIB	SAKLEI	Lignite	Straw
Moisture	2.00	2.00	2.00	6.70
Volatiles	39.53	24.07	51.85	68.76
Ash	5.00	14.49	5.28	7.37
C	76.14	71.51	62.70	44.80
N	1.41	1.75	0.71	1.10
S	0.81	0.63	0.40	0.20
Cl	0.01	0.01	0.05	0.73
P	0.004	0.11	0.02	0.14
Na	0.01	0.02	0.01	0.02
K	0.07	0.08	0.01	1.90

COPRIB: Columbia high volatile bituminous coal. SAKLEI: South African medium volatile bituminous coal. Lignite: Brown coal

Full scale tests on the impact on the SCR catalyst by combusting biofuels have been investigated by several authors [20-22, 24]. The studies showed that the SCR catalyst exhibits significant deactivation over a relatively short time, as shown in Figure 1.5, where the relative activity versus time is plotted for three different fuel compositions. By combustion of 100% sawdust the catalyst was deactivation more than 75% after 1500 hours on stream. However, their results also indicated that, in the case of sawdust, the deactivation could be delayed by clever co-combustion bio fuel and coal.

That alkali indeed is responsible for the deactivation observed in the full scale study of the SCR catalyst is verified in Figure 1.6, where model-poisoning with potassium has been done on a commercial SCR catalyst. Severe deactivation is observed already at K/V = 0.3 mol/mol, where 90% of the initial activity is lost. The high content of alkali present in the biomass (cf. Table 1.1) thus acts as a chemical poison towards the catalyst. The potassium salts in the fuel are transported to the catalyst in the gas phase, diffuses into the catalyst, condensates in the pore system and reacts with the surface species. As the final proof for a chemical poisoning it was observed that there was no significant decrease of the surface area after exposure [20,21].

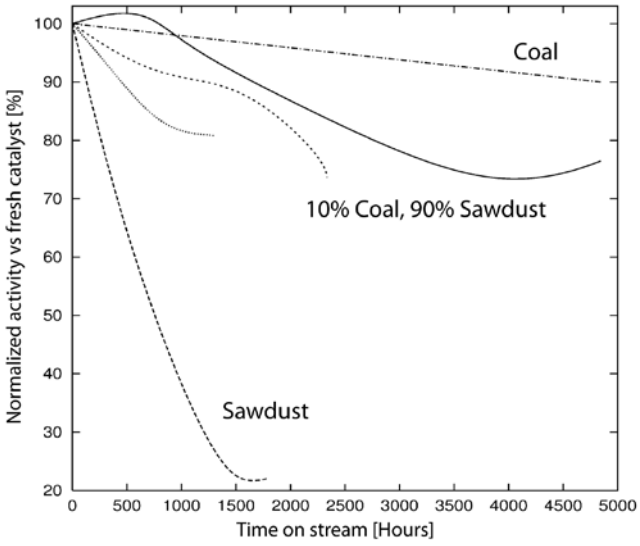

Figure 1.5 Activities of a commercial V_2O_5-WO_3/TiO_2 catalyst (installed in power plant) versus time in units with different fuel compositions. Adapted from [24]

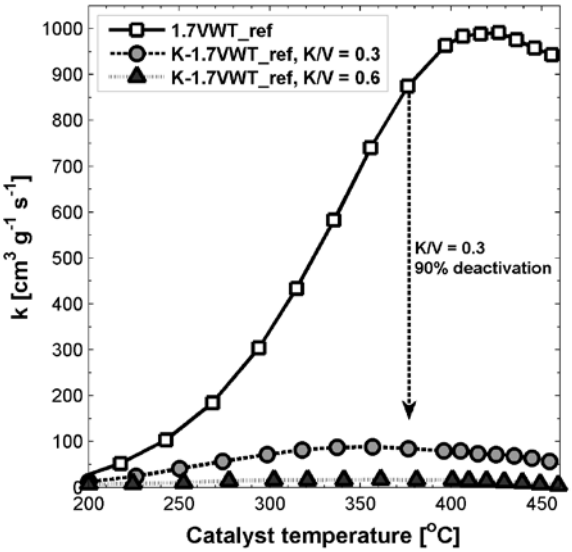

Figure 1.6 SCR activity (lab scale) profile of fresh commercial V_2O_5-WO_3/TiO_2 catalyst and model doped with potassium (K/V = 0.3 and 0.6 mol/mol)

It was found that the rate constant was still of first order with respect to NO after poisoning, and FTIR measurements indeed confirmed that the poisoning effect was due to a decrease in Brønsted acid sites (V-OH) – while the number of Lewis sites appeared unchanged. Zheng et al. [25] suggested an early mechanism, based on a substitution reaction on the Brønsted acid site, whereby the reactive site is blocked by potassium by condensation of HCl, as outlined in (1-2).

$$\text{V-OH} \xrightarrow{\text{KCl}} \text{V-O-K} \qquad (1\text{-}2)$$

This mechanism requires an equimolar ratio of vanadium and potassium to completely deactivate the catalyst. Although the model provides a very intuitive understanding of the deactivation, several groups report of almost complete loss of catalyst activity already at K/V≈ 0.5 mol/mol [23,26]. Recent DFT studies suggest mechanisms in better agreement with experimental findings. The results show that the deactivating agent preferentially occupy hole sites between V_2O_5 centers, thereby inhibiting both Brønsted and V^{5+}=O sites [21] (Figure 1.7), even at low alkali/vanadium rations. Kiwi-Minsker et al. [29] reported of the disappearance of monomeric vanadium species

upon potassium doping, which fit well with the findings suggested in Figure 1.8. This suggests that potassium is also involved in the reaction and cleavage of bridging V-O-V bonds. Furthermore, it is worth noticing that the deactivation mechanism illustrated in Figure 1.8 also fits the experimentally observed complete deactivation of the catalyst at K/V = 0.5.

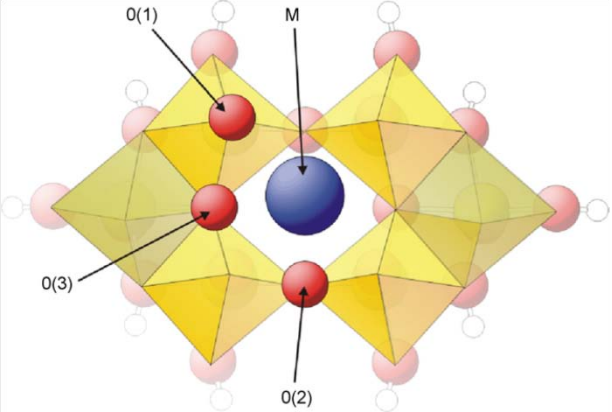

Figure 1.7 The V_2O_5 surface ($V_6O_{20}H_{10}$ cluster) used for the theoretical calculations. Here the deactivating atom (M) is located in the non-atomic hole between the oxygen centers [21]

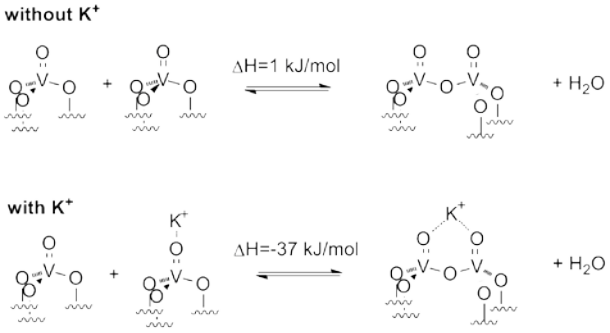

Figure 1.8 Effect of potassium on the equilibrium between monomeric and dimeric vanadia complexes calculated by DFT. Dimerization is clearly favored in enthalpy [22]

1.4 Alkali-resistant SCR catalyst

Although tungsta is added to the V_2O_5/TiO_2 formulation to decrease the poisoning effect of alkali, the traditional catalyst is still far from being resistant to deactivating agents typically found in the flue gas of biomass, confirmed by several full-scale experiments with the V_2O_5-WO_3/TiO_2 catalyst, as discussed in the previous section. The key issue is that the alkaline potassium in blocking the Brønsted V_2O_5 acid sites of the working SCR catalyst. This phenomenon motivates the current project, which deals with searching for alternative deNO$_x$ technologies which are less affected by alkali salts from the fuel. During the project, several approaches can be applied to design alkali-resistant catalysts or technologies:

- *Increase of substrate acidity*. By increasing the substrate acidity (adding sacrificial acid sites) the incident alkali species would interact stronger with the support than the active vanadia sites. Various types of zeolites as well as sulfated zirconia possess very strong acidity, and are thus a suitable candidate. By promoting the support material with heteropoly acids, the same effect in acidity enhancement can also be achieved. Finally, applying a mixed oxide of ceria zirconia (CeO_2-ZrO_2) a significant improvement in surface acidity can also be attained.

- *Substituting the active species of the catalyst*. A crucial part of the SCR mechanism is the Brønsted acid sites of vanadia, which is much more affected than the Lewis acid sites by

potassium doping. Hence, by using metal oxides which mainly possess Lewis acidity, the catalyst could avoid deactivation by alkali. CuO and Fe_2O_3 are attractive under these conditions, since they are well known Lewis acids and have also exhibited NH_3-SCR activity [1].

- *Improving the activity of the existing V_2O_5/TiO_2 formulation* by preparing nano-sized vanadia-particles (being significantly more active than bulk vanadia) on a high surface area TiO_2 anatase support. Thereby it is possible to prolong the catalyst time on stream by increasing the amount of initial active sites.

- *Non-catalytic NO_x absorption*. Finally, a more exotic non-catalytic method of NO removal, is by means of gas capture in ionic liquids. The technology has already been used for CO_2 (although some challenges are still to be overcome) and SO_2 absorption, but has so far never been applied to the removal of NO.

1.5 References

[1] G. Busca, L. Lietti, G. Ramis, and F. Berti, Appl. Catal. B: Environ. 18 (1998) 1-36.
[2] H. Falsig, T. Bligaard, C. H. Christensen, and J. K. Nørskov, Pure and Applied Chemistry 79 (2007) 1895–1903.
[3] R. da Silveira, A. de Oliveira, S. Pergher, V. da Silva, and I. Baibich, Catal. Lett. 129 (2009) 259–265.
[4] H. Yahiro and M. Iwamoto, Appl. Catal. A: Gen. 222 (2001) 163–181.
[5] S. Brandenberger, O. Kröcher, A. Tissler, and R. Althoff, Catalysis Reviews: Science and Engineering 50 (2008) 492-531.
[6] P. Forzatti, Appl. Catal. A: Gen. 222 (2001) 221-236.
[7] J.P. Dunn, P.R. Koppula, H.G. Stenger, I.E. Wachs, Appl. Catal. B: Environ. 19 (1998) 103-117.
[8] N.-Y. Topsøe, Cattech 1 (1997) 125-134.
[9] M. Inomata, A. Miyamoto, Y. Murikami, J. Catal. 62 (1980) 140-148
[10] F.J.J.G. Janssen, F.M.G. van den Kerkhof, H. Bosch, J.R.H. Roos, J. Phys, Chem. 91 (1987) 5921-5927
[11] L. Singoredjo, R. Korver, F. Kapeijn, J. Moulijn, Appl. Catal. B: Environ. 1 (1992) 297-316
[12] S.C. Wood, Chem. Eng. Prog. 90 (1994) 32-38
[13] J.A. Dumesic, N.-Y. Topsøe, H. Topsøe, Y. Chen, T. Slabiak, J. Catal. 163 (1996) 409-417
[14] Z. Zhu, Z. Liu, S. Liu, H. Niu, Appl. Catal. B: Environ. 23 (1999) L229-L233
[15] F. Liu, H. He, Y. Ding, C. Zhang, Appl. Catal. B: Environ. 93 (2009) 194-204
[16] I.E. Wachs, Catal. Today 27 (1996) 437-455.
[17] N.-Y. Topsøe, Science, 265 (1994) 1217-1219.
[18] I.E. Wachs, B.M. Weckhuysen, Appl. Catal. A: Gen. 157(1997) 67–90.
[19] M. Takagi, T. Kawai, M. Soma, T. Onishi, K. Tamaru, J. Catal. 50 (1977) 411-446.
[20] Å. Kling, C. Andersson, Å. Myringer, D. Eskilsson, S.G. Järås, Appl. Catal. B: Environ. 69 (2007) 240-251.
[21] Y. Zheng, P. A. Jensen, A.D. Jensen, B. Sander, H. Junker, Fuel, 86 (2007) 1008–1020.
[22] H. Jensen-Holm, J.R. Thøgersen, P. Lindenhoff, Presented at Power-Gen Europe, Germany, 2009.
[23] J.P. Chen, R.T. Yang, J. Catal. 125 (1990) 411-420.
[24] C. Andersson, C.U.I. Odenbrand, L.H. Andersson, Värmeforsk 646 (1998).
[25] Y. Zheng, A.D. Jensen, J.E. Johnsson, Ind. Eng. Chem. Res. 43 (2004) 941-947.
[26] A. Kustov, S. Rasmussen, R. Fehrmann, P. Simonsen, Appl. Catal. B: Environ. 76 (2007) 9-14.
[27] D. Nicosia, I. Czekaj, O. Kröcher, Appl. Catal. B: Environ. 77 (2008) 228-236.
[28] J. Due-Hansen, S. Boghosian, A. Kustov , P. Fristrup, G. Tsilomelekis, K. Ståhl, C.H. Christensen, R. Fehrmann, J. Catal. 251 (2007) 459-473.
[29] L. Kiwi-Minsker, D.A. Bulushev, F. Rainone, A. Renken, J. Mol. Catal. A: Chem. 184 (2002) 223-235.

2. ZrO_2-based catalysts

In the following chapter the results are presented for various catalysts, all constitute on zirconia (ZrO_2) as support material. The motivation for employing zirconia as catalyst carrier over the traditional TiO_2 can be found in the acidic properties. By adding promoters, e.g. MoO_3, WO_3, SO_4^{2-}, or by mixing the oxide with e.g. CeO_2, it is possible to enhance the acidity of zirconia significantly.

The acid-enhancement of the catalyst support was pursued as a strategy to develop an alkali-resistant catalyst. The scope of this strategy was to create catalysts with acidic surface groups, by which alkali can be hosted, instead of reacting with vanadium species. By producing catalysts with high surface acidity it is possible to keep the alkali compounds away from the active vanadium sites, by having sacrificial acid sites co-impregnated on the surface.

Early in the study of zirconia-based catalysts, we found that a series of commercial zirconia-based samples from Saint-Gobain Norpro (NP) proved suitable as support material, competitive with the SCR activities of vanadia-loaded synthesized zirconia which was previously published [1]. Since the zirconia already was commercially available on extruded form (pellets), the exploitation of this material as possible SCR catalyst is a step closer to industrial relevance. Hence, the commercial zirconia is setting the frame for all the catalysts synthesized in this chapter, except the CeO_2-ZrO_2 mixed oxide catalyst.

2.1 The crystal phases of zirconia

The initial selection of suitable support materials was primarily based on the surface area and crystalline form. The monoclinic phase of ZrO_2 provides weak acid sites when sulfated, whereas the tetragonal form is responsible for the generation of strong acid sites [2,3].

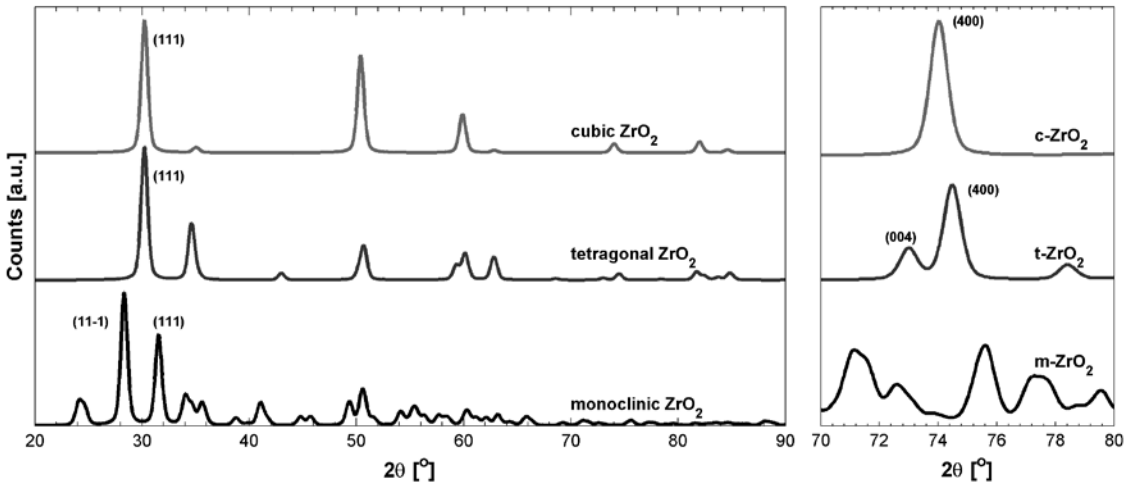

Figure 2.1 Calculated diffraction patterns of the three phases of ZrO_2. The plots are for $CuK_{\alpha 1}$ X-rays. Unit cells of zirconia: **m-ZrO_2** (space group $P2_1/c$}), a = 5.107 Å, b = 5.174 Å, c = 5.332 Å, $\alpha = \gamma = 90^o$, $\beta = 99^o$; **t-ZrO_2** ($P4_2/nmc$}), a = b = 3.6 Å, c = 5.18 Å, $\alpha = \beta = \gamma = 90^o$; **c-$ZrO_2$** (Fm3m), a = b = c = 5.118 Å, $\alpha = \beta = \gamma = 90^o$.

Zirconia has three stable polymorphs: tetragonal (t-ZrO_2), monoclinic (m-ZrO_2), and cubic (c-ZrO_2), and the occurrence and transformation between the phases depend on doping and/or thermal

treatment. With X-ray diffraction (XRD) it is easy to identify the monoclinic phase of ZrO_2, whereas tetragonal and cubic zirconia can be difficult to distinguish between as can be observed in Figure 2.1.

The monoclinic phase is stable up to 1050ºC, where it transforms into the tetragonal phase, which further changes into the cubic phase at 2400ºC. The cubic phase of zirconia is stable up to the melting point at about 2700ºC. Thus, tetragonal and cubic ZrO_2 are only metastable phases below 1050ºC, where monoclinic is the thermodynamically preferred form. In the case of i.e. sulfate or tungsta promoted zirconia catalysts, the crystalline structures of the samples behave differently from that of pure ZrO_2. Amorphous zirconia has been reported to undergo crystallization around 350-450ºC [4,5], but when doping the matrix with e.g. a promoter, the phase transition temperature from amorphous to tetragonal zirconia is shifted to higher temperatures [1,4,6,7]. Zirconia can thus easily be stabilized in its tetragonal phase by e.g. a promoter, which hinders the phase transition to monoclinic.

2.2 Sulfate-promoted zirconia catalysts

2.2.1 The commercial support materials

The phases of zirconia can easily be discriminated by refining the XRD data with the Rietveld method. In Figure 2.2 the diffraction patterns of the commercial supports is depicted together with the difference curve from the Rietveld fit. If the Rietveld analysis results in a perfect fit (thereby accounting for the presence of all phases present) the difference curve would yield a straight line, located on the baseline.

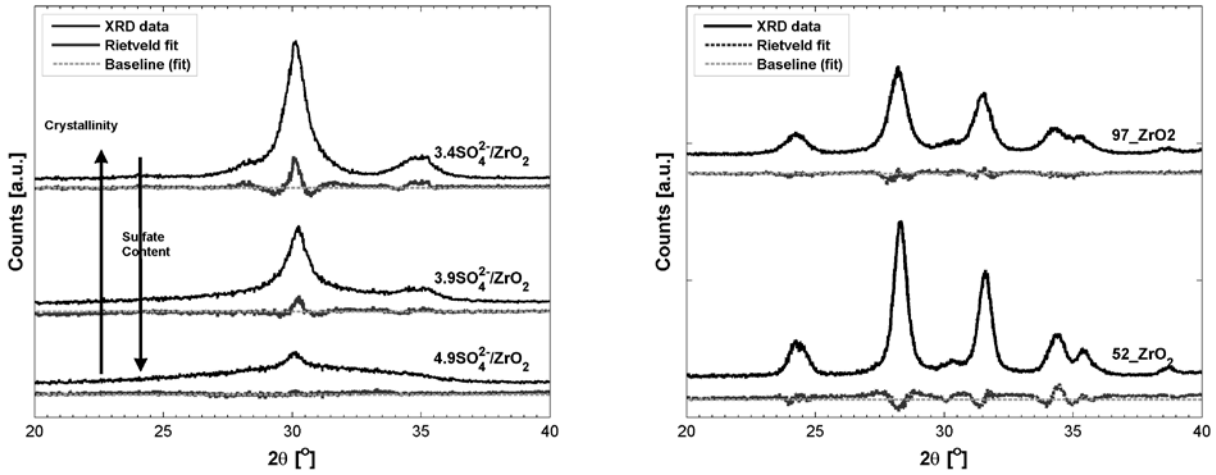

Figure 2.2 Powder X-ray diffraction and Rietveld refinement of commercial zirconia-bases supports from Saint-Gobain Norpro. Left: Sulfated samples, Right: pure ZrO_2-based samples.

From the diffraction patterns in Figure 2.2 it is clear that the pure ZrO_2 samples primarily consist of monoclinic ZrO_2, whereas the samples containing sulfate mainly contain tetragonal and cubic ZrO_2.

The numbers in the name of the pure zirconia samples correspond to their surface area (m^2/g), and in the sulfated samples they denote the loading of sulfate measured as SO_3 (wt%) (from here on, sulfate is abbreviated as "S", and zirconia as "Z"). Through Rietveld refinement the phase distributions can be obtained, which is collected in Table 2.1. Although synthesis details for these commercial materials can not be obtained, a trend can be extracted regarding the concentration of sulfate versus the crystallinity, being inverse proportional. Assuming that the sulfated materials are calcined under similar conditions, the degree of crystallinity obtained agrees well with results from literature, where increasing the dopant would retard the temperature of crystallization [4].

The phase distribution of the three crystalline ZrO_2 configurations of the commercial samples is outlined in Table 2.1, where the two pure ZrO_2 samples consist almost entirely of m-ZrO_2. The sulfated samples are all polymorph mixtures, comprising mostly of monoclinic and cubic zirconia. Only 3.4SZ_NP holds significant amounts of the tetragonal phase, namely 10 vol%. However, the high content of c- ZrO_2 in the samples is slightly surprising when comparing with literature. The majority of XRD-studies on promoted zirconia report only of the monoclinic and tetragonal ZrO_2 phase, only using the strong (111) reflection around 30º of the latter phase, without mentioning the cubic phase [5,8-11]. Only a few distinguishes the phases [12,13]. On the other hand, differentiation between the two is not straight forward, and only few differences exist, as can be seen in Figure 2.1. Only using the (111) reflection line would therefore not be enough to discriminate t-ZrO_2 from c-ZrO_2, which is located at almost the same angle. However, the relative intensity of the (111) reflection to the line of $2\theta \approx 35º$ or the (004) reflection at 73º 2θ can be used to identify the tetragonal phase.

Table 2.1 Properties of commercial zirconia samples. The phases (tetragonal, cubic, and monoclinic) of zirconia are given as volumetric percent of the crystalline phase. Full TPD profile is shown in Figure 2.3.

Sample	BET area	Crystallinity†	Phase distribution‡			Surface acidity	
			t-ZrO_2	c-ZrO_2	m-ZrO_2	Total*	<500ºC
	[m^2/g]	[%]	[Vol%]			[µmol/g]	
52Z_NP	52	75	3	0	97	372	372
97 Z_NP	97	100	0	0	100	648	648
3.4SZ_NP	145	73	10	67	23	2004	896
3.9SZ_NP	130	60	5	36	59	2109	785
4.9SZ_NP	125	53	3	58	39	2351	910
1.7VWT						1324	930

† Calculated with the program Winprep

‡ Phase distribution found through Rietveld refinement. Program used: Winpow

* Total amount of desorbed NH_3 in temperature range 100-1000ºC

The ammonia desorption profiles of the commercial samples are depicted in Figure 2.3. The total amount of adsorbed ammonia, which is listed in Table 2.1, corresponds to molecular adsorbed ammonia or ammonium ions on Lewis or Brønsted acid sites, respectively. The relative strength of the acid sites are reflected by the temperature of maximum ammonia desorption, these are listed in the figure legend.

The broad nature of the low-temperature desorption peaks of sulfated zirconia in Figure 2.3 can be attributed to a wide range of surface acid sites present with different acid strengths. However, categorizing the exact nature of the acid sites are not possible with NH_3-TPD alone, but a commonly used technique is infrared spectroscopy (IR) coupled with pyridine adsorption.

The TPD curve for the supports 52Z_NP and 97Z_NP showed a bi- and tri-modal desorption profile with peaks at about 190, 300, and 427ºC, whereas no desorption peaks are observed at higher temperatures. The overall acidity of the two pure monoclinic ZrO_2 samples contains an order of magnitude less surface acidity compared to the sulfated ZrO_2. Only desorption peaks above 430ºC are observed for sulfated zirconia, which tentatively can be attributed to the presence of Brønsted acid sites [14], which does not exist on the pure monoclinic ZrO_2. Moreover, the absence of any ammonia desorption peak of 1.7VWT around 430ºC, suggests a low concentration of Brønsted acid sites on this type of catalyst.

At lower temperatures, roughly two types of acid sites can be identified on the sulfated samples, one around 165ºC, which is likely to originate from very weakly bound or physisorbed ammonia, and one at around 270-300ºC. A number of high-temperature peaks exist for the sulfated samples, the strongest at 660ºC, 732ºC, and 763ºC for 1.7V-4.9SZ_NP, 1.7V-3.9SZ_NP, and 1.7V-3.4SZ_NP, respectively. The temperature of desorption from these strong acid sites are consistent with the findings of Barthos et al. [14], which detected ammonia desorption on sulfated zirconia at about 630ºC, attributed to be of Lewis-acid nature. Besides the very low temperature desorption peaks observed around 165ºC in Figure 2.3, the Brønsted and Lewis acid site designation of Barthos et al. could tentatively be extrapolated to the results observed of the commercial sulfated ZrO_2. However, the NH_3-desorption peak of 3.9SZ_NP and 4.9SZ_NP from the apparent Brønsted acid site are located at a slightly higher temperature than they reported, namely above 500ºC.

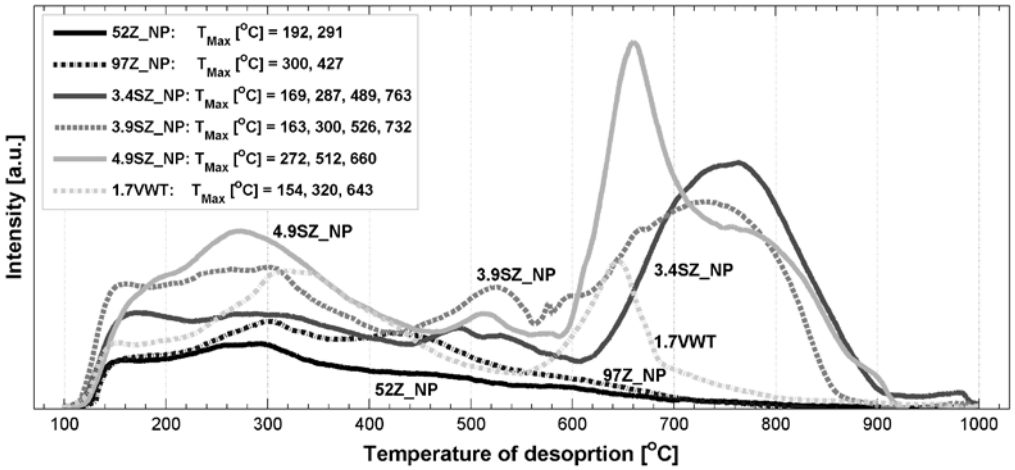

Figure 2.3 NH_3-TPD profiles of the commercial supports and the $3V_2O_5$-$10WO_3$-TiO_2 reference catalyst. The amount of desorbed ammonia is listed in Table 2.1.

Haw et al. [15] postulates that the number of Brønsted acid sites on sulfated zirconia are moderate, consisting only of about 7% of the number of sulfur atoms on the basis of ^{15}N NMR

of adsorbed pyridine-^{15}N. This was confirmed by Katada et al. [16], which found a slightly higher number of Brønsted acid sites, namely 12-18%, whereas Wachs and Weckhuysen [17] reported that around 5-10% of the surface vanadia species are surface Brønsted acid sites. Assuming that the peaks observed at 489-526ºC of the sulfated zirconia supports are due to Brønsted acid sites. An integration of the peak area versus the total desorption area would then result in the fraction of Brønsted acid sites, where the number of Brønsted acid sites versus total acidity is in the range of 9-15%. Although this number is encumbered with some uncertainty, it is close to those observed in literature.

2.2.2 Vanadia-based catalysts

The commercial samples were impregnated with vanadyl (incipient wetness impregnation, IWI) corresponding to a vanadia loading of 3.0 wt% and calcined at 400ºC for 2 hrs in air. The reference catalyst is based on commercial 10 wt% WO_3-TiO_2 (DT-52, Millennium), which was stabilized with 5 wt% of Bentonite (Tolsa, >95%) and 5 wt% of Hymod Excelsior (Imerys Minerals Ltd) and $VOSO_4 \cdot 5H_2O$ (aq). A small amount of water were added to the slurry, and the paste were extruded from a 20 ml syringe (Ø=2 mm) and dried and calcined at 500ºC, resulting in a vanadium loading of 3 wt% V_2O_5.

The SCR activity of the vanadium-impregnated samples have been measured from room temperature to 550ºC, presented in Figure 2.4. The SCR activity of unpromoted 1.7V-97Z_NP reaches maximum conversion of NO around 500ºC, only yielding a k-value around 170 $cm^3g^{-1}s^{-1}$. 1.7V-52Z_NP yields even lower activities, and is therefore not shown here. In contrast, the sulfate-promoted catalysts render somewhat higher SCR activities, where the total activity follow the order 1.7V-4.9SZ_NP < 1.7V-3.9SZ_NP < 1.7V-3.4SZ_NP, with a concurrent decrease in temperature of maximum NO conversion.

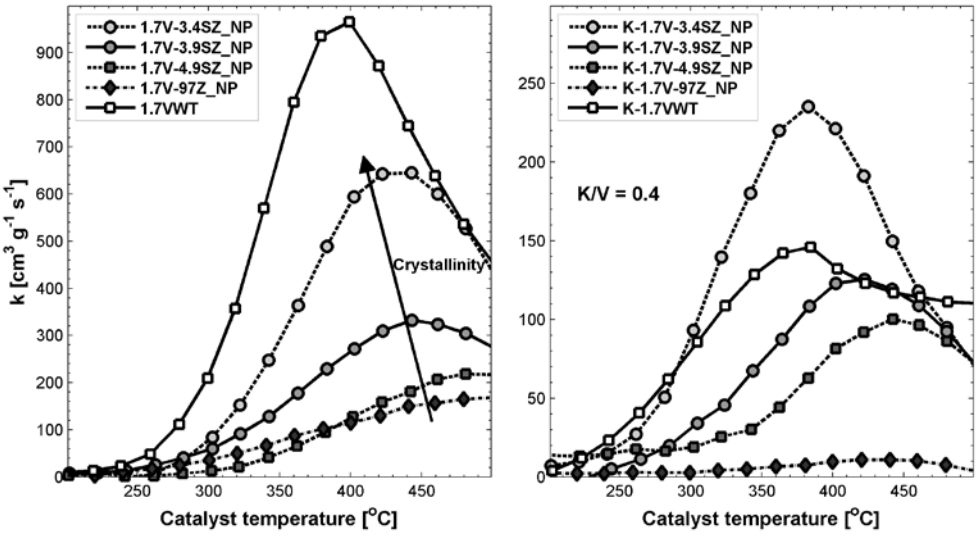

Figure 2.4 Left: SCR profile of various vanadia-loaded commercial supports and a 1.7VWT reference catalyst. Markers indicate SCR activity while heating, lines the activity while cooling from 550ºC. Right: SCR activity of the corresponding potassium-doped commercial supports and the reference catalyst, K/V = 0.4.

Thus, 1.7V-3.4SZ_NP presents the highest SCR activity of the vanadium-loaded sulfated-zirconia catalysts at the lowest temperature, namely 430ºC. In the absence of potassium, the reference catalyst 1.7VWT, based on the traditional vanadia-based catalyst, display a somewhat higher activity with a maximum at 400ºC. However, the first order rate constant is here given on a weight basis of the catalyst, and the density of titania is somewhat lower than for zirconia (particle density for titania-based catalyst ≈ 0.2 g/ml, zirconia-based catalyst ≈ 0.5 g/ml). Since similar catalyst mass is used for the activity measurements, the difference in density (catalyst volume) should be taken into consideration in the evaluation of catalyst performance.

Impregnation of the catalysts with potassium (K/V = 0.4) leads to a considerable decrease of their catalytic activity (Figure 2.4, right). This deactivation is pronounced for all catalysts, but in the case of the unpromoted K-1.7V-97Z_NP, an almost complete deactivation observed. In the case of the potassium-doped reference catalyst, severe deactivation is also detected, whereas the sulfate-promoted samples still exhibit SCR activity, especially K-1.7V-3.4SZ_NP. Moreover, the addition of potassium results in a shift of maximum catalytic activity towards lower temperatures compared with the corresponding catalyst. A possible explanation of such a shift in temperature is that potassium reduces the activity of the main SCR reaction while the rate of the competitive oxidation of ammonia remained constant or even increased.

A rough indicator for high resistance toward the poisoning of the basic alkali can be found in the initial surface acidity of the supports. The un-promoted ZrO_2-based catalysts possess relatively low surface acidity (less than 650 μmol/g) and suffer from significant deactivation, as does the 1.7VWT reference catalyst (total surface acidity = 1324 μmol/g). If we take into account that the catalytically active Brønsted acid sites consist of less than ca. 20% of all surface acid sites [15-17], it emphasize the vulnerability of the catalyst. Thus, even a small amount of alkali potentially can deactivate the majority of Brønsted sites, which are essential for the SCR reaction on vanadia catalysts.

2.2.3 Concluding remarks

Binary V_2O_5-ZrO_2 catalysts were shown to provide low catalytic activity and almost complete deactivation was observed upon alkali-doping due a combination of low surface acidity and/or high abundance of monoclinic ZrO_2 in the matrix.

The 3 wt% V_2O_5-10wt% WO_3-TiO2} reference catalyst also suffered from significant deactivation, where less than 20% of the initial SCR activity was present after potassium doping (K/V = 0.4). The low overall surface acidity and apparent absence of Brønsted acid sites are likely contribute to a high sensitivity to the basic potassium.

The sulfated zirconia catalysts of commercial grade presented here contain high surface acidity, and especially 3.4SZ_NP contains the smallest fraction of monoclinic zirconia among the samples studies and the highest surface area. The corresponding vanadia-loaded catalyst exhibited much higher resistance toward potassium (only deactivating 38%) than the two titania-based reference catalysts. Utilization of sulfated zirconia as support material is thus a promising candidate for increasing the catalysts resistance when confronted with deactivating potassium in the flue gas.

2.3 Iron-Copper-based catalysts

2.3.1 Introduction

Studies similar to those reported for vanadium-based catalysts in the previous section have recently also been performed with other oxide catalysts such as copper- [18-22] and iron-based catalysts [19,23,24]. Since the metal oxides of copper and iron mainly possess Lewis acidity [18] they belong to an interesting class of SCR catalysts in principle less sensitive to deactivation of the Brønsted acid sites. The SCR mechanism therefore takes place via different routes, collected in a review by Busca et al. [25]. This strategy was exploited by Kustov et al. [19, 26] who studied the effect of potassium on vanadium, copper and iron oxides supported on sulfated zirconia (monoclinic), where a slight increase in alkali resistance was found using the metal oxides of copper and iron compared to vanadium. However, samples with less or no monoclinic phase of ZrO_2 were not investigated, and sulfation was performed after calcination of zirconia, which has been found to result in less acidic samples than sulfation of the hydroxide $Zr(OH)_2$ [27]. Thus, in continuation of the study of copper and iron oxides on sulfated zirconia, a series of mixed Cu and Fe oxides supported on the best commercial sulfated zirconia support from previous section were investigated in the following.
The catalysts studied in this section consist of iron-copper mixed oxides in different molar ratio, with a constant total metal loading of 364 μmol/g (similar loading as in [19]) and doped with potassium to K/M = 0.4. The optimal support, 3.4SZ_NP, was used in all catalysts.

2.3.2 Results and discussion

The TPD profiles of the iron-copper mixed oxide on sulfated zirconia are collected in Figure 2.5. The fresh catalysts primarily consisting of copper oxide (i.e. samples with the iron mole fraction: X_{Fe} = 0.00-0.33) show roughly a tri-modal desorption profile and a shoulder around 260-290ºC, whereas for the catalysts comprising mainly iron oxides (i.e. X_{Fe} = 0.50-1.00) only two major desorption peaks are observed and the shoulder is disappeared. The first major desorption peak can be attributed to acid sites generated by the copper and iron oxides, considering that only the small peak at 489ºC was present on the TPD profile of 3.4SZ_NP. Moreover, a gradual increase in temperature of desorption is observed with the relative content of iron oxide in the samples, suggesting an increase in the strength of acid sites as iron oxide species displaces copper oxide on the sulfated zirconia. The gradual displacement of CuO with Fe_2O_3 does almost not affect the overall acidity (cf. inset figure in Figure 2.5). The disappearance of the minor peak around 490--520ºC, combined with the small decrease in overall surface acidity when increasing the fraction of iron oxide, could be attributed to physical coverage of acid sites with Fe_2O_3 species. At X_{Fe} = 0, the CuO loading is 3.5 wt% with a corresponding surface density of 2.4 CuO/nm^2, whereas at X_{Fe} = 1, the equimolar concentration of Fe_2O_3 is 7.7 wt%, corresponding to a surface density of 5 FeO_x/nm^2. Although monolayer capacity probably is not reached for either of the pure metal oxide catalysts [28], the coverage of iron species is higher, covering or weakening the acid sites of sulfated zirconia.

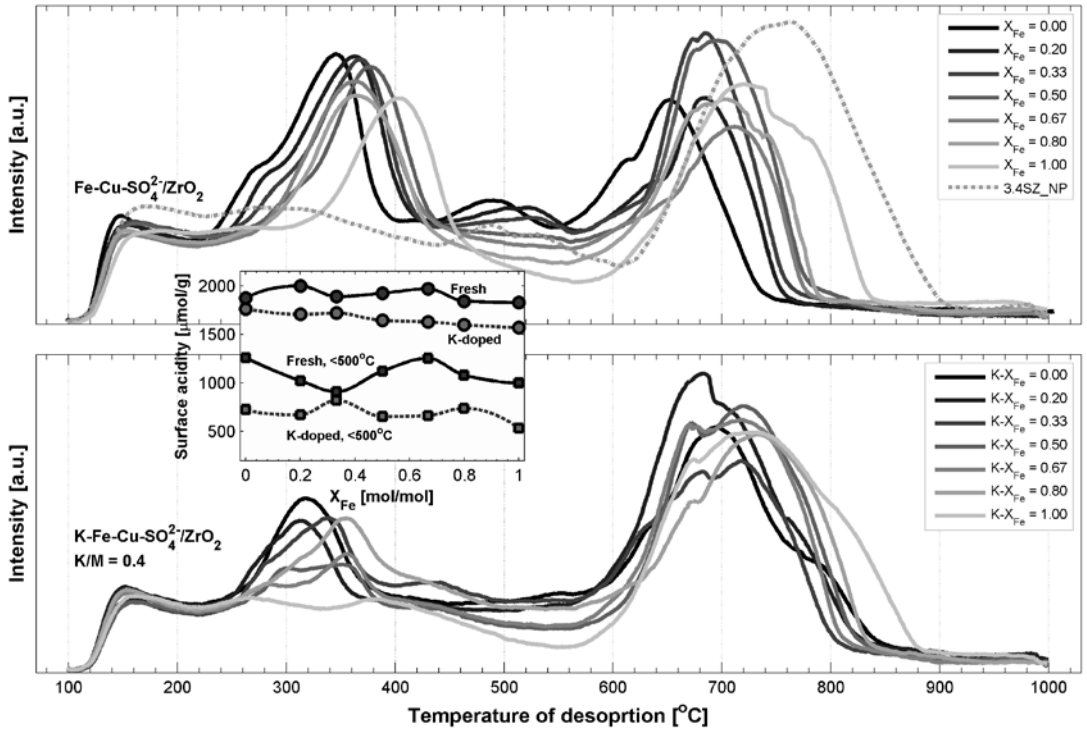

Figure 2.5 NH_3-TPD profiles for fresh iron-copper oxides hybrid catalyst and the pure support material as reference (top) and the corresponding potassium-treated samples (bottom), same scale. Inset figure show the trends in the surface acidity of the Fe-Cu mixed oxide catalysts.

For all the catalysts, the addition of potassium results in a significant reduction in total acidity, in agreement with previous observations [1,19]. Especially the amount of ammonia desorbed at low-temperature peaks around 340-400ºC is reduced considerably, whereas the peaks observed at temperatures above 650ºC does not seem to have changed upon treatment with alkali. This could suggest that the unaffected desorption peak originates from decomposing sulfate. Furthermore, it should be noticed that the desorption-peak around 340-400ºC is shifted towards lower temperatures for the K-treated samples, whereby the acid sites and ammonia adsorption are weakened, presumably due to electron donation from the basic potassium oxide. An interesting behavior in the surface acidity of the K-doped compared to the fresh catalysts is the trend in overall acidity (cf. inset figure in Figure 2.5). Linear fitting of the total surface acidity versus iron mole fraction of the fresh series, reveals an almost constant slope, corresponding to a difference between the pure CuO-based and Fe_2O_3-based catalysts of on 75 µmol/g, whereas the overall decline of the K-treated catalysts show a difference of around 200 µmol/g. In other words, copper oxide catalysts maintain the surface acidity better upon potassium doping than catalysts consisting mainly of iron oxide.

The activity of the Fe-Cu oxide catalysts in the catalytic removal of NO were measured in the temperature range of 25-500ºC. Here, the catalysts based solely on CuO (on sulfated zirconia) is denoted $X_{Fe} = 0.00$, whereas the iron-based catalyst without any copper oxide is denoted $X_{Fe} = 1.00$. In general, the temperature of maximum SCR activity is shifted from 400ºC for the reference catalyst to around 460ºC for the hybrid catalysts, along with a decrease in maximum

activity (data not shown here, c.f. [29]). All the fresh catalysts roughly possess similar SCR activity up to around 440ºC, at which point the SCR activity is decreasing rapidly for catalysts comprising mainly copper oxide (X_{Fe} = 0.00-0.67), whereas the two samples with highest content of iron oxide maintain, or even increase, their high-temperature activity. The shift of the catalytic activity towards higher temperatures for the catalysts with most iron oxide, agrees well with the increase of the overall strength of the acid sites with iron content, as reflected by TPD measurements.

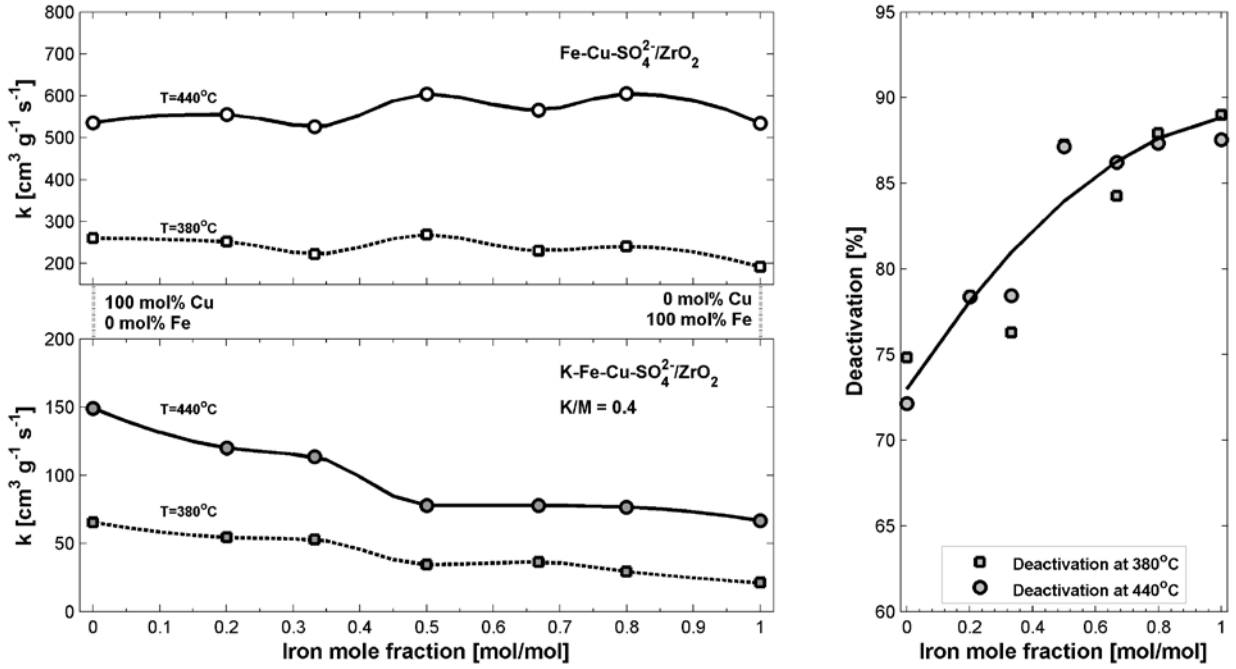

Figure 2.6 Left: interpolated SCR activities of Fe-Cu "alloy" catalysts at 380ºC and 440ºC versus iron loading for fresh hybrid and corresponding K-doped samples. Total metal loading 364 µmol/g (equivalent of 3.5 wt% CuO loading). Right: loss of SCR activity versus Fe-Cu oxide composition at 380ºC and 440ºC.

A significant difference in reversibility of the hybrid catalysts SCR activity was observed upon cooling down from 500ºC. Almost complete reversibility of copper-based catalysts was revealed, whereas the iron-based catalysts exhibit some degree of deactivation after treatment at 500ºC. Thus, the copper-based catalysts are not thermally deactivated at the highest temperatures, and the reversibility suggests that competing reactions to SCR are dominating at higher temperatures. In contrast, the high coverage of Fe_2O_3-species (5 FeO_x/nm^2) compared to CuO, could promote sintering of active centers in close vicinity.

To obtain a clearer trend in the performance of the Fe-Cu series supported on sulfated zirconia, the activities of the fresh and K-doped catalysts at two selected temperatures are compared and presented in Figure 2.6. Based on the interpolated activities[1] at 380 and 440ºC, the activity of the fresh Fe-Cu mixed oxide catalyst at these temperatures is almost constant, regardless of composition, although catalysts containing most iron oxide exhibit slightly higher activity at 440ºC.

[1] The temperature obtained during experiment deviate slightly from set-point, and to obtain comparable values the activities are linear interpolated

However, a different trend is observed when the catalysts have been deactivated with potassium, where it is clear that predominantly the copper oxide-containing catalysts (X_{Fe} = 0.00-0.50) exhibit higher activity than the corresponding iron-samples.

The degree of deactivation through the series, based on the interpolated values, is depicted in Figure 2.6 (right). Here, the catalysts with pure CuO as active component, or a high relative content of copper oxides, display somewhat better alkali resistance than catalysts with increasing content of iron oxide. Compared to the V_2O_5-WO_3-TiO_2 reference catalyst, which deactivated 83% at 360ºC, slightly lower activity loss is observed for the CuO-SO_4^{2-}-ZrO_2 (X_{Fe} = 0.00), deactivating around 75%, whereas the Fe_2O_3- SO_4^{2-}-ZrO_2 is losing almost all SCR activity, around 90%.

For the potassium-treated catalysts, a similar decreasing trend is observed in surface acidity as well as in SCR activity with increasing iron-oxide content (i.e. inset figure in Figure 2.5 and Figure 2.6), suggesting a relationship. Based on TPD observations, the basic potassium is deactivating a higher number of acidic sites on iron-based catalysts than on copper-based. On the pure Fe_2O_3-based catalyst, the potassium treatment resulted in complete removal of the TPD peak at 402ºC on the fresh catalyst. This indicates that potassium is attacking the Lewis sites generated by iron oxides or because of the high surface coverage of iron-oxides, whereby sulfate-generated acid sites are weakened or covered by iron-oxides, unable to effectively host the incident potassium. Furthermore, the presence of the stronger acid site (TPD peak at 489 ºC for X_{Fe} = 0.00), introduced by sulfated zirconia, is likely to appear as a more attractive site for potassium than relatively weaker sites, such as the Lewis sites of the active catalyst.

Finally, only linear behavior were observed in the TPD experiments and SCR activity measurements of the iron-copper mixed oxide series as a function of the molar Cu-Fe content, suggesting that no predominant metal alloys are formed on the catalysts or other symbiotic effects occur.

2.3.3 Concluding remarks

All the catalysts with equimolar copper and iron loadings, a mixture of 3.5 wt% CuO-SO_4^{2-}-ZrO2 and 7.7 wt% Fe_2O_3-SO_4^{2-}-ZrO2, display similar surface acidity, although iron oxides displaces the apparent Brønsted sites (490--520ºC), originating from the sulfated zirconia support. Increasing the molar fraction of iron oxides in the catalysts, is accompanied by a strengthening of the low-temperature acid site, desorbing ammonia around 345-402ºC, which is reflected by the corresponding higher SCR activity of high iron content catalysts (i.e. X_{Fe} = 0.80-1.00) at elevated temperatures (<460ºC).

SCR activities up until ca. 440ºC are almost similar for all fresh catalysts. However, after K-doping it is evident that catalysts comprising mainly copper oxide (X_{Fe} = 0.00-0.50) exhibit higher resistance to potassium-poisoning, which were attributed to the presence of strong acid-sites of the sulfated zirconia. These sites were either covered or chemically weakened by the Fe_2O_3-species at higher iron mole fractions.

Although interesting trends were found in the Fe-Cu mixed oxide catalyst series, the "best" catalyst, namely CuO-SO_4^{2-}-ZrO2, deactivated around 70%, and was thus only marginally more resistant than the 1.7VWT reference catalyst which deactivated 83%.

2.4 CeO_2-ZrO_2 catalysts

2.4.1 Introduction

V_2O_5 supported on WO_3-ZrO_2 or sulphated-ZrO_2 has previously shown to be promising carriers for NO abatement with ammonia in alkali-containing flue gases [1,6,30]. CeO_2 is one of the important additives in three-way catalysts [31]. It provides oxygen storage capability through redox cycling between the trivalent and tetravalent oxidation states of the Ce ions. However, pure ceria is not suitable for the applications due to its high reduction temperature (700^{o}C) and loss of surface area due to sintering. By adding zirconium oxide into ceria, the oxygen storage capacity (OSC) and the thermal stability of CeO_2 are significantly improved. These materials are generally prepared either at low temperature by co-precipitation of the corresponding salts (soft chemical method) or at high temperature by firing the respective oxides together. The former method usually produces relatively pure and homogeneous materials. Depending on Ce/Zr atomic ratio and calcination temperature, three different phases are frequently reported for $Ce_{(1-x)}Zr_xO_2$ solid solutions [32, 33]. Interestingly, the phase composition strongly influences the redox behavior of cerium oxide [34, 35]. The optimum resulting $Ce_{(1-x)}Zr_xO_2$ material facilitate high oxygen storage capacity (OSC), excellent thermal stability, and resistance to sintering.

Many groups have extensively investigated the surface structure of vanadia on various single and mixed-oxide supports in the literature [36, 37]. However, catalytic studies on V_2O_5 supported on ceria-zirconia mixed oxides have not been reported for SCR of NO with NH_3. In this study, CeO_2-ZrO_2 (1:1 mole ratio) and ZrO_2 oxides were prepared by soft chemical routes, impregnated with 3 wt% V_2O_5 and subjected to thermal treatments from 400-600ºC. 3 wt% V_2O_5 is the optimum composition in traditional commercial catalysts as higher content compromises the selectivity to N_2.

2.4.2 Experimental

A $CeO(H)_4$-$Zr(OH)_4$ composite oxide (1:1 mole ratio based on oxides) was prepared by a co-precipitation with dilute ammonium hydroxide. The required amounts of $ZrO(NO_3)_2 \cdot 6H_2O$ and $Ce(NO_3)_3 \cdot 6H_2O$ (Aldrich, 99.9%) were dissolved in water, and the hydroxides were precipitated by drop wise addition of an ammonia solution to maintain the pH at about 9. The precipitate was collected by filtration and dried at 120ºC in air overnight. Pure $Zr(OH)_4$ was also prepared by an analogous procedure. 3 wt% V_2O_5 modified catalysts were prepared by wet impregnation of the $Ce(OH)_4$-$Zr(OH)_4$ or $Zr(OH)_4$ as support material by dissolving the required amount of the precursor ammonium meta-vanadate (Aldrich, 99.999%) in 2 M oxalic acid solution. Each impregnated catalyst was oven dried at 120^{o}C for 12 h followed by calcination at temperatures between 400-600^{o}C for 5 h prior to use.

2.2.4.2.2 NO SCR with ammonia

The SCR activity measurements were carried out at atmospheric pressure in a fixed-bed quartz reactor loaded with 10-20 mg of fractionized (180-300 µm) or 1.7 x 1.7 cm^2 (catalyst late) catalyst samples positioned between two layers of inert quartz wool. The reactant gas composition was adjusted to 1000 ppm NO, 1100 ppm NH_3, 3.5% O_2, 2.3% H_2O and balance N_2 by mixing 1% NO/N_2 (±0.1% abs.), 1% NH_3/N_2 (0.005% abs.), O_2 (≥99.95%) and balance N_2 (≥99.999%) (Air Liquide) using Bronkhorst EL-Flow F-201C/D mass-flow controllers. The total flow rate was maintained at 500 ml/min (ambient conditions). During the experiments the temperature was increased stepwise from 200 to 600ºC while the NO and NH_3 concentrations were continuously monitored by a Thermo Electron's Model 17 C chemiluminiscent NH_3-NO_x gas analyzer. The catalytic activity is represented as the first-order rate constant (cm^3/g·s), since the SCR reaction is known to be first-order with respect to NO under stoichiometric NH_3 conditions [38].

2.4.3 Results and Discussion

The catalytic activity of the V_2O_5/ZrO_2 and V_2O_5/CeO_2-ZrO_2 catalysts was measured in the temperature range 200-460ºC. In Figure 2.7 the catalytic activities obtained are shown as first-order mass based rate constant (cm^3/g.s). The V_2O_5/ZrO_2 catalysts showed increase in activity with increase in calcination temperature from 400 to 600ºC However, the catalysts calcined at 400 and 450ºC were comparable less activity than the other catalysts calcined above 450ºC, due to the low crystallinity of the support. All the catalysts showed maximum activity above 440ºC except the V_2O_5/ZrO2-600 sample. Similar activity profiles were also observed by Kustov et al. [30] in their studies on V_2O_5/ZrO_2 catalysts applicable for alkali-containing NO flue gas treatment, the rate constant vales are comparable with reported V_2O_5/ZrO_2 catalysts (280 cm^3/g·s) [30].

V_2O_5/CeO_2-ZrO_2 catalysts showed higher low-temperature activity compared to V_2O_5/ZrO_2 catalysts, i.e. the temperature window and conversion level were large for the V_2O_5/CeO_2-ZrO_2 samples. The catalytic activities of V_2O_5/CeO_2-ZrO_2 catalysts were found to follow in order: 450ºC>400ºC>500ºC>550ºC>600ºC. The rate constant vales are comparable with highly active V_2O_5/sulphated-ZrO_2 catalysts (430 cm^3/g·s) [30].

The catalytic selectivity was measured in terms of N_2O formation vs. the operating temperature in the range 200-460ºC. The N_2O formation vs. temperature dependencies of the most active V_2O_5/ZrO_2-600 and V_2O_5/CeO_2-ZrO_2-450 catalysts are shown in Figure 2.8.

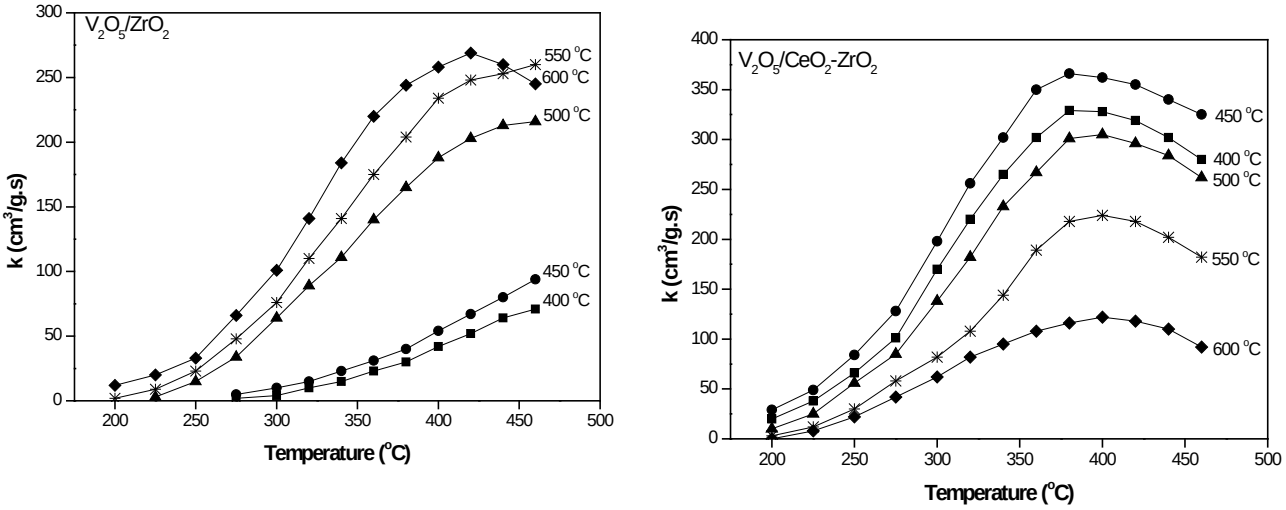

Figure 2.7 Temperature dependency of first-order rate constant profiles for V_2O_5/ZrO_2 and V_2O_5/CeO_2-ZrO_2 catalysts.

Formation of N_2O was observed from 300ºC on the V_2O_5/ZrO_2-600 catalyst and the amount of N_2O increased gradually with temperature up to 105 ppm at 460ºC. In contrast, the V_2O_5/CeO_2-ZrO_2-450 catalyst began producing N_2O only from 380ºC which further removed less than 40 ppm within the operating temperature. This moderate loss in selectivity is due to partial oxidation of NH_3 to N_2O. Composite materials of CeO_2-ZrO_2 are able to decrease the rate of partial oxidation of ammonia even at high temperatures.

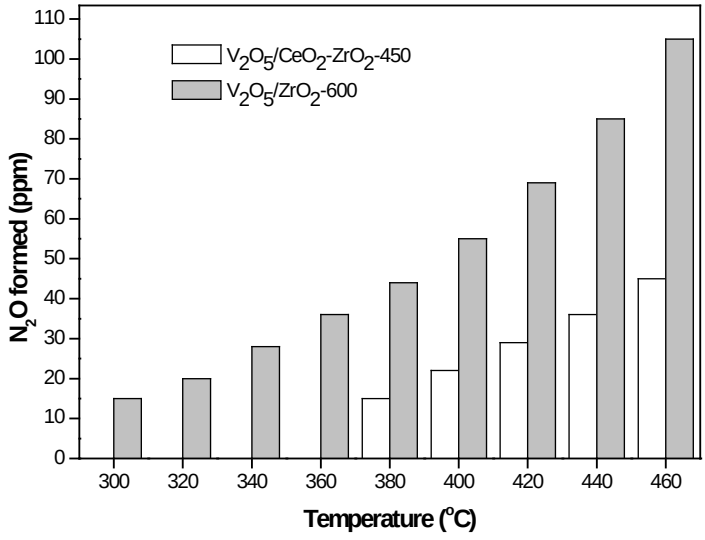

Figure 2.8 N_2O formation profiles of V_2O_5/ZrO_2-600 and V_2O_5/CeO_2-ZrO_2-450 catalysts.

2.4.4 Conclusion

The catalytic behavior of V_2O_5/ZrO_2 and V_2O_5/CeO_2-ZrO_2 catalysts calcined at different temperatures were tested for the reduction of NO with ammonia. The V_2O_5/CeO_2-ZrO_2 catalysts

showed maximum catalytic activity at lower temperatures than the V_2O_5/ZrO_2 catalysts and the catalysts were more selective by being less prone to partial oxidation of ammonia to N_2O.

2.5 References

[1] J. Due-Hansen, S. Boghosian, A. Kustov , P. Fristrup, G. Tsilomelekis, K. Ståhl, C.H. Christensen, R. Fehrmann, J. Catal. 251 (2007) 459-473

[2] C. Morterra, G. Cerrato, F. Pinna, M. Signoretto, J. Catal. 157 (1995) 109–123

[3] M.A. Cortes-Jacome, J.A. Toledo, C. Angeles-Chavez, M. Aguilar, and J.A. Wang, J. Phys. Chem. B, 109 (2005) 22730–22739

[4] J.R. Sohn, M.R. Park, Langmuir 14 (1998) 6140-6145

[5] L. D'Souza, A. Suchopar, K. Zhu, D. Balyozova, M. Devadas, R.M. Richards, Microporous and Mesoporous Materials 88 (2006) 22–30

[6] J. Due-Hansen, A.L. Kustov, S.B. Rasmussen, R. Fehrmann, C.H. Christensen, Appl. Catal. B: Environ. 66 (2006) 161–167

[7] K. Arata, M. Hino, Materials Chemistry and Physics 26 (1990) 213–237

[8] J. Pasel, V. Speer, C. Albrecht, F. Richter, H. Papp, Appl. Catal. B: Environ. 25 (2000) 105–113

[9] B.H. Davis, R.A. Keogh, R. Srinivasan, Catal. Today 20 (1994) 219–256

[10] M.A. Cortes-Jacome, J.A. Toledo, C. Angeles-Chavez, M. Aguilar, J.A. Wang, J. Phys. Chem. B 109 (2005) 22730–22739

[11] C. Morterra, G. Cerrato, F. Pinna, M. Signoretto, J. Catalysis 157 (1995) 109–123

[12] V. Ramaswamy, M. Bhagwat, D. Srinivas, A.V. Ramaswamy, Catal. Today 97 (2004) 63-70.

[13] C.J. Howard, R.J. Hill, J. Mater. Sci. 26 (1991) 127-134.

[14] R. Barthos, F. Lónyi, G. Onyestyák, J. Valyon, Solid State Ionics 141-142 (2001) 253–258.

[15] J.F. Haw, J. Zhang, K. Shimizu, T.N. Venkatraman, D.-P. Luigi, W. Song, D.H. Barich, J.B. Nicholas, J. Am. Chem. Soc. 122 (2000) 12561–12570.

[16] N. Katada, T. Tsubaki, M. Niwa, Appl. Catal. A: Gen. 340 (2008) 76–86.

[17] I.E. Wachs, B.M. Weckhuysen, Appl. Catal. A: Gen. 157 (1997) 67-90.

[18] G. Ramis, L. Yi, G. Busca, M. Turco, E. Kotur, R.J. Willey, J. Catal. 157 (1995) 523–535.

[19] A. Kustov, S. Rasmussen, R. Fehrmann, P. Simonsen, Appl. Catal. B: Environ. 76 (2007) 9–14.

[20] G. Centi, C. Nigro, S. Perathoner, G. Stella, Catal. Today 17 (1993) 159-166.

[21] D. Pietrogiacomi, D. Sannino, S. Tuti, P. Ciambelli, V. Indovina, M. Occhiuzzi, F. Pepe, Appl. Catal. B: Environ. 21 (1999) 141–150.

[22] G. Centi, S. Perathoner, Appl. Catal. A: Gen. 132 (1995) 179-259.

[23] N. Apostolescu, B. Geiger, K. Hizbullah, M. Jan, S. Kureti, D. Reichert, F. Schott, W. Weisweiler, Appl. Catal. B: Environ. 62 (2006) 104–114.

[24] V. Indovina, M. C. Campa, F. Pepe, D. Pietrogiacomi, S. Tuti, Appl. Catal. B: Environ. 60 (2005) 23–31.

[25] G. Busca, L. Lietti, G. Ramis, F. Berti, Appl. Catal. B: Environ. 18 (1998) 1-36.

[26] S.B. Rasmussen, A. Kustov, R. Fehrmann, J. Due-Hansen, Alkali resistant catalysts, patent WO/2008/037255 (2007).

[27] B. Li, R.D. Gonzalez, Ind. Eng. Chem, Res., 35 (1996) 3141–3148.

[28] I.E.Wachs, Catal. Today 27 (1996) 437–455.

[29] J. Due-Hansen, Alternative deNO$_x$ catalysts and technologies, Ph.D. thesis, DTU Chemistry, June 2010.

[30] A.L. Kustov, M.Yu. Kustova, R. Fehrmann, P. Simonsen, Appl. Catal. B 58 (2005) 97.

[31] Y. Li, H. Cheng, D. Li, Y. Qin, Y. Xie, S. Wang, Chem. Comm (2008) 1470.

[32] S. Letichevsky, CA Tellez, R. de Avillez, M.A Fraga, Appl. Catal. B 58 (2005) 203.

[33] C. Bozo, F. Gaillard, N. Guilhaume, Appl. Catal. A 220 (2001) 69.

[34] M.Y. Sinev, G.W. Graham, L.P. Haach, M. Shelef, J. Mater. Res. 11(1996) 1960.

[35] S. Damyanova, B. Pawelec, M.V. Martinez Huerta, J.L.G. Fierro, Appl. Catal. A 337 (2008) 86.

[36] G.C. Bond, S.F. Tahir, Appl. Catal. 71(1991)1

[37] B.M. Reddy, A. Khan, Y.Yamada, T. Kobayashi, J.C. Volta, Langmuir. 19 (2003) 3025.

[38] R.Q. Long, R.T. Yang, J. Catal. 196 (2000) 73.

3. Improvement of V_2O_5/TiO_2 based catalysts

3.1 Introduction

This chapter describes the improvements of the alkali resistivity and overall activity of the traditional deNO$_x$ catalyst. Catalysts used for cleaning flue gasses from NO$_x$ via selective catalytic reduction (SCR) with ammonia are based on anatase (TiO_2) particles with a single monolayer of amorphous V_2O_5 corresponding to a vanadia loading of 3-5 wt%. If the monolayer is exceeded due to high loading, crystalline vanadia will form on the catalyst surface and cause a dramatic drop in activity and unwanted increase in SO_2 and NH_3 oxidation [1]. The efficiency of commercial state-of-the-art catalysts is high when applied to flue gases from fossil fuels like oil and coal. However, use of biomass (straw, wood) alone or as co-fuel is of increasing importance since this type of fuel is considered CO_2 neutral. Unfortunately, the flue gas becomes very poisonous towards the catalyst due to increased content of especially alkaline potassium salts originating from the biomass combustion [2].

One approach to overcome this problem is to improve the overall initial activity of the deNO$_x$ catalyst and thereby prolong the catalyst lifetime. This can be achieved by preparation of nano-sized particles with much higher surface area that can accommodate much higher vanadium loadings. Sulfation of the catalyst is also increasing the alkali resistivity by binding the potassium species. A third option is to choose other kinds of active metals e.g. copper and iron that is more resistant to deactivation. In the present work, very active deNO$_x$ catalysts based on anatase nano-particles containing up to 25wt% V_2O_5 were synthesized [3]. The catalysts were tested for SCR deNO$_x$ activity and compared to a state-of-the-art commercial catalyst. The method was further demonstrated on other supported oxide systems with V_2O_5, Fe_2O_3 and CuO as the active monolayer phases on anatase [4]. The formation of N_2O by side reactions using a SCR catalyst is also a new concern, because the N_2O have been classified as a greenhouse gas. Current commercial catalysts are not very selective and are producing small but considerable amounts of N_2O. As mentioned earlier the use of biomass is increasing demanding higher alkaline resistance ensuring long term SCR activity [5; 6]. This calls for new and more active and selective deNO$_x$ catalysts [2].

3.2 Experimental

Vanadia/anatase catalysts were prepared by hydrolysis of an acetous ethanol solution containing titanium(IV) isopropoxide (97%, Lancaster) and vanadium(V) oxytriethoxide (95%, Aldrich) with an aqueous solution of ammonium nitrate (99.0%, Aldrich) or ammonium chloride (99.5%, Fluka) forming solid seeds. In a typical preparation the $Ti(OC_3H_7)_4$, $VO(OC_2H_5)_3$ and acetic acid mixture was first diluted in absolute ethanol and then cooled to 0◦C in an ice bath. The aqueous ammonium salt (NH_4NO_3 or NH_4Cl) solution was then added drop wise to the ethanolic solution under magnetic stirring to form a sol-gel. The molar ratio of the reactants was adjusted to Ti:V:acetic acid:water:ethanol:ammonium salt = 1:x:2:15:30:2, where x was varied according to the desired amount of vanadium required to obtain catalysts with vanadia loading between 0-25 wt%. Subsequently, the sol-gel was aged at room temperature for 48 hours under stirring, in some cases sulfuric acid were added to sulfate the titania and simultaneous remove acetic acid by esterfication. Then excess ethanol, water, acetic acid and liberated isopropanol were removed under reduced

pressure (12 mbar, 70ºC). Finally the remaining powder was calcined at 380ºC in an air stream (300 mL min^{-1}) to decompose the ammonium template and convert amorphous titania into crystalline anatase. The calcination temperature was chosen to match normal maximum operating temperature of the SCR unit in a power plant.

The iron and copper containing catalysts were prepared in the same way just instead of adding vanadium(V) oxytriethoxide a strong ethanol solution of the metal precursor was used (Iron(III) acetyl acetonate or Copper(II) acetate monohydrate). Potassium poisoning was done by incipient wetness, doping the catalysts using an aqueous solution of KNO_3 (99%, Riedel-de Haën). After the impregnation the sample was dried for 1 h at 100ºC and calcined at 300ºC for 2h. This allowed the KNO_3 to decompose and form K_2O, which was deposited on the surface of the catalyst now. This is a well-known and frequently used way of alkaline poisoning catalysts [8; 9].

BET surface areas of samples were determined by physical adsorption of nitrogen using a Micromeritics ASAP 2020 analyzer. XRPD diffractograms were obtained by collecting data for 30 minutes with a Huber Guinier G670 camera at 25°C using CuK_α radiation. FT-IR spectra were recorded of pressed wafers of 1 mg of sample mixed with 100 mg KBr using a Perkin-Elmer 1710 Infrared Fourier Transform Spectrophotometer. The spectra were measured in air at room temperature using 30 scans.

NO-SCR reactions were performed with 50 mg fractionized (180-295 μm) samples containing 2-10 mg catalysts diluted in silica. The flue gas consisted of 1000 ppm NO, 1100 ppm NH_3 and 9% O_2 (balanced with He) at a total flow of 280 ml min^{-1}. Catalyst performance (as the first-order rate constant k) was obtained from measuring gas outlet concentrations of NH_3 and NO (λ = 201 and 226 nm) by UV-Vis and N_2O by gas chromatography, at NO conversions <80%.

3.3 Catalytic activity

From the BET surface measurements (see table 3.1) it can be concluded that the sulfation has a positive effect on the surface area and the acidity also increased. This can explain the additional activity by sulfation. Crystal size were following the same trend but adding iron and copper has an additional positive effect on the crystallite size.

Table 3.1 BET surface area, Crystallite size calculated from XRPD, Acidity calculated from NH3 TPD measurements, Loading is calculated from active metal content and BET surface area.

Catalyst	**BET [m^2/g]**	**Crystal size [nm]**	**Desorbed NH_3 [cm^3/g]**	**Acidity [molecules/mn^2]**	**Loading [AM atoms/nm^2]**
15 wt% V_2O_5/TiO_2, sulfated	159	6.1	71	10.9	6.23
15 wt% V_2O_5/TiO_2	127	7.9	22.39	4.2	7.82
4 wt% CuO/TiO_2, sulfated	219	5.6	80	8.9	1.38
3 wt% Fe_2O_3/TiO_2, sulfated	177	5.2	59	8.1	1.28

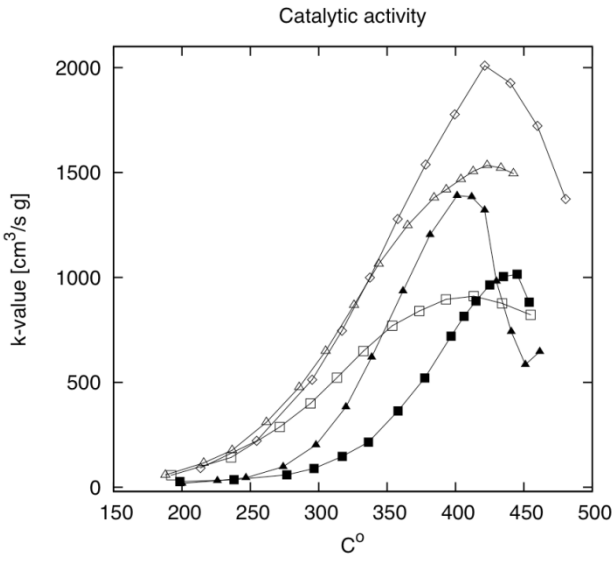

Figure 3.1 Catalyst activity (as a rate constant k) as function of reaction temperature of (◊) 15 wt. V_2O_5/TiO_2 sulfated, (△) 15 wt % V_2O_5/TiO_2 unsulfated, (■) 4 wt % CuO/TiO_2 sulfated, (▲) 3% Fe_2O_3/TiO_2 sulfated, (□) commercial ref. catalyst. (3 wt% V_2O_5, 10 wt% WO_3 on TiO_2)

All the new nano deNO$_x$ catalysts showed remarkable SCR activity, as can be seen from the plot of catalyst activity vs. temperature. Catalysts containing vanadium showed the highest activity with an optimal catalyst loading of 15 wt. % vanadium for either sulfated or unsulfated samples. Comparing with the state-of-the-art commercial catalyst the sulfated V_2O_5/TiO_2 catalyst is 2.3 times as active at 400ºC. Catalysts containing iron and copper also show very high activities, exceeding the activity of the commercial catalyst. Looking at the activities it is clear that the initial activity is much higher than a conventional catalyst and the lifetime in a poisonous biomass flue gas should also be longer. But the alkali resistivity has to be tested to prove this. All the catalysts in figure 3.1 have been optimized regarding the active metal content and maximum activity.

In order to investigate the alkaline resistivity all the catalysts was impregnated with 1 wt% KNO_3. From figure 3.2 it is clear that the catalyst suffering the worst deactivation was the commercial deNO$_x$ catalyst, having an activity of only 22% of the original at 400ºC. The unsulfated V_2O_5/TiO_2 catalyst also suffered high deactivation ending with an activity of 41% of the original. But the starting point was much higher so compared with the commercial catalyst the deactivated catalyst activity at 400ºC was 3 times as high. This shows that the high loading of vanadium must yield many active sites, hence a lower deactivation pr. g of potassium compared to the commercial catalyst.

Despite the low active metal oxide content of the iron based catalyst it only suffered a medium activity loss ending up at 49% of the start activity having a 2.5 times as good activity as the commercial catalyst at 400ºC. The best results were obtained by the sulfated titania vanadia catalysts and the copper titania catalyst. These catalysts had an activity of 75% of the fresh catalyst, which is up to 7 times the commercial catalysts activity. This shows clearly that the sulfation of catalysts is enhancing the potassium resistance, and that a high loading of vanadium is also leading

to higher resistance. By combining the two strategies, a very high potassium tolerance is achieved. But the copper catalyst showed also very high activities, as mentioned earlier this system has been proven before to be very alkaline resistant due to the Lewis acidity nature of copper sites [8]. Kustov et al. have also shown that surface sulfate groups represent attractive sites for hosting potassium oxide leading to lower deactivation [9].

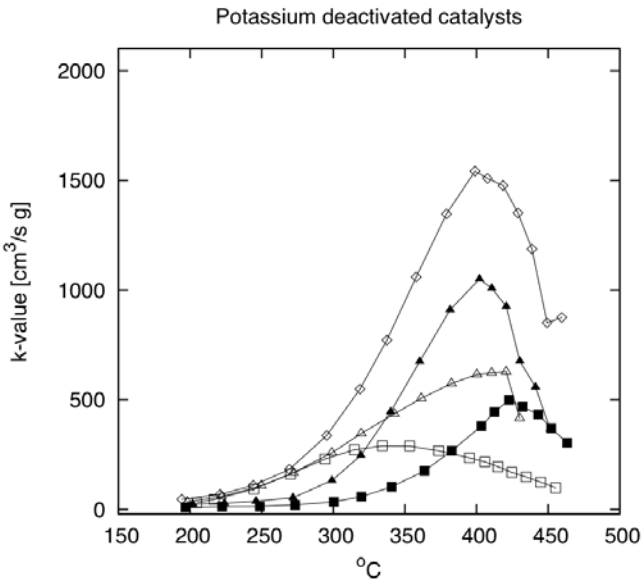

Figure 3.2 Catalyst activity (as a rate constant k) as function of reaction temperature of potassium deactivated catalysts all containing 1 wt % KNO_3 (◇) 15 wt. V_2O_5/TiO_2 sulfated, (△) 15 wt % V_2O_5/TiO_2 unsulfated, (■) 4 wt % CuO/TiO_2 sulfated, (▲) 3% Fe_2O_3/TiO_2 sulfated, (□) commercial ref. catalyst. (3 wt% V_2O_5, 10 wt% WO_3 on TiO_2) [7].

As mentioned earlier the production of N_2O is unfavorable due to various reasons, and it has been shown that normal SCR catalysts to some extent are producing N_2O [10]. Thus selectivity measurements have been performed on every of the 7 catalysts doped with and without potassium. These measurements are done in dry conditions, because water is suppressing the formation of N_2O under good detection levels. Formation of N_2O is reduced by over 90% in wet conditions [11] and because the catalysts are performing equally better under wet conditions they can be compared under dry conditions. Even though the formation of N_2O is vastly reduced in wet conditions, it is still a major concern because of the massive amounts of flue gas.

Looking at figure 3.3 it is obvious that the NO selectivity is the same for all the titanium vanadium based catalysts except small deviations. The sulfated V_2O_5/TiO_2 is performing better than the commercial and nonsulfated catalyst. NH_3 selectivity is also higher for the sulfated catalyst and again better than the commercial catalyst. Both the copper oxide and iron oxide based catalyst is almost 100% selective in conversion of NO. So if the formation of N_2O is a big issue an iron or copper based nano catalyst is the catalyst of choice.

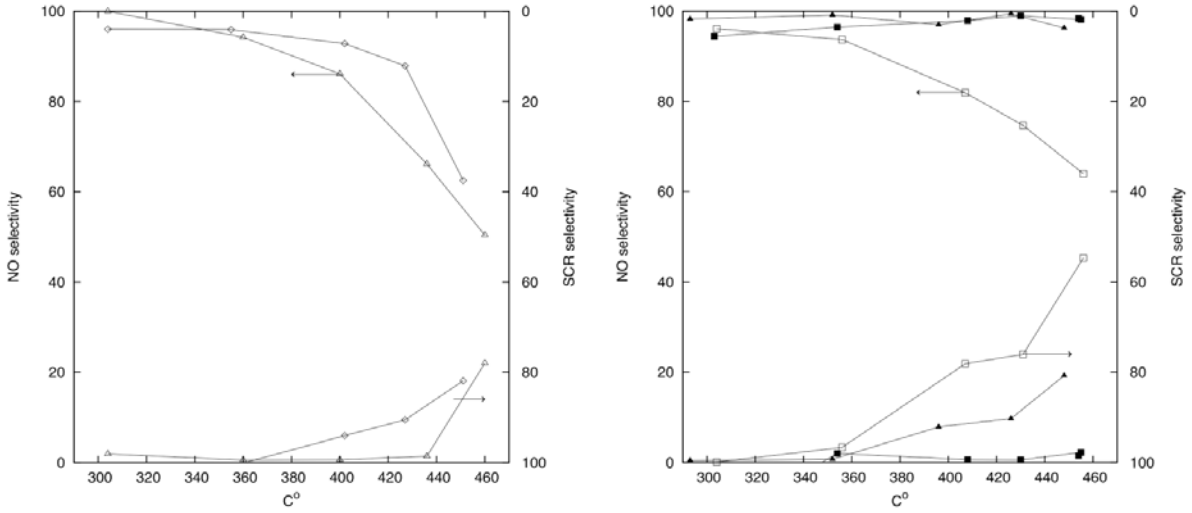

Figure 3.3 A SCR and NO selectivity comparison between (◊) 15 wt. V_2O_5/TiO_2 sulfated, (△) 15 wt % V_2O_5/TiO_2 unsulfated, (■) 4 wt % CuO/TiO_2 sulfated, (▲) 3% Fe_2O_3/TiO_2 sulfated, (□) commercial ref. catalyst. (3 wt% V_2O_5, 10 wt% WO_3 on TiO_2) in dry environment [7].

3.4 In situ FTIR investigation of the active sites on the 15 wt%-V_2O_5/TiO_2 –SO_4^{2-}

NH_3-TPD showed that the acidity with respect to the specific surface area was increased roughly by a factor of 2.5 upon sulfation, whereas the peak activity of the catalyst increased by a factor of 1.4 [12]. The alkali resistance was increased significantly upon sulfation. It is well known that performance of various metaloxide-based deNO$_x$ catalysts is increased by sulfation [13,14]. But the underlying mechanisms are poorly understood, and the more precise roles of the sulfates have so far only been of little interest. Various models based on IR spectroscopy have been proposed in the last three decades [15-24]. But interpretation of these spectra is rather complex and has developed into a controversial subject in the catalytic and surface science communities. The main side of the controversy is to establish whether the sulfates forms bi- or tridentate species. Good arguments for both types of species have been presented over time, and the discussion has been complicated as the spectra are very moisture and temperature sensitive and changes completely when going from ambient conditions to typical catalyst working conditions [15,21]. For a long period of time the majority of authors thought that sulfates were best understood through bidentate species, as the tridentate species would require penta-coordination of the sulfate [15-19].

In the last decade the availability to powerful computers has assisted in the understanding on how to interpret these spectra of sulfated metal oxides, through DFT calculations, though most studies have been conducted for sulfated zirconia and not for titania [23,24-28]. In these studies it has become clear the tridentate species in general give a much better agreement with the actual sulfated metal oxide surfaces. Today there is an overwhelming proof for the tridentate species [20-22, 25-28] although the bidentate species exists on some metal oxide surfaces e.g. the zirconia (001) surface [28]. The species involves a free S=O bond whereas the other S-O bonds are in between an double and a single bond [25,26,28].

Also the acidity of the metal oxides is still a debated subject. Even though it has been suggested that the acidity can be understood barely as supported sulfuric acid species [23, 24], Most authors agree that the acidity arises from the inducing effect of the sulfates, which means that if bases react with adjacent acidic sites adjacent to the sulfate, the sulfates stabilize the bond between the acidic surface site and the incoming base [15, 16, 19, 26]. Thereby the sulfate itself is not the actual acid site but instead it generates strong acidity in the surrounding surface environment. But this effect also arises from the creation of surface defects introduced by the sulfates. Several theoretical independent studies show that sulfation creates oxygen vacancies on zirconia, which gives the possibility of highly acidic under coordinated surface metal centers [25-28]. This theory has experimentally been supported for zirconia [29,30] and anatase as well [31,32]. This oxygen vacancy would allow the surface titanium centers to maintain coordination 5 even though sulfate is directly coordinated to the titanium sites, generating strong Lewis acidity – se figure 3.4. As shown in [26] water adsorbed at a site of this type will exhibit rather strong Brønsted acidity.

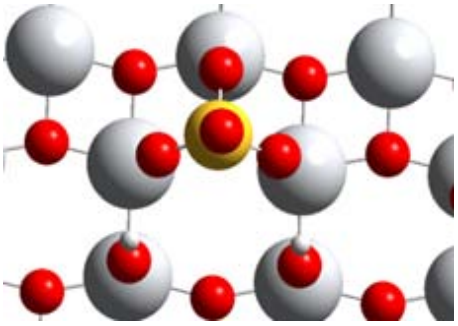

Figure 3.4 A cut out of the assumed environment around the sulfate site on the (101) top layer of the sulfated anatase. The assumption of an oxygen vacancy analogous to the zirconia system will result in 3 strong Lewis acidic 5-coordinated titanium atoms [12]. Red: Oxygen, White: Titanium, Yellow: Sulfur.

We have performed a thorough in situ FTIR investigation of the V_2O_5/TiO_2 and V_2O_5/TiO_2 $-SO_4^{2-}$ at realistic operation conditions (350°C) as well as pyridine adsorption experiments at 200 and 300°C. These studies provide a new understanding on how the sulfates generate new SCR active species as well as spectators in the mechanism [12]. Though the V_2O_5 species only has poor IR activity the great mechanistic insight could be obtained by monitoring the tridentate sulfates species, and their interaction with ammonia and water. The tridentate species has a strong S=O stretching band at 1400-1360 cm^{-1} which is strongly pertubated by the presence of bases such as ammonia or water absorbed adjacent to the sulfate species. The in situ experiments were performed at 350°C in dry and wet gas (3 vol% H_2O), respectively. In each series of experiments spectra in three gas mixtures:

- Oxidizing gas: 1000 ppm NO, 3% O_2 in helium
- Diluted ammonia: 1100 ppm NH_3 in helium
- SCR gas: 1100 ppm NH_3, 1000 ppm NO, 3% O_2 in helium

By careful comparison of these spectra several conclusions could be reached: The ammonia coordinated strongly to the Ti sites around the sulfate. The majority of this strongly bound ammonia was not able to be activated by an adjacent redox site, and this ammonia signal was constant when switching to SCR gas after saturation with NH_3. Only weaker coordinated ammonia seemed to be able to be activated. By saturation with ammonia a small fraction of the S=O at 1374 cm^{-1} band shifted down to 1326 cm^{-1}, which suggests that the most or all Ti sites around these sulfate species was saturated with ammonia. When switching to SCR gas this band disappeared together with some of the signal from the weaker Lewis coordinated ammonia, suggesting that this kind of ammonia could be activated and thereby take place in the reduction of NO. This weakening of the strength of the acidic Ti sites around the highly saturated sulfates could be explained by the formation of a relative short-lived monodentate sulfate complex, lowering the barrier for ammonia activation, as shown in figure 3.5(a) [12, 25].

From FTIR spectra obtained of the catalysts saturated with pyridine in dry gas, it was observed that a significant amount of new Brønsted acidic sites were generated upon sulfation [12]. Even though the resolution in the OH stretching region was poor, these sites are probably acidic Ti-OH group analogous to the similar and well descried ZrO_2-SO_4^{2-} system [25,26,28]. This was consistent with a significant increase in the NH_4^+ signal in situ, when saturating with ammonia. But quite surprisingly these sites could be assigned as spectator sites as the NH_4^+ signal was constant when switching to SCR gas. An example of this kind of site is shown in figure 3.5(b), as a terminal hydroxyl.

If water is introduced to the gas mixture the S=O stretching frequency drops to 1289 cm^{-1} suggesting formation of a monodentate sulfate complex, stabilized by hydrogen bonding to three coordinating water molecules around it [12, 25]. Along with this inversion of the sulfate species, the formation of new Brønsted acidic sites were observed through a significant increase in the intensity of the band due to NH_4^+ species upon saturation with NH_3. The intensity of the NH_4^+ band decreased significant when switching to the SCR gas suggesting that these species were a new type of active Brønsted sites of the type $Ti_4SO_4(H_2O)_3$ (see figure 3.5(c)). There was the same drop in the signal from the weaker coordinated ammonia when switching from 1100 ppm NH_3 to the SCR gas mixture, which analogous to the experiment without water, suggests a new type of active Lewis acidic Ti in the presence of sulfates. But the peak at 1326 cm^{-1} that was interpreted as monodentate $Ti_4SO_4(NH_3)_3$ (see fig. 5 (a)) was not identified. One explanation could be that one water ligand in the $Ti_4SO_4(H_2O)_3$ complex could be exchanged by ammonia, long enough to activate the ammonia – se figure 3.5(d).

Because of the weak and broad nature of the IR signals arising from V_2O_5 a complete mechanistic picture cannot be drawn from this study. But evaluating the mechanism in terms of a dual site mechanism where the acid site and redox sites are two adjacent but relatively independent sites, the study suggests new types of catalytic active sites [14, 33]. The actual intermediate of the SCR reaction is today proposed through a nitrosamide intermediate [34-38]. In the case of a Lewis acidic ammonia adsorption, the activation of ammonia starts by abstraction of a hydrogen atom to a bridging V-O species [38]. The electron can be transferred through the conduction band of the anatase to the vanadium oxide [39]. The odd electron is transferred to the vanadium thereby reducing vanadium from oxidation state +5 to +4 [34, 39]. The formed amide radical reacts with

gaseous NO and forms the nitrosamide intermediate [34,35,37,38]. The nitrosamide intermediate is thereafter catalytically decomposed on the vanadium site[35]. A thorough review and discussion on resent literature in the SCR mechanism can be found in [12], with further arguments for the chosen interpretation the SCR mechanism.

a

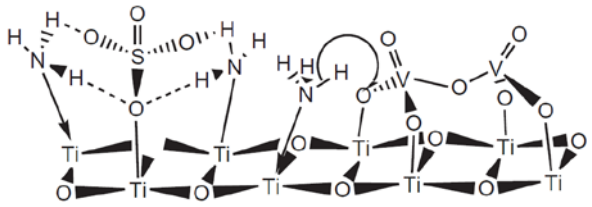

Active Lewis acid site – dry gas

b

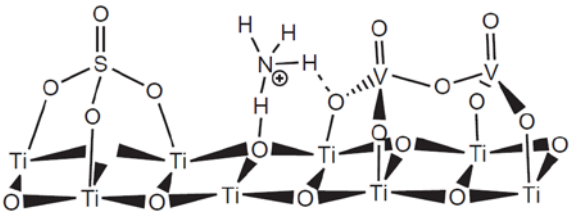

Spectator Brønsted acid site – dry gas

c

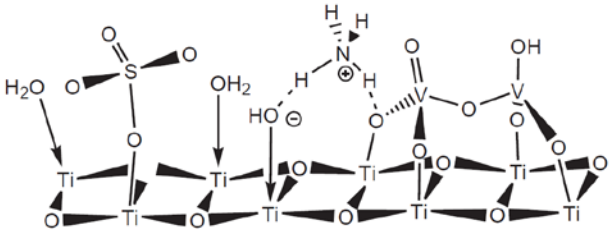

Active Brønsted acidic complex – wet gas

d

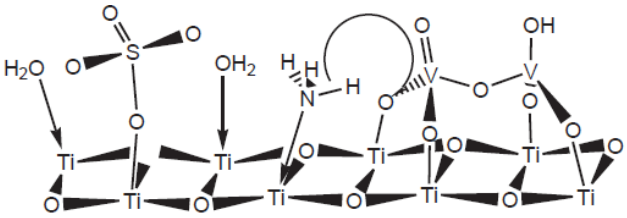

Active Lewis acid site – wet gas

Figure 3.5 Suggested new types of acidic sites. a) short-lived complexation between sulfate, possible in monodentate form, and ammonia molecules generates active acid site. b) according to [25] new types of M-OH are formed by sulfation, these where seen with in situ experiment and by pyridine adsorption, but was not active. c) stable sulfate-water complex formed in wet gas was active Brønsted acidic site. d) [12]

3.4.1 In situ FTIR investigation of potassium poisoning

The previous described catalysts poisoned with 1 wt% K_2O were also investigated with in situ FT-IR. First of all it was obvious that a lot of the acidic surface sites as expected were poisoned which was indicated by a significant loss of intensity of the signals from ammonia and ammonium on the surface at saturation with ammonia. Further it was clear that the acidic sites involving sulfate was heavily poisoned. The S=O stretch found at 1374 cm^{-1} was shifted downwards to 1296 cm^{-1}. This was investigated through two hypothesis': In the first it was assumed that the potassium oxide

attacked the sulfates and formed a type of bidentate potassium sulfate, se figure 3.6(a). This structure was simulated using DFT and the vibration frequencies were calculated. The S=O stretching frequency should be located at 1273 cm^{-1} and 1146 cm^{-1}. The stretch at 1146 cm^{-1} could not be identified possibly due to overlap with a broad intense band originating from S-O stretching. The second band at 1273 cm^{-1} has some similarity to the band at 1296 cm^{-1}. A second hypothesis could be that the potassium oxide attacked the Lewis acidic Ti sites adjacent to the sulfates as demonstrated in the three schemes in figure 3.6(b). The shift of the S=O stretch is almost identical to the shift observed on the fresh catalyst in the presence of water vapor. This shift was, based on DFT calculations in [25], interpreted as the inversion from tridentate sulfate into a monodentate species. Therefore it seems likely that the main sites of the attack are on those Lewis acidic sites, which are also thought to be the most acidic [15-17, 19, 26]. This theory could explain the well known "protecting effect" of sulfates towards alkali poisoning of metal oxide SCR catalysts. But this would also mean that the sulfates would be significantly destabilized, a phenomenon previously described in the literature [40].

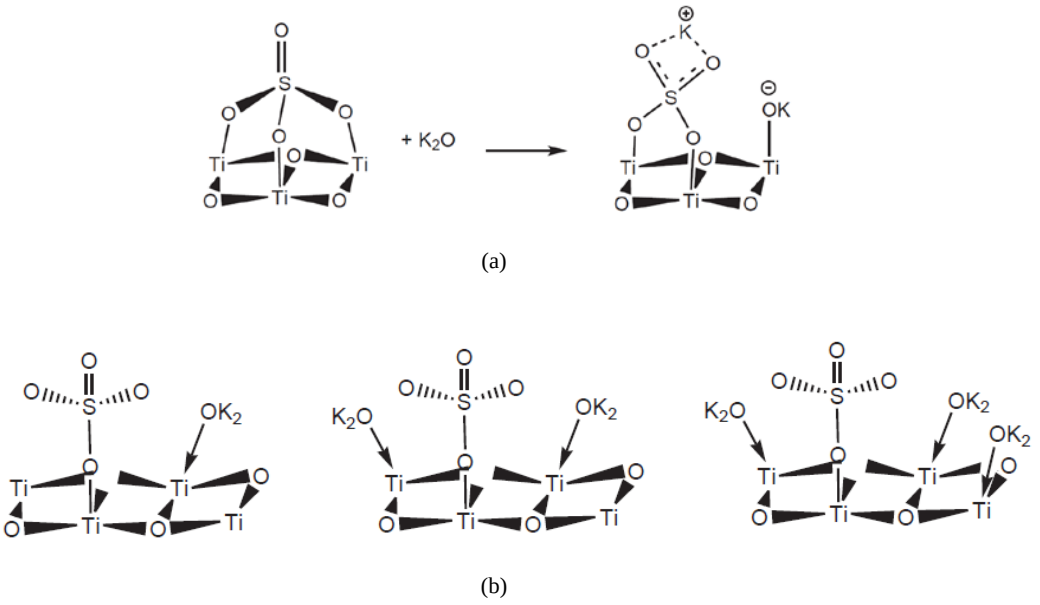

(a)

(b)

Figure 3.6 Schematic representation of two possible ways that the potassium could interact with the acidic sulfate sites: (a) formation of a potassium sulfates surface species (b) Coordination to the acidic titanium atoms around the sulfate species, thereby the sulfate is forced into a monodentate configuration [12].

3.5 Conclusion

A new type of highly active nano particle based SCR catalysts has been synthesized. The sol-gel synthesis showed great potential for nano-catalyst preparation indicated by the catalytic activity, XRPD and BET measurements. The catalysts did not only show high SCR activity but also high selectivity for a large range of V-loadings. Thus new regulations towards N_2O emissions might also make these catalysts very interesting alternatives to the current commercial SCR catalyst.

Comparing the potassium resistance with state of the art commercial catalysts, the advance of having a high surface area acidic catalyst was shown. With new and stricter CO_2

regulations the use of biomass will increase and the demand for such catalysts with higher potassium resistance will undoubtedly increase.

3.6 References

[1] G. Busca, L. Lietti, G. Ramis, F. Berti, Appl. Catal. B: Environ. 18 (1998) 1-36.
[2] H. Kamata, K. Takahashi, C.I. Odenbrand, J. Mol. Catal. A: Chem 139 (1999) 189-198.
[3] A.J. Kruse, S.B. Kristensen, A. Riisager, S.B. Rasmussen, R. Fehrmann, J. Mater. Sci. 44 (2009) 323.
[4] R. Fehrmann, A. Riisager, S.B. Rasmussen, S.B. Kristensen and A.J. Kunov-Kruse, Patent application 08169238.6-2104, 2008 (DTU).
[5] Y. Zheng, A. D. Jensen, J. E. Johnsson, Appl. Catal. B 60 (2005) 253–264.
[6] P. Overgaard, K. Wieck-Hansen, O. Larsen, Biomass Bioenergy 19 (2000) 395–409.
[7] S. B. Kristensen, Kandidat speciale, Nano deNOx calysts, 2009
[8] A. Kustov, S.B. Rasmussen, R. Fehrmann, P. Simonsen, Appl. Catal. B 76 (2007) 9–14.
[9] H. Kamata, K. Takahashi, C.I. Odenbrand, J. Mol. Catal. A: Chem. 76 (2007) 9–14.
[10] M. Gutierrez, D. Baxter, C. Hunter, K. Svoboda, Waste Manage. Res. 23 (2005) 133–147.
[11] B.L. Duffy, H.E. Curry-Hyde, N.W. Cant, P.F. Nelson, J. Phys. Chem. 98 (1994) 7153–7161.
[12] A.J. Kunov-Kruse, Marsterthesis, Department of Chemistry of DTU feburay 2010, "Synthesis and Spectroscopic Characterization of Sulfated Metaloxide SCR Catalysts"
[13]J. Due-Hansen, S. Boghosian, A. Kustov, P. Fristrup, G. Tsilomelekis, K. Stahl, C. Christensen, R. Fehrmann, J. Catal 251 (2007) 259.
[14]I. Wachs, G. Deo, B. Weckhuysen, A. Andreini, M. Vuurman, M. de Boer, M. Amiridis, J. Catal. 161 (1996) 211.
[15] M. Hino, K. Arata, Chem. Comm. 18 (1980) 851.
[16] M. Hino, K. Arata, Mater. Chem. Phys. 26 (1990) 213.
[17] J. R. Sohn, Ind. Eng. Chem. 10 (2004) 1.
[18] C. Morterra, G. Cerrato, E.F. Pinna, M. Signoretto, J. Catal 157 (1995) 109.
[19] J. Sohn, H. Kim, J. Mol. Catal. 52 (1989) 361.
[20] O .Saur, M. Bensitel, A.M. Saad, J. Lavalley, C. Tripp, B.A. Morrow, J. Catal. 99 (1986) 104.
[21] M. Bensitel, O. Saur, J. Lavalley, B.A. Morrow, Mater. Chem. Phys. 19 (1988) 141.
[22] M. Waqif, J. Bachelier, O. Saur, J. Lavalley, J. Mol. Catal. 72 (1992) 127.
[23] F. Babou, B. Bigot, P. Sautet, J. Phys. Chem. 97(1993) 11501.
[24] F. Babou, G. Coudurier, J. Vedine, J. Catal. 152 (1995) 341.
[25] A. Hofmann, J. Sauer, J. Phys. Chem. B 108 (2004) 14652.
[26] T. Kanougi, T. Atoguchi, S.Yao, J. Mol. Catal. A: Chem. 177 (2002) 289.
[27] K. Meinel, A. Hofmann, S. Förster, R. Kulla, K.-M Schindler, H. Neddermeyer, J. Sauer, W. Widdra, Phys. Chem. Chem. Phys. 8 (2006) 1593.
[28] F. Hasse, J. Sauer, J. Am. Chem. Soc. 120 (1998) 13512.
[29] I. Bobricheva, I. Stavitsky, V Yermolaev, V. Shamchkova, D. Kochubey, Catal. Lett 56 (1998) 23.
[30] H. Liu, L. Feng, X. Zhang, Q. Xue, J. Phys. Chem. B 99 (1995) 332.
[31] G. Colón, J. Sánches-España, M. Hidalgo, J. Navío, J. Photochem. Photobiol. A 179(2006) 20.
[32] R. Kun, S. Tarján, A. Oszkó, T. Seemann, V. Zöllmer, M. Busse, I. Dékány, J. Solid State Chem. 182 (2009) 3076.
[33] J. Dumesic, N. Topsøe, H. Topsøe, Y. Chen, T. Slabiak, J. Catal 163(1996)
15679.
[34] G. Ramis, G. Busca, F. Bregani, P. Forzatti, Appl. catal. 64 (1990) 259.
[35] M. Anstrom, N. Topsøe, J. Dumesic, J. Catal. 213 (2003) 115.
[36] S. Soyer, A. Uzun, S. Senkan, I. Onal, Catal. Today 118 (2006) 268.
[37] F. Gilardoni, J. Weber, A. Baiker, J. Phys. Chem. 101 (1997) 6069.
[38] F. Gilardoni, J. Weber, A. Baiker,. Int. J. Quantum Chem. 61(1997) 683.
[39] M. Calatayud, C. Minot, J. Phys. Chem. B 108 (2004) 15679.
[40] A. Kustov, M. Kustova, R. Fehrmann, P. Simonsen, Appl. Catal. B 58 (2005) 97.

4. Heteropoly acid promoted SCR catalysts

4.1 Introduction

Heteropoly acids (HPAs) and salts are a class of compounds that have attracted much scientific interest. Because of their unique structure and the resulting acidic and redox properties, they have been studied as possible catalysts for a variety of reactions [1-5]. Catalysis by HPAs is at the forefront of fundamental and applied catalysis [1-5]. Most typical Keggin HPAs such as $H_3PW_{12}O_{40}$, $H_4SiW_{12}O_{40}$ and $H_3PMo_{12}O_{40}$ are commercially available. HPAs possess stronger (Brønsted) acidity than conventional solid acid catalysts such as acidic oxides and zeolites. The acid strength of Keggin HPAs decreases in the order: $H_3PW_{12}O_{40}$ >$H_4SiW_{12}O_{40}$ >$H_3PMo_{12}O_{40}$ >$H_4SiMo_{12}O_{40}$ [5].

It has been found that the 12-tungstophosphoric acid (TPA) effectively can absorb NO at flue gas temperatures, and upon rapid heating, the absorbed NO is effectively decomposed into N_2 [6, 7]. The results showed that the quantities of NO_2 abstracted from the gas phase follow the order $H_3PW_{12}O_{40}$ >$H_4SiW_{12}O_{40}$ >$H_3PMo_{12}O_{40}$ and the quantity of NO_2 retained on HPA is strongly dependent on temperature, reaching a maximum in the range from 423 to 573 K, and decreases to small values from 773 to 873 K. Supplementary experiments showed that the maximum quantity of NO taken up by the solid is approximately equal to those of NO_2 [7]. Later Pt/TPA and TPA supported metal oxides were also used extensively for the abatement of NO_x majorly, for mobile applications [8, 9]. Recently, Pd was loaded on dispersed $H_3PW_{12}O_{40}$ (TPA) on SiO_2, and the catalyst was applied for selective reduction of NO with aromatic hydrocarbons in stationary applications. The catalyst exhibited high SCR activity when branched aromatic hydrocarbons, such as toluene and xylene, were used as reductants [10,11].

Several authors [12-14] have reported the deactivation effect of alkaline metals on the activity of V_2O_5/TiO_2 catalysts for biomass fired applications in power plants. Most of them conclude that poisonous additives (e.g. potassium, barium) are affecting the Brønsted acid sites, which are responsible for the ammonia adsorption, thus decreasing both their number and activity in NO reduction. One of the possible ways to increase catalyst resistance to alkaline poisons is the use of supports, revealing high or super-acidic properties which would interact stronger with alkali than vanadium species. Such super-acidic characteristics are available in heteropoly acids [15].

In the present work, the promotional effect and alkali resistance of heteropoly acid supported TiO_2 with 3 wt% V_2O_5, Cu and Fe as the active materials on the activity of the SCR reaction with NH_3 as a reducing agent were studied. The influence of potassium oxide additives on the activity was also studied and compared with unpromoted SCR catalysts. All the catalysts were characterized by various techniques to allow detailed discussion of the compositional effects on the SCR performance.

4.2 Experimental

TiO_2 anatase-supported heteropoly acids $H_3PW_{12}O_{40}$ (TPA), $H_4SiW_{12}O_{40}$ (TSiA), and $H_3PMo_{12}O_{40}$ (MPA) (Aldrich, 99.9%) were prepared by suspending a known amount of dried TiO_2 anatase powder in aqueous solution of corresponding heteropoly acids. The suspension mixture (optimum

heteropoly acids loading, 15%) were dried at 120^{o}C for 12 h [16, 17]. 3 wt% V_2O_5 modified catalysts were prepared by wet impregnation by dissolving the required amount of ammonium meta- vanadate (Aldrich, 99.9%) as a precursor in 2 M oxalic acid solution to the pure TiO_2 and heteropoly acid -TiO_2 supports. Each impregnated catalyst was oven dried at 120^{o}C for 12 h followed by calcination at 400-700^{o}C for 4 h prior to use. 3 wt% Cu and 3 wt% Fe modified catalysts were also prepared by wet impregnation by dissolving the required amount of copper nitrate (Aldrich, 99,9%) and iron nitrate (Aldrich, 99,9%) as a precursor in water to the pure TiO_2 and heteropoly acid -TiO_2 supports.

The potassium-doped catalyst was prepared by co-impregnation with a solution of KNO_3 (Aldrich, 99.9%) to obtain a potassium loading of 100 µmol/g catalyst. Each impregnated catalyst was oven dried at 120^{o}C for 12 h followed by calcination at 400^{o}C for 4 h prior to use.

X-ray powder diffraction (XRPD) measurements were performed on a Huber G670 powder diffractometer using CuK_α radiation within a 2θ range of 10–60° in steps of 0.02°. BET surface area, NH_3-TPD and H_2-TPR experiments were performed as described in Chapter 2.2.3. The SCR activity measurements were carried out at atmospheric pressure in a fixed-bed quartz reactor loaded with 20 mg of fractionized (180-300 µm) catalyst samples positioned between two layers of inert quartz wool. The reactant gas composition was adjusted to 1000 ppm NO, 1100 ppm NH_3, 3.5% O_2, 2.3% H_2O and balance N_2 by mixing 1% NO/N_2 (±0.1% abs.), 1% NH_3/N_2 (±0.005% abs.), O_2 (≥99.95%) and balance N_2 (≥99.999%) (Air Liquide) using Bronkhorst EL-Flow F-201C/D mass-flow controllers. The total flow rate was maintained at 500 ml/min (ambient conditions).

4.3 Results and Discussion

4.3.1 Vanadium based catalysts

The XRD patterns of VTPATi, VTSiATi, and VMPATi samples calcined at various temperatures are shown in Fig. 4.1. At 400°C no diffractions lines attributing to crystalline V_2O_5 or HPAs were observed only support TiO_2 patterns can be observed indicating that the vanadium and HPAs are highly dispersed on the support. Both anatase (2θ = 25.3°, 37.9°, 47.8° and 54.3°) and very small rutile (2θ = 27.4°, 36.1°, and 54.2°) phases are present in the catalysts. Partial phase transformation from anatase to rutile can be seen at 600°C and complete transformation into rutile rich phase occurs around 700°C. The concentration of the rutile phase is varying for each catalyst and they are in the order VMPATi > VTSiATi > VTPATi. At 700°C calcination temperature some decomposition products of HPAs (MoO_3 and WO_3) can be seen along with rutile rich phase support. Potassium doped catalysts showed further increase in rutile phase in the order KVMPATi > KVTSiATi > KVTPATi.

The results of the N_2-BET surface area are summarized in Table 4.1 for fresh and potassium deactivated catalysts calcined at 400°C. Surface area of VTi catalyst showed 128 m^2/g, while those of the HPA-promoted catalysts showed a small decrease. Potassium deactivated catalysts showed further decrease in surface area might be due to pore blocking. All the catalysts showed two ammonium desorption regions; one due to moderate acid strength (high $T_{max}2$ region) and the other due to weak acid strength (low $T_{max}1$ region). The $T_{max}1$ peak attributed to the weak acid sites was

observed at around 200°C, while the $T_{max}2$ peak attributed to the strong acid sites was observed between 300- 500°C.

Fig. 4.2 shows NH_3-TPD profiles of VTPATi, VMPATi, and VTSiATi catalysts calcined at 400°C in the temperature range of 100-650°C and the results are summarized in Table 4.1. The acidity of the pure VTi catalyst without promoters showed 571 µmol/g and that of VMPATi, VTPATi and VTSiATi impregnated catalysts showed increased acidity with the presence of vanadium. It is known that acidity of the catalysts is enhanced with presence of vanadium on the support [18]. Total acidity of the VHPATi catalysts are in the order of VTPATi > VTSiATi > VMPATi. Acid strength of the catalysts can best be described by their desorption temperatures. The VTPATi catalyst revealed high $T_{max}1$ and $T_{max}2$ peaks, indicating its high acid site density.

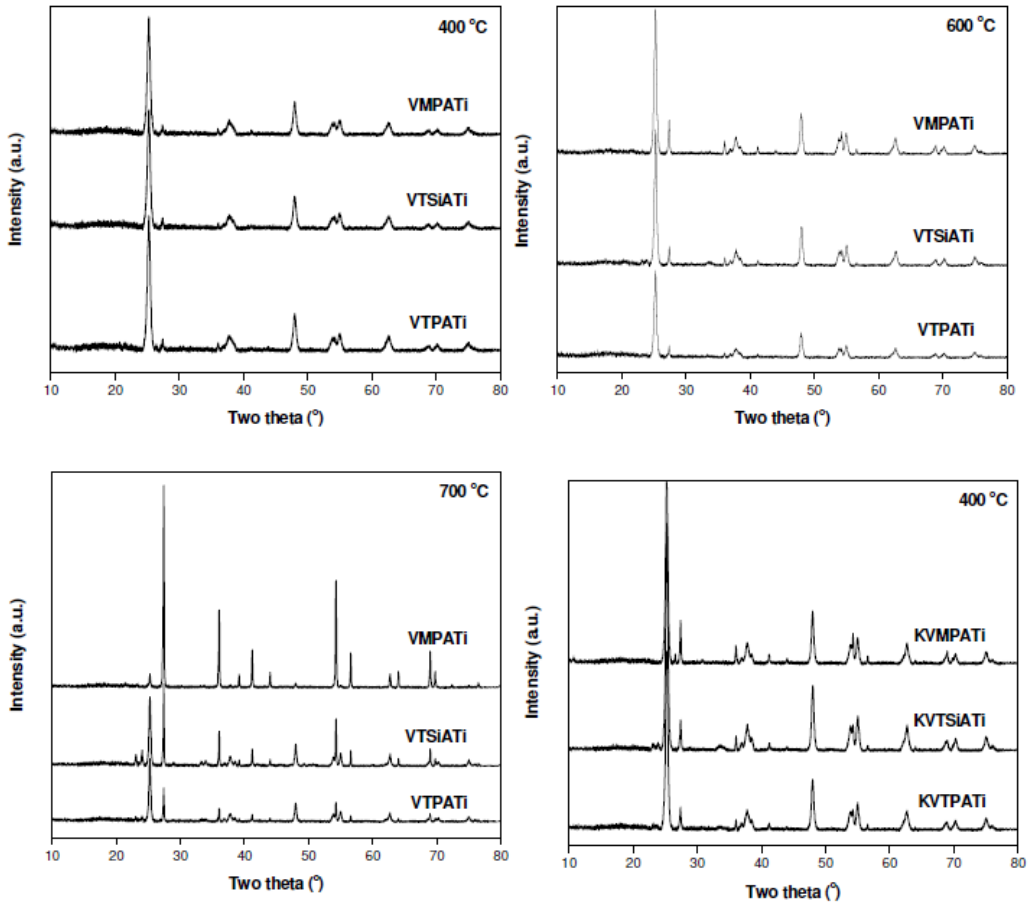

Figure 4.1 XRPD patterns of fresh and deactivated VTPATi, VMPATi, and VTSiATi catalysts at various calcination temperatures.

Table 4.1 Surface area and NH_3-TPD results of fresh and potassium doped catalysts calcined at 400°C.

Catalyst	Surface area (m^2/g)	Acidity (µmol/g)	T_{max} of desorption	
VTi	128	571	….	….
VTPATi	112	839	281	417
VTSiATi	114	809	265	401
VMPATi	96	787	256	350
KVTi	120	108	….	….
KVTPATi	102	503	178	338
KVTSiATi	104	463	191	344
KVMPATi	84	491	193	342

Acid strength of the catalysts are in the order of VTPATi > VTSiATi > VMPATi. The acid sites in HPA are more uniform and easier to control than those in other solid acid catalysts. Usually, tungsten HPAs are the catalysts of choice because of their stronger acidity, higher thermal stability and lower oxidation potential compared to molybdenum acids. Being stronger acids, HPAs are generally more active catalysts than the conventional solid acid catalysts, which allow efficient operation under milder conditions.

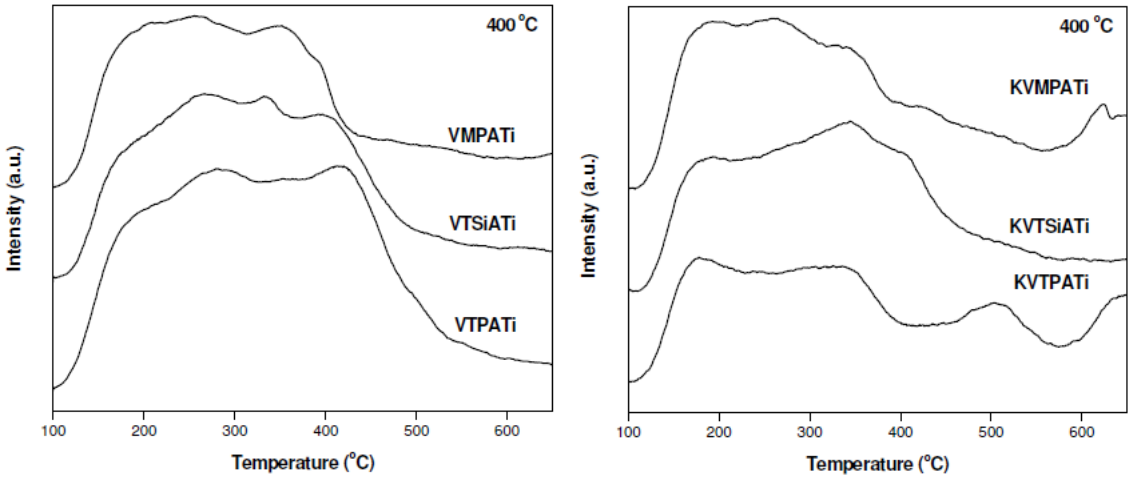

Figure 4.2 NH_3-TPD profiles of fresh and deactivated VTPATi, VMPATi, and VTSiATi catalysts calcined at 400°C.

Fig. 4.2 also shows the NH_3-TPD profiles of potassium deactivated catalysts calcined at 400°C and the results are summarized in Table 4.1. Overall there is a drastic decrease in acidity and T_{max} peak positions can be seen. It is rather obvious to assume that potassium oxide first occupy the strongest acid sites and then due to electron donation weakens the remaining acid sites, and therefore is T_{max} in potassium deactivated catalysts shifted towards lower temperature regions. Especially KVTi catalyst acidity dropped (81%) from 571 to 108 µmol/g and those of KVTPATi (40%), KVTSiATi (43%) and KVMPATi (38%) catalysts showed less drop in acidity after deactivation. It is known that the surface modified or promoted V_2O_5 catalysts showed similar type of performance in terms of alkali resistance [12-14].

Catalytic activity of VHPATi catalysts calcined at between 400-700°C is shown in Fig. 4.3. VMPATi, VTPATi, and VTSiATi catalysts showed maximum activity at 400°C calcination

temperature. However, the catalysts calcined at 500ºC, 600ºC and 700ºC were comparatively less active than the catalysts calcined at 400ºC. From the calcination effect it is evident that the HPAs are sensitive to the calcination process. Further, low calcination temperatures are not studied since optimum reaction temperatures are around 400ºC and inactive amorphous TiO_2 phase can be seen. At 400ºC calcination temperature the catalyst is rich in anatase phase and there is no crystalline V_2O_5 or HPAs present. By further increase in calcination temperature there is a partial phase transformation of anatase to rutile phase and chances of formation of less active HPAs decomposition products (WO_3 or MoO_3). It is evident that WO_3 and MoO_3 are excellent promoters, in the present case when they are in the stable HPA form they have high acidity and SCR activity as well.

Yoshimoto et al. [11] performed SCR with various aromatic hydrocarbons on Pd-TPA/ SiO_2 and ultimately they couldn't achieve 100% NO conversion and the N_2 selectivity is very poor. The present catalysts are highly active and can easily replace the conventional catalysts since the operating conditions are very similar. For the VMPATi catalysts K_{max} values are observed at 440ºC and by further increase in reaction temperature the activity decreases. Whereas VTPATi and VTSiATi catalysts showed K_{max} at 460ºC and also by further increase in reaction temperature the activity decreases due to predominant ammonia oxidation (SCO) over SCR [19]. Low temperature activity of VMPATi catalyst is well appreciated and all thermal deactivations could be easily avoided with low temperature performance catalysts. Over all the best VMPATi, VTPATi and VTSiATi catalysts showed k_{max} values of 803, 966 and 963 $cm^3/g.s$, respectively at their optimum conditions. The rate constant values are much higher than the commercial V_2O_5-WO_3/TiO_2 catalyst and highly active V_2O_5/Sulphated-ZrO_2 catalysts (430 $cm^3/g.s$) [13, 14]. This critical comparison with the mass based rate constants gives clear idea about the HPAs ability to enhance the SCR. Jentys et al. [20] performed SCR on Pt-TPA on MCM-41 with C_3H_6 as a reducing agent, they couldn't achieve 100% NO_x conversion and also C_3H_6 slip was large. Pt-TPA/MCM-41 catalysts are sensitive to water and high concentration of oxygen and it has much smaller operational window for the reaction. Thermal stability of VHPAs can best be compared at 700°C with the help of XRD and the SCR activity. At 700ºC SCR activity and anatase phase intensities by XRD are in the order of VTPATi>VTSiATi>VMPATi. Overall WO_3-containing VTPA and VTSiA catalysts are more active than MoO_3 containing VMPA catalysts.

Doping the optimum catalysts (calcined at 400ºC) with potassium (of K/V=0.3 or 100 µmol/g) resulted in decrease in activity and a small shift of k_{max} towards lower temperature (Fig. 4.3). A possible explanation for such a temperature shift is that the potassium loading reduced the activity of the main NO-SCR reaction while the rate of the side reaction of ammonia oxidation remained constant or even increased. All the potassium doped HPA catalysts showed similar profiles as that of undoped catalysts. KVMPATi catalyst showed k_{max} value at 400ºC and KVTPATi and KVTSiATi catalysts showed k_{max} at 440ºC. Especially the KVTi catalyst showed decrease in k_{max} from 500 to 155 $cm^3/g.s$ which implies the severe poisoning effect of alkali in the absence of HPAs. On VTi catalyst potassium seems to preferably coordinate with the vanadium sites and make them inactive for the SCR reaction. Whereas HPA promoted V_2O_5/TiO_2 catalysts showed better deactivation resistance as compared to that of VTi catalyst. The super acidic nature of HPAs can host the potassium poisons where by the SCR active vanadium can be protected from deactivation.

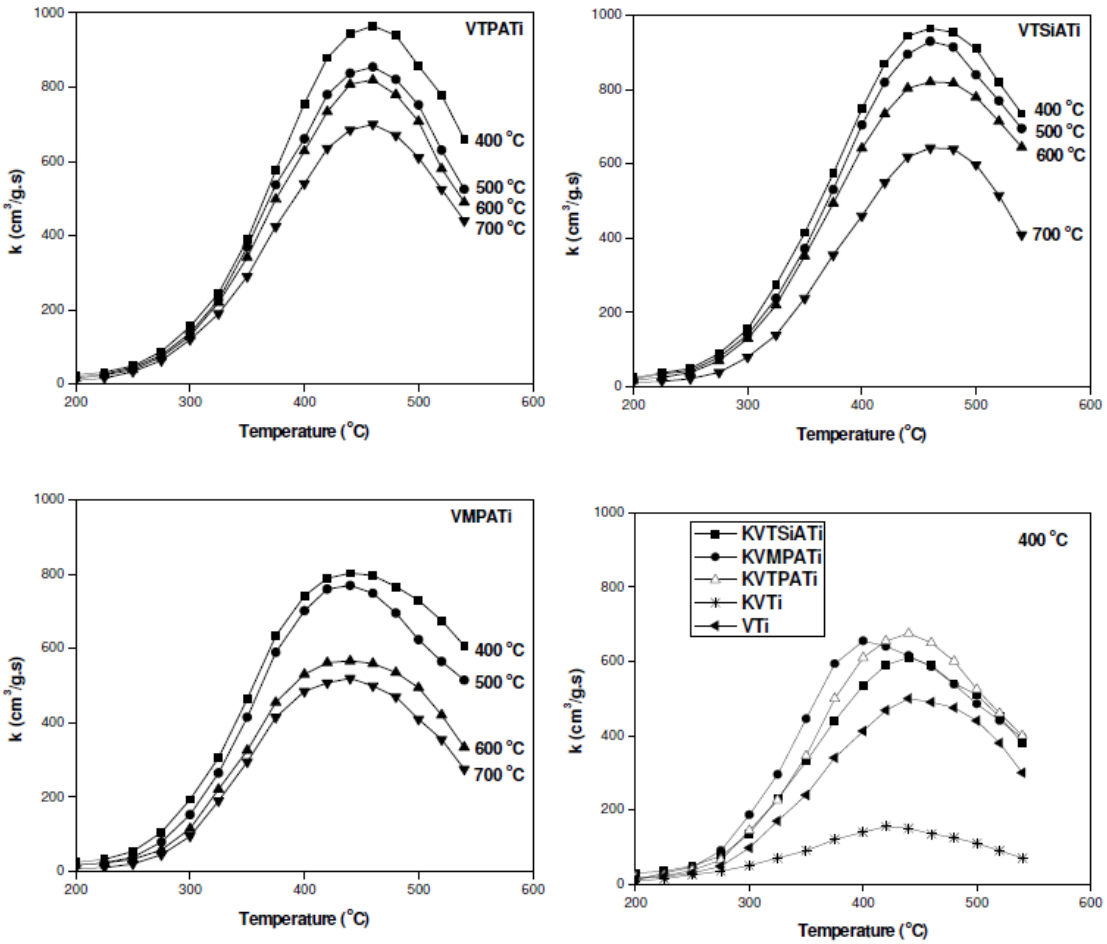

Figure 4.3 Temperature dependency of first-order rate constant for SCR of NO with VTPATi, VMPATi, and VTSiATi fresh and deactivated catalysts calcined at indicated temperature (^{o}C).

KVTi catalysts showed a relative activity of 33% and that of KVMPATi, KVTPATi, KVTSiATi catalysts showed 88%, 81%, 71%, respectively at 400ºC. For all catalysts the deactivation increases with reaction temperature which is connected with the shift of the maximum activity towards lower temperatures for potassium-poisoned catalysts. Especially the KVMPATi catalyst is very resistant to alkali poisons as compared to other catalysts which could be due to the low temperature performance of this catalyst as well as its moderate loss of acidity after potassium poisoning. Consequently, the potassium deactivation was significantly lower in the present catalysts compared to that of traditional SCR catalysts. Highly active V_2O_5-WO_x/ZrO_2 catalysts reported in literature for biomass fired applications also showed 40% relative activity even with less potassium concentration of 80 µmol/g [21].

4.3.2 Copper and Iron based catalysts

The XRPD patterns of Cu-Ti and Fe-Ti based catalysts with and without HPA promoters are shown in Fig. 4.4. Only diffractions corresponding to the TiO_2 support can be observed indicating that CuO or Fe_2O_3 are highly dispersed in an amorphous state on the surface of the support. Furthermore, absence of phases of HPAs or their decomposition products (like MoO_3 and WO_3) suggests that

also HPAs are highly dispersed and thermally stable at the calcination temperature of 400ºC. Potassium-doped catalysts showed similar XPRD patterns as the corresponding undoped catalysts (not shown in Figure).

BET surface areas of the Cu and Fe based catalysts are presented in Table 4.2 the surface area of the Cu-Ti and Fe-Ti catalysts was measured to 128 and 120 m^2/g, respectively, while the areas of the HPA-promoted catalysts were slightly lower in the range of 90-110 m^2/g. It is know that an increase in metal content on the surface of the support can induce pore blocking which results in decreasing the overall surface area [13].

NH_3-TPD is used to evaluate the acidity of the catalysts. The ammonia desorption profiles of both the Cu- and Fe-impregnated catalysts and corresponding potassium-doped samples are presented in Fig. 4.5. For all samples the total amount of desorbed ammonia and T_{max} of desorption are listed in Table 4.2. The total amount of adsorbed ammonia corresponds to molecular adsorbed ammonia or ammonium ions on Lewis or Brønsted acid sites [13]. The relative strength of the acid sites are reflected by the temperature of maximum ammonia desorption. The NH_3-TPD profile of the fresh Cu-Ti and Fe-Ti catalysts showed primarily a sharp desorption temperature peak around 290ºC, whereas the Cu-HPA-Ti and Fe-HPA-Ti catalysts showed a broad desorption T_{max} peak above 350ºC, which probably are due to Brønsted acid sites from the HPAs. As calculated in Table 4.2, Cu-Ti and Fe-Ti catalysts have total acidities of 490 and 452 µmol/g, respectively, whereas Cu-HPA-Ti and Fe-HPA-Ti catalysts are more acidic with values above 630 µmol/g due to the super acidic nature of the HPA promoters. The acid strength of the fresh HPA-promoted samples with Cu follows the order: Cu-TSiA-Ti > Cu-TPA-Ti > Cu-MPA-Ti > Cu-Ti, whereas the surface acidity are in the order: Cu-TPA-Ti > Cu-MPA-Ti > Cu-TSiA-Ti > Cu-Ti. Fresh Fe-HPA-Ti catalysts showed similar acid strength order as that of Cu-HPA-Ti catalysts, whereas the surface acidity of the iron based catalysts are in the order: Fe-MPA-Ti > Fe-TSiA-Ti > Fe-TPA-Ti > Fe-Ti. Thus, HPA-promoted catalysts showed high surface acidity and acid strength compared to that of unpromoted catalysts.

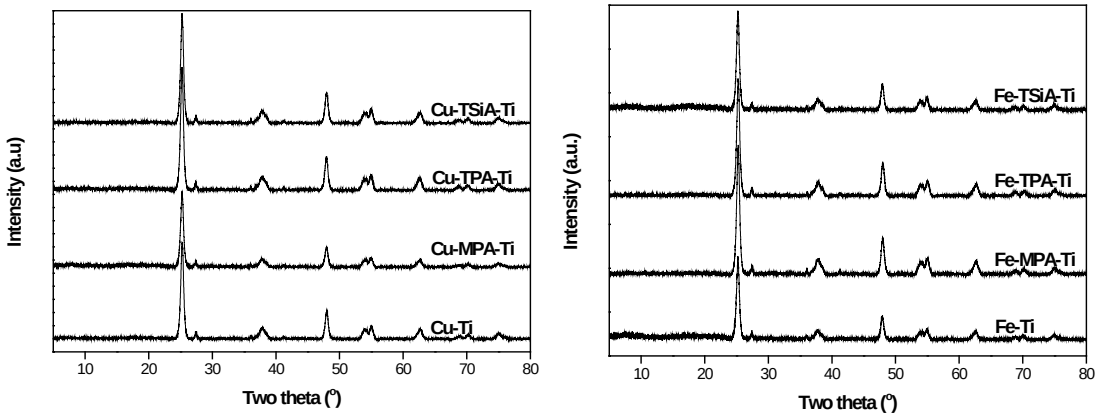

Figure 4.4 XRPD patterns of Cu and Fe based catalysts.

The NH_3 desorption profiles of the potassium-poisoned catalysts showed an overall decrease in surface acidity as reported in Table 4.2. Moreover, the alkali doping is associated with a decrease in acid strength on all catalysts, in agreement with earlier reports [12, 14, 22]. The weakening of the acid sites is due to occupation of potassium on the strongest acid sites, which

decreases the strength of the remaining acid sites through electron donation. Especially KCu-Ti and KFe-Ti catalysts showed acidity drop of 61% and 55%, respectively. In comparison the acidity of the HPA-promoted catalysts decreased 33% upon potassium-doping. Similar alkali resistivity results were observed on TiO_2 and ZrO_2 surface modified catalysts [13, 22].

Table 4.2 Surface area and NH_3-TPD results of Cu and Fe based catalysts.

Catalysts	Surface area (m^2/g)	Acidity (µmol/g)		T_{max} of desorption (^{o}C)	
		Fresh	K-doped	Fresh	K-doped
Cu-Ti	128	490	190	291	288
Cu-MPA-Ti	95	687	455	349	316
Cu-TPA-Ti	108	745	536	386	341
Cu-TSiA-Ti	115	630	514	405	338
Fe-Ti	112	452	200	293	291
Fe-MPA-Ti	92	709	515	380	342
Fe-TPA-Ti	100	613	505	412	347
Fe-TSiA-Ti	108	683	540	419	344

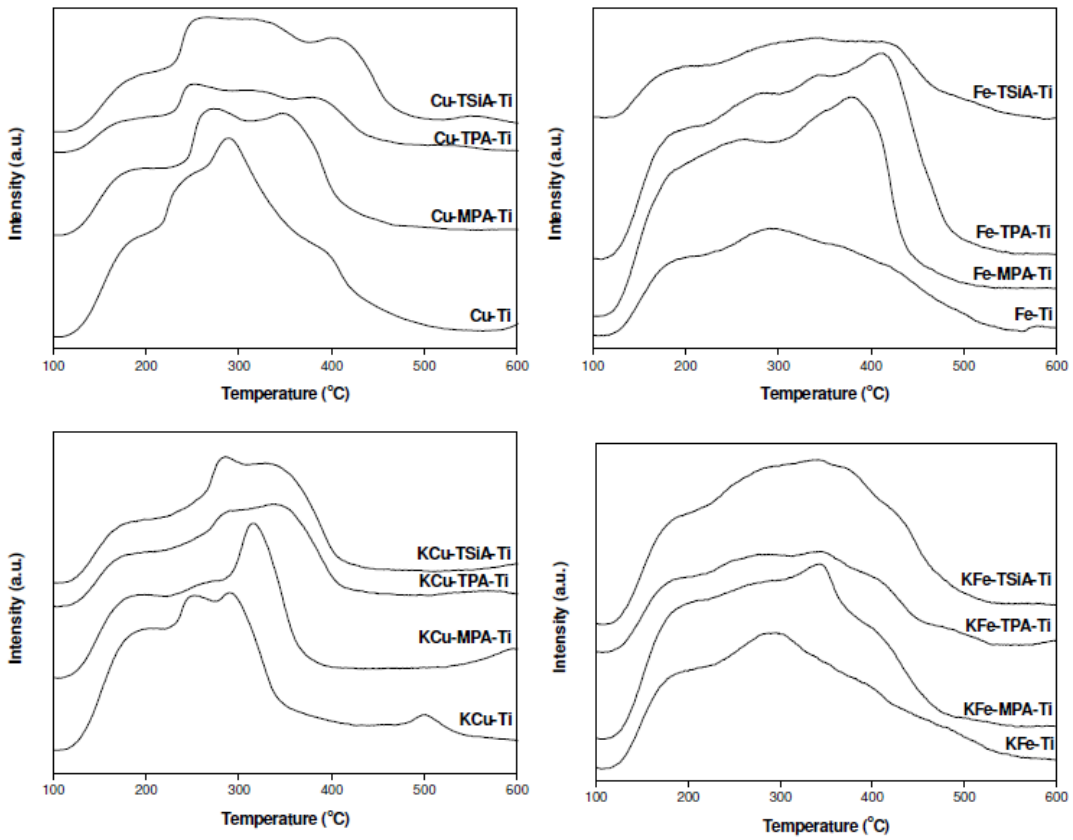

Figure 4.5 NH_3-TPD profiles of fresh and potassium doped Cu and Fe based catalysts.

H_2-TPR is frequently used to study the redox property of metal oxide catalysts. In Fig. 4.6 the TPR patterns of both fresh and potassium-doped Cu and Fe catalysts are shown. All the Cu catalysts showed three reduction peaks; A sharp low temperature peak with maximum between 100-200^{o}C, a small shoulder at medium temperature around 300^{o}C and a broad high temperature peak between 560-730^{o}C. Cu-Ti catalysts yielded only low and medium temperature peaks while all three peaks were observed in Cu-HPA-Ti catalysts. The high temperature peak is due to the reduction of HPAs [23, 24], whereas the low and medium temperature peaks are ascribed to reduction of CuO [25, 26]. In more detail, the two or three reduction peaks observed for the Cu catalysts in the low temperature region, can be ascribed to sequential reduction of CuO species on the TiO_2 support, while the medium temperature reduction peak has been attributed to interacted or anchored CuO on TiO_2 [25, 26].

Table 4.3 H_2-TPR results of Cu and Fe based catalysts.

Catalysts	**T_{max} of low temperature peak (^{o}C)**		**T_{max} of high temperature peak (^{o}C)**	
	Fresh	**K-doped**	**Fresh**	**K-doped**
Cu-Ti	171	130	….	….
Cu-MPA-Ti	154	166	621	602
Cu-TPA-Ti	141	151	656	633
Cu-TSiA-Ti	132	132	637	587
Fe-Ti	325	306	….	….
Fe-MPA-Ti	352	369	632	610
Fe-TPA-Ti	313	309	666	578
Fe-TSiA-Ti	286	310	595	569

Potassium-doped Cu catalysts showed similar H_2-TPR profiles with some changes in reduction temperatures as indicated in Table 4.3. Hence, in the Cu-Ti catalyst the T_{max} position of the low temperature reduction is decreased from 171 to 131°C, whereas increased or unchanged T_{max} reduction temperature was found for Cu-HPA-Ti catalysts upon potassium addition. In contrast the high temperature reduction peaks in Cu-HPA-Ti catalysts are decreased upon potassium addition, indicating that the active Cu species are protected from the potassium species in the promoted catalysts. The Fe-Ti catalyst revealed only one reduction peak and Fe-HPA-Ti catalysts two reduction peaks. The low temperature peak around 300-320°C is ascribed to iron oxide reduction [27]. Potassium doped Fe catalysts also showed similar shift in low and high temperature T_{max} position as observed with the Cu catalysts.

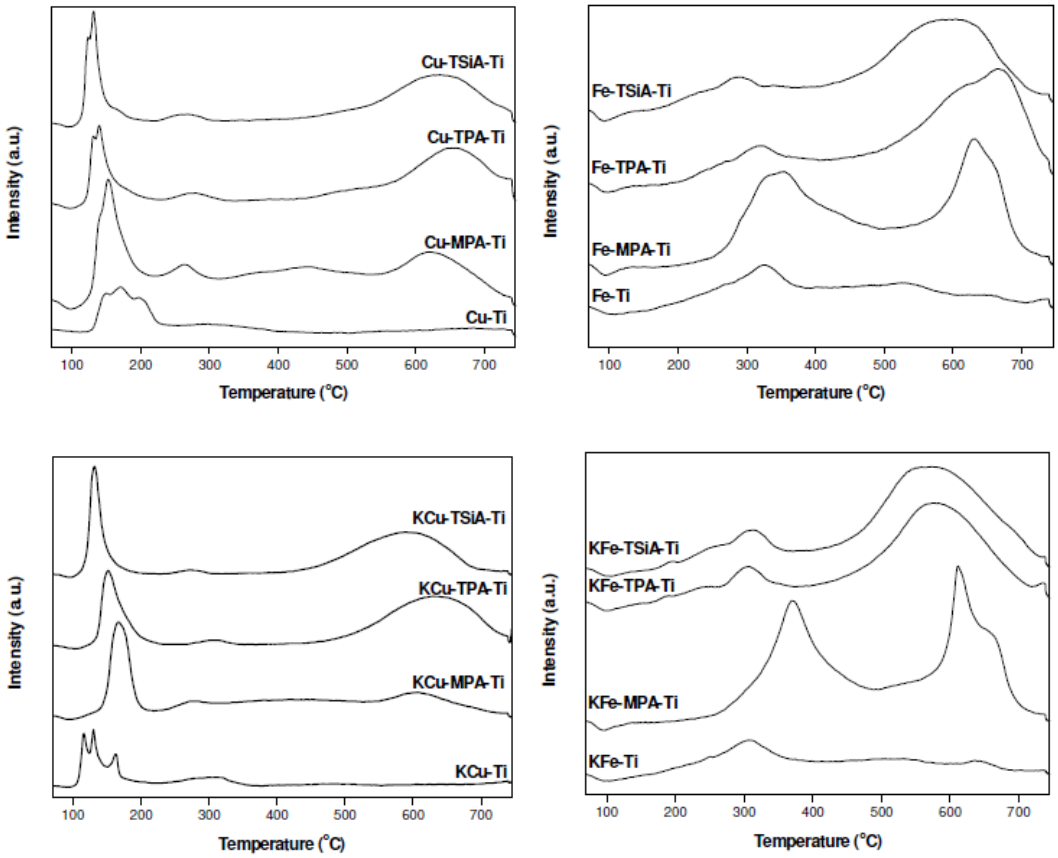

Figure 4.6 H_2-TPR profiles of fresh and potassium doped Cu and Fe based catalysts.

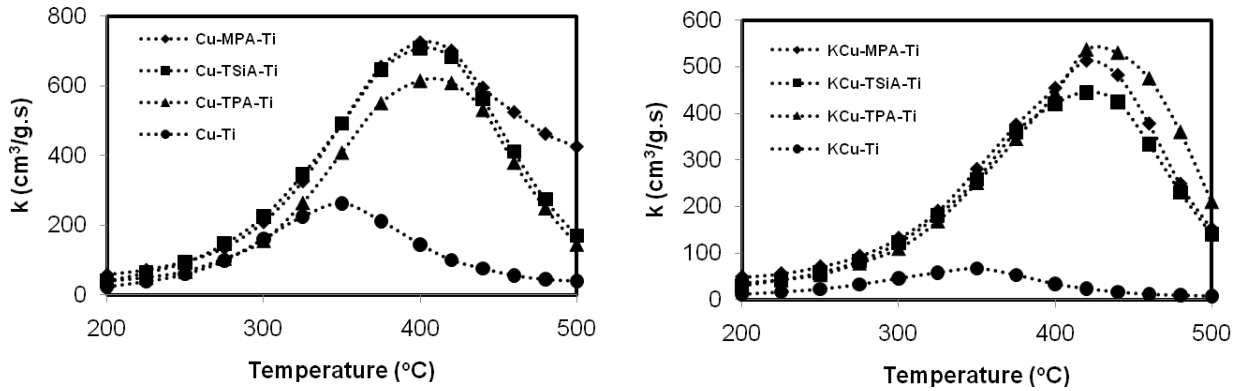

Figure 4.7 Temperature dependency of first-order rate constant for SCR of NO with fresh and potassium doped Cu based catalysts.

The SCR activity of the fresh and potassium-doped Cu catalysts was measured in the temperature range 200-500°C. In Fig. 4.7 the measured catalytic activities are reported as first-order mass based rate constants k ($cm^3/g{\cdot}s$). The catalytic activity is generally increasing with catalyst temperature until a optimum temperature is reached between 350-400^{o}C. Upon further increase in temperature the SCR activity decreases due to predominant ammonia oxidation [28, 29]. HPA-promoted catalysts showed higher activity compared to that of unpromoted Cu-Ti catalyst with an order corresponding to Cu-MPA-Ti ≈ Cu-TSiA-Ti > Cu-TPA-Ti > Cu-Ti. Thus, Cu-MPA-Ti, Cu-

TSiA-Ti, Cu-TPA-Ti and Cu-Ti catalysts showed k_{max} values of 724, 709, 616 and 262 $cm^3/g{\cdot}s$, respectively, at their T_{max} temperatures. No reports are available in literature for the SCR of NO with NH_3 on HPA promoted catalysts for direct comparison with the observed values. However, Yoshimoto et al. [11] found low NO conversion and N_2 selectivity in SCR performed with various aromatic hydrocarbons on Pd-TPA/SiO_2. Potassium-doped Cu based catalysts (100 µmol K/g) was less active than the undoped catalysts showing k_{max} values of 513, 445, 537 and 67 $cm^3/g{\cdot}s$ for KCu-MPA-Ti, KCu-TSiA-Ti, KCu-TPA-Ti and KCu-Ti catalysts, respectively, at their T_{max} temperatures. Importantly, some of the rate constants are higher than obtained with the commercial V_2O_5-WO_3/TiO_2 catalyst and the highly alkali resistant V_2O_5/sulphated-ZrO_2 catalysts (430 $cm^3/g{\cdot}s$) under identical reaction conditions [13, 14].

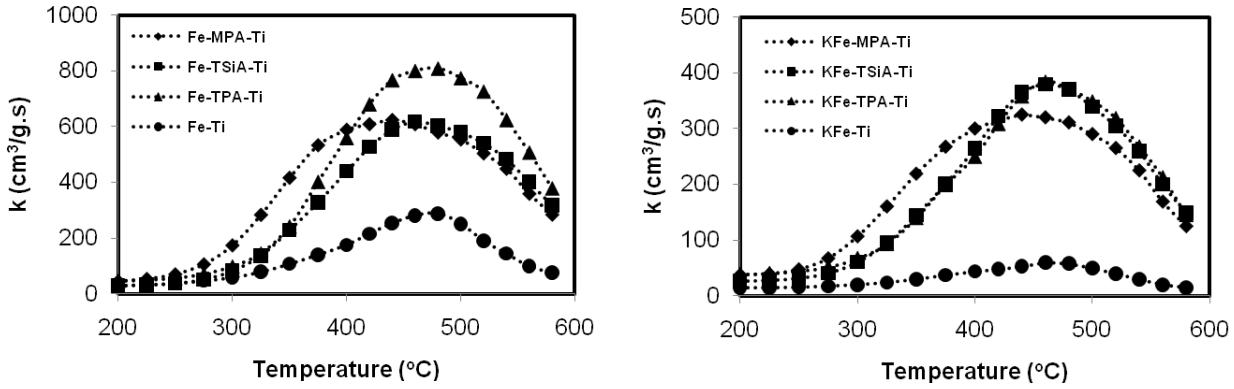

Figure 4.8 Temperature dependency of first-order rate constant for SCR of NO with fresh and potassium doped Fe based catalysts.

The SCR activities of the fresh and potassium-doped Fe catalysts were measured in the temperature range 200-580°C (Fig. 4.8). Fe-based catalysts are showing maximum catalytic activity at higher temperatures (440-480°C) compared to that of Cu based catalysts. The order of catalytic activity (k_{max}) of fresh catalysts is: Fe-TPA-Ti (810 $cm^3/g{\cdot}s$) > Fe-MPA-Ti (625 $cm^3/g{\cdot}s$) > Fe-TSiA-Ti (619 $cm^3/g{\cdot}s$) > Fe-Ti (288 $cm^3/g{\cdot}s$) at T_{max} temperatures. This order is different from the one observed for the Cu catalysts where the molybdenum-containing MPA was the most active catalyst. Potassium-doping of the Fe catalysts also resulted in decrease of SCR activity resulting in k_{max} values at Tmax temperature of 325, 380, 385 and 60 $cm^3/g{\cdot}s$ for KFe-MPA-Ti, KFe-TSiA-Ti, KFe-TPA-Ti and KFe-Ti catalysts, respectively. The observed change in catalytic activity after doping with potassium seems to correlate well with the loss in total acidity of the catalysts (listed in Table 4.2).

The decrease in activity after potassium doping is represented as relative activity (%). Cu-Ti catalysts possessed a relative activity of 23% at 400°C, whereas Cu-MPA-Ti, Cu-TSiA-Ti and Cu-TPA-Ti catalysts showed 63, 59 and 72%, respectively. Similarly, the Fe-Ti, Fe-MPA-Ti, Fe-TSiA-Ti and Fe-TPA-Ti catalysts showed a relative activity of 21, 52, 62, 47%, respectively at 440°C. Notably, these potassium deactivation values are significantly lower compared to that of traditional SCR catalysts. Highly active V_2O_5-WO_x/ZrO_2 catalyst reported in literature for biomass fired

applications also showed severe deactivation [13, 14]. Hence, overall the HPA promoted catalysts are both very active and resistant to alkali poisons compared to unpromoted catalysts.

4.4 Conclusions

Distribution of the heteropoly acids, MPA, TPA or TSiA on V-Ti, Cu-Ti and Fe-Ti entailed a substantial increase in acid strength and surface acidity. All the HPA promoted catalysts exhibited better SCR activity than unpromoted catalysts. Furthermore, the impact of potassium doping (100 µmol/g) on the Cu-HPA-Ti and Fe-HPA-Ti catalysts is less severe than that found on corresponding unpromoted V-Ti, Cu-Ti and Fe-Ti catalysts. Accordingly, heteropoly acid promoted V_2O_5/TiO_2 and Cu/TiO_2 and Fe/TiO_2 catalysts are promising new, SCR catalysts for flue gas cleaning in both coal and biomass fired power plants.

4.5 References

[1] T. Okuhara, N. Mizuno, M. Misono, Adv. Catal. 41 (1996) 113.
[2] C.L. Hill (Ed.), Polyoxometalates, 98, Chem. Rev., 1998.
[3] I.V. Kozhevnikov, Chem. Rev. 98 (1998) 171.
[4] N. Mizuno, M. Misono, Chem. Rev. 98 (1998) 199.
[5] I.V. Kozhevnikov, Catalysts for Fine Chemicals, Vol.2. Catalysis by Polyoxometalates, Wiley, Chichester, England, 2002.
[6] R.T. Yang, N. Chen, Ind. Eng. Chem. Res. 33 (1994) 825.
[7] R. Belanger, J.B. Moffat, J. Catal. 152 (1995)179.
[8] K. Vaezzadeh, C. Petit, V. Pitchon, Catal. Today 73 (2002) 297.
[9] M.A. Gomez-Garcia, V. Pitchon, A. Kiennemann, Catal. Today 107 (2005) 60.
[10] K. Okumura, R. Yoshimoto, K. Suzuki, M. Niwa, Bull. Chem. Soc. Jpn. 78 (2005) 361.
[11] R. Yoshimoto, T. Ninomiya, K. Okumura, M. Niwa, Appl. Catal. B 75 (2007) 175.
[12] J. Chen, R. Yang, J. Catal. 125 (1990) 411.
[13] A.L. Kustov, M. Yu. Kustova, R. Fehrmann, P. Simonsen, Appl. Catal. B 58 (2005) 97.
[14] J. Due-Hansen, S. Boghosian, A. Kustov, P. Fristrup, G. Tsilomelekis, K. Ståhl, C.H. Christensen, R. Fehrmann, J. Catal. 251(2007) 459.
[15] R.S. Drago, J.A. Dias, T. Maier, J. Am. Chem. Soc. 119 (1997) 7702.
[16] B.M. Devassy, S.B. Halligudi, J. Catal. 236 (2005) 313.
[17] A. Alsalme, E.F. Kozhevnikova, I.V. Kozhevnikov, Appl. Catal. A 349 (2008) 170.
[18] S.S.R. Putluru, A. Riisager, R. Fehrmann, Appl. Catal. B 97 (2010) 333.
[19] M. Yates, J.A. Martín, M. Ángeles Martín-Luengo , S. Suárez, J. Blanco, Catal Today 107–108 (2005) 120
[20] A. Jentys, W. Schieber, H. Vie, Catal. Today 59 (2000) 313.
[21] J. Due-Hansen, A.L. Kustov, S.B. Rasmussen, R. Fehrmann, C.H. Christensen, Appl. Catal. B 66 (2006) 161.
[22] A.L. Kustov, S.B. Rasmussen, R. Fehrmann, P. Simonsen, Appl. Catal. B 76 (2007) 9.
[23] A.A. Spojakina, N.G. Kostova, B. Sow, M.W. Stamenova, K. Jiratova, Catal. Today 65 (2011) 315.
[24] L.M. Gomez Sainero, S. Damyanova, J.L.G. Fierro, Appl. Catal. A. 208 (2001) 63.
[25] S. Guerrero, I. Guzmán, G. Aguila, P. Araya, Catal. Commun. 11 (2009) 38.
[26] J. Xiaoyuan, D. Guanghui, L. Liping, C. Yingxu, Z. Xiaoming, J. Mol. Catal. A 218 (2004) 187.
[27] G. Pecchi, P. Reyes, J. Sol-Gel. Sci Techn. 27 (2003) 205.
[28] G. Ramis, L. Yi, G. Busca, M. Turco, E. Kotur, R.J. Willey, J. Catal. 157(1995) 523.
[29] R.Q. Long, R.T. Yang, J. Catal. 186 (1999) 254.

5. Catalysts based on the zeolite support

5.1 Introduction

Zeolites are crystalline, aluminosilicate molecular sieves that have pores of molecular dimensions [1, 2]. Zeolites are nontoxic and environmentally benign materials that can be synthesized with a wide range of pore sizes and topologies. Zeolites are classified as microporous materials that have pore dimensions in the subnanometer to nanometer size range. The zeolite framework typically consists of SiO_4^{-4} and AlO_4^{-5} moieties in tetrahedral coordination with shared oxygen atoms.

The faujasite zeolites, X and Y, are widely used as catalysts in the industry. Zeolites X and Y have the same structure but differ in silicon to aluminum ratio. The faujasite structure consists of sodalite cages and 12-membered oxygen rings that form a three-dimensional channel system with 7.4 Å apertures. The zeolite ZSM-5 (or MFI) has a silicon to aluminum ratio >10. The framework of ZSM-5 is composed of straight 10-ring, elliptical channels (pore dimension: 5.3 x 5.6 Å) running along the [0 1 0] direction and sinusoidal 10-ring, elliptical channels (pore dimension: 5.1 x 5.5 Å) along the [1 0 0] direction [3]. The framework of zeolite Beta is similar in topology to ZSM-5, but the pore size is larger. The framework of Beta is composed of straight 12-ring channels (pore dimension: 5.5 x 5.5 Å) along the [0 0 1] direction and sinusoidal 12-ring, elliptical channels (pore dimension: 7.6 x 6.4 Å) along [1 0 0] direction [3]. Zeolites ferrierite and mordenite have silicon to aluminum ratios around 5 and have two-dimensional channel systems. In recent years, applications for catalysts related to environmental issues have been driven by legislation that has placed regulations on air and water pollutants. This has led to a growth in the development of catalytic processes designed to alleviate environmental problems. Some examples of zeolites use or potential use as environmental catalysts are SCR of NO_x with hydrocarbons, SCR of NO_x with ammonia, N_2O decomposition, VOC removal and caprolactam in an oxidation processes.

In the present work, V, Cu and Fe metal oxides were optimized for various zeolites to achieve maximum activity in the SCR reaction. The influence of potassium oxide additives on the activity was also studied and compared with traditional SCR catalysts. All the catalysts were characterized by various techniques to allow detailed discussion of the effect of the catalyst composition on the SCR performance.

5.2 Experimental

5.2.1 Powder catalyst Preparation

Commercial NH_4-ZSM5, NH_4-BETA, NH_4-Mordenite and NH_4-Y (Zeolyst International, USA) zeolites with different Si/Al were initially calcined at 550 ^oC for 5 h to obtain the H-ZSM5, H-BETA, H-Mordenite and H-Y supports, respectively.

V_2O_5-zeolite catalyst with 3 to 16wt% V_2O_5 were prepared by wet impregnation of the supports with 0.5 to 1.25 M vanadium oxalate solution. This vanadium oxalate solution is prepared with ammonium meta-vanadate and oxalic acid solution with a stoichiometric ration of 1:2 at 70^oC. Cu-zeolite catalysts were prepared by incipient wet impregnation using appropriate amounts of copper nitrate (Aldrich, 99.99%) as a precursor and H-Mordenite (400 m^2/g), H-ZSM5 (500 m^2/g)

or H-BETA (680 m^2/g), respectively as supports (Zeolyst International). Each impregnated catalyst was oven dried at 120^{o}C for 12 h followed by calcination at 500^{o}C for 5 h prior to use.

Fe-zeolite catalysts were prepared by ion-exchange methods. Commercial zeolite supports H-ZSM5 (500 m^2/g), H-Mordenite (400 m^2/g) and H-BETA (680 m^2/g) were purchased from Zeolyst International. In the ion-exchange method 2 g of zeolite sample was added to 1 liter of 2 mM iron (III) nitrate nonahydrate (Aldrich, 99.99%) solution. The mixture was stirred for 24 h at 80 ^{o}C, where after the solid iron-exchanged zeolite catalyst was filtered off, washed there times with 1 liter water, dried at 120^{o}C for 12 h and finally calcined at 500^{o}C for 5 h.

Optimum catalysts were then poisoned by incipient wet impregnation with 0.05–0.15 M solution of potassium nitrate (Aldrich, 99.99%) to obtain a potassium loading of 100, 250 and 500 µmol/g. The prepared catalysts were oven dried at 120^{o}C for 12 h and finally calcined at 500^{o}C for 5 h before use.

5.2.2 Cu based monolith preparation and potassium chloride aerosol exposure

Glass fiber plate type monoliths (Haldor Topsøe, Denmark) were used as substrates for the dip coating purpose. Fiber material consists primarily of SiO_2 and also alumina and calcium to a lesser extent. The catalysts were prepared by immersing the fiber plate into zeolite suspension. Two different types of zeolites (Zeolyst International) H-Mordenite (Si/Al=10) and H-ZSM5 (Si/ Al=15) were used. The suspension was prepared by mixing the 20 wt% zeolite powder and 1wt% colloidal silica (LUDOX®HS- 30 colloidal silica, 30 wt % suspension in H_2O) with demineralized water in a wet fluid mill till a stable uniform slurry was formed. The fiber plates were immersed in the suspension for 3 min each, and the excess suspension from the channels was removed by air blowing. The coated samples were dried at 383 K for 2 h and weighed to find the gain in weight. 4 wt% Cu-zeolite plate type catalysts were prepared by incipient wet impregnation using appropriate amounts of copper nitrate (Aldrich, 99.99%) solution as a precursor on zeolite coated plates. The samples were finally calcined at 500^{o}C for 4 h at a heating rate of 2^{o}C/min.

To expose the Cu/zeolite catalysts to alkali poisons under more realistic conditions monolith catalysts were placed in a pilot plant reactor and exposed to well-defined aerosols of KCl [4]. For the comparison purpose commercial vanadium catalyst (VWT) provided by Haldor Topsøe, Denmark is also placed in the reactor for the exposure.

5.2.3 Characterization

BET surface areas of the samples were determined from nitrogen physisorption measurements on about 100 mg sample at liquid nitrogen temperature with a Micromeritics ASAP 2010 instrument. The samples were heated to 200^{o}C for 1 h prior to the measurement.

NH_3-TPD experiments were conducted on a Micromeritics Autochem-II instrument. In a typical TPD experiment, about 100 mg of dried sample was placed in a quartz tube and pretreated in flowing He at 500^{o}C for 2h. Then, the temperature was lowered to 100^{o}C and the sample was treated with anhydrous NH_3 gas (Air Liquide, 5% NH_3 in He). After NH_3 adsorption, the sample was flushed with He (50 ml/min) for 100 min at 100^{o}C. Finally, the TPD operation was carried out by heating the sample from 100 to 650^{o}C (10^{o}C/min) under a flow of He (25 ml/min).

H_2-TPR studies were also conducted on a Micromeritics Autochem-II instrument. In a typical experiment, 100 mg of oven-dried sample was placed in one arm of a U-shaped quartz tube

on quartz wool. Prior to TPR, the catalyst sample was pretreated by flushing with air at 300 ^oC for 2 h. After pretreatment, the sample was cooled to ambient temperature thereafter the TPR analysis was carried out in a reducing mixture (50 ml/min) consisting of 5% H_2 and balance Ar (Air Liquide) from ambient temperature to 900^oC (10^oC/min). The hydrogen concentration in the effluent stream was monitored by a thermal conductivity detector (TCD) and the H_2 consumption values were calculated from calibration experiments.

The SCR activity measurements were carried out at atmospheric pressure in a fixed-bed quartz reactor loaded with 10-20 mg of fractionized (180-300 µm) or 1.7 x 1.7 cm^2 (catalyst late) catalyst samples positioned between two layers of inert quartz wool. The reactant gas composition was adjusted to 1000 ppm NO, 1100 ppm NH_3, 3.5% O_2, 2.3% H_2O and balance N_2 by mixing 1% NO/N_2 (±0.1% abs.), 1% NH_3/N_2 (0.005% abs.), O_2 (≥99.95%) and balance N_2 (≥99.999%) (Air Liquide) using Bronkhorst EL-Flow F-201C/D mass-flow controllers. The total flow rate was maintained at 500 ml/min (ambient conditions). During the experiments the temperature was increased stepwise from 200 to 600^oC while the NO and NH_3 concentrations were continuously monitored by a Thermo Electron's Model 17 C chemiluminiscent NH_3-NO_x gas analyzer. Fresh and poisoned catalysts are compared by change in relative activity (%) of the corresponding catalysts. The catalytic activity is represented as the first-order rate constant (cm^3/g.s), since the SCR reaction is known to be first-order with respect to NO under stoichiometric NH_3 conditions [4].

5.3 Results and Discussion

5.3.1 Vanadium based catalysts

Fig. 5.1 shows the catalytic activity profiles for the optimum zeolite catalysts. Among all the supports HMORDENITE showed the highest rate constant followed by HZSM5, HY and HBETA. Importantly, the rate constant value of 12% V_2O_5-MOR (430 cm^3/g.s) catalyst was comparable to that of commercial V_2O_5–WO_3/TiO_2 catalyst (500 cm^3/g.s) reported in the literature [5] at 420^oC reaction temperature. Catalytic activity of zeolite supports was studied at 420 ◦C. Supports showed rate constant (cm^3/g·s) values of 46, 38, 28 and 26 for HMORDENITE, HZSM5, HBETA and HY, respectively. All these rate constant values are well below 10% of the NO conversion.

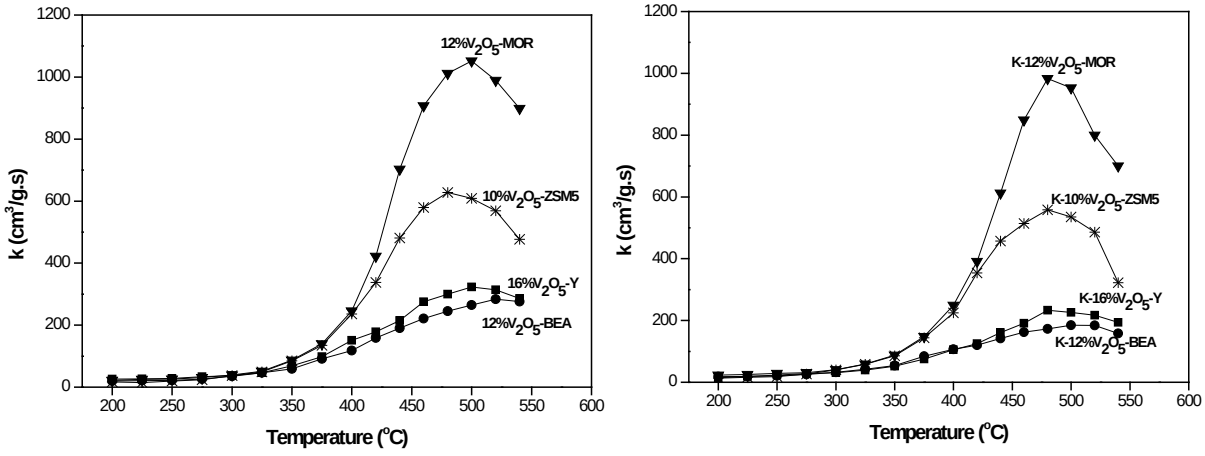

Figure 5.1 Catalytic activity profiles of undoped and potassium-doped catalysts with optimum V_2O_5 content.

Doping the optimum catalysts with potassium (100 µmol/g) resulted in slight decrease in activity and a small shift of maximum catalytic activity towards lower temperature (Fig. 5.1). Especially the HMORDENITE catalyst showed increased resistance to the alkali poisoning and was deactivated by 9% only at 500^{o}C, whereas the other catalysts with HZSM5, HY and HBETA support material were deactivated by 11%, 30% and 35%, respectively at their T_{max} temperatures. The deactivation was even lower at 400^{o}C, the temperature of operation in most power plants. In general, high dispersion of vanadium, high surface area and high surface acidity of zeolites enable hosting of potassium oxide with relatively little change in total acidity. Consequently, the potassium deactivation was significantly lower in the present catalysts compared to that of traditional SCR catalysts. In traditional catalysts 45% deactivation has been observed at around 400^{o}C on highly active V_2O_5–WO_x/ZrO_2 catalyst with even less potassium loading, i.e. of 80 µmol/g [6]. The important deactivation resistance parameters for metal oxide support materials suggested by Due-Hansen et al. [5] are low vanadium coverage (below monolayer), high surface area, and high surface acidity. These three crucial parameters are all reached by the HZSM5 and HMORDENITE catalysts studied in this work. For zeolite supports an additional structural parameter concerned with the size of micropores can also alter the SCR catalytic activity [7,8], as also found in this study.

Table 5.1 Maximum rate constant, surface area, pore volume and NH_3-TPD characterization results of undoped and potassium-doped catalysts with optimum V_2O_5 content.

Catalyst	k_{max} ($cm^3/g.s$)	Surface area (m^2/g)	Micropore volume (cm^3/g)	Acidity (µmol/m^2)	$T_{max}1$ (°C)	$T_{max}2$ (°C)
16% V_2O_5-Y	323	524	0.24	2.42	176	321
12% V_2O_5-HBEA	284	510	0.19	3.24	184	339
10% V_2O_5-ZSM5	628	324	0.10	3.72	188	376
12% V_2O_5-MOR	1052	348	0.13	4.58	188	410
K-16% V_2O_5-Y	233	488	0.23	2.00	171	318
K-12% V_2O_5-BEA	185	497	0.18	3.04	179	330
K-10% V_2O_5-ZSM5	558	298	0.09	3.59	184	370
K-12% V_2O_5-MOR	983	322	0.12	4.56	177	396

$T_{max}1$ (°C) and $T_{max}2$ (°C) are low temperature (100–300°C) and high temperature (300–500°C) NH_3-TPD regions, respectively.

The results of the NH_3-TPD are also summarized in Table 5.1. The order of the acidity and the SCR activity of the catalysts were: 12%V_2O_5-MOR > 10% V_2O_5-ZSM5 > 12% V_2O_5-BEA > 16% V_2O_5-Y. All the catalysts showed $T_{max}1$ peak at around 175–190 ^{o}C, while the strong acid sites $T_{max}2$ peak was significantly increased to 410^{o}C for the HMORDENITE catalyst due to its high acid site density. It was also interesting to see the influence of vanadium presence on support in enhancing the total acid sites. Pure zeolites exhibited acid site density (µmol/m^2) values of 2.83, 2.53, 2.15 and 2.07 for HMORDENITE, HZSM5, HBEA and HY, respectively. When the supports were impregnated with vanadium enhanced acid site density (µmol/m^2) values of 4.58, 3.72, 3.24 and 2.42 for 12%V_2O_5-MOR, 10% V_2O_5-ZSM5, 12% V_2O_5-BETA and 16% V_2O_5-Y, respectively.

Hence, both structural and acidic characteristics favored the HMORDENITE catalysts in SCR of NO compared to the other catalysts, in accordance with the activity measured.

The results of the N_2-BET surface area, surface density of V_2O_5, micropore volume and acidity measurements are also summarized in Table 5.1 for potassium-doped catalysts. Upon the addition of potassium the surface area and pore volume slightly decreased, which can be the result of specific interaction of the potassium with the support material as well as partial physical blocking of the support pores. Total acidity of the potassium oxide doped catalysts also decreased slightly compared to the analogous undoped samples. Furthermore, the $T_{max}1$ and $T_{max}2$ positions of the potassium doped catalyst shifted about 10^{o}C to lower temperatures, indicative of lower relative strengths of the acid sites. Assuming that potassium oxide first occupy the strongest acid sites present on the support and then weakens the remaining acid sites due to electron donation, the T_{max} should be expected to shift towards lower temperature region, as observed.

5.3.2 Iron based catalysts

Table 5.2 shows the surface Fe content of the catalysts measured by EDX analysis. Fe-MOR, Fe-ZSM5 and Fe-BEA catalysts were found to be have Fe composition of 3.0, 3.2 and 5.6 wt%, respectively. In general, the metal exchange capacity of a zeolite is a function of Si/Al ratio, surface area and pore size [9].

Table 5.2 Characterization of Fe-zeolite catalysts.

Catalyst	Si/Al ratio	Fe content[a] (wt%)	K/Fe[b] ratio	Fe/Al ratio	Surface acidity (µmol/g)		
					Support	catalyst	K-doped[b]
Fe-MOR	10	3.0	0.93	0.38	1418	1837	905
Fe-ZSM5	15	3.2	0.87	0.58	1062	1286	660
Fe-BEA	25	5.6	0.49	1.60	1008	1242	637

[a] Fe content measured by EDX analysis.
[b] Potassium-doped catalysts containing 500 µmol/g of potassium.

The catalytic activity of undoped and potassium-doped Fe-zeolite catalysts from 200-600^{o}C is reported in Fig. 5.2 by the rate constant k (cm^3/g.s). The Fe-BEA catalyst reached maximum activity about 500^{o}C while Fe-ZSM5 and Fe-MOR catalysts reached maximum around 525^{o}C, all yielding rate constants around 1600 cm^3/g.s above 450^{o}C. These T_{max} activities were higher than that obtained with commercial vanadium catalysts at the optimal reaction temperature i.e. (420^{o}C) [5,6,10]. Generally, Fe-zeolite catalysts obtain their maximum activity over a wide temperature range between 425-575^{o}C, whereas vanadium-based formulations perform best in a much more narrow temperature range from 375-425^{o}C. Consequently, Fe-zeolite catalysts with high activity and a wider range of operating temperatures could also prove applicable for automotive applications. The potassium-doped Fe-zeolite catalysts with a maximum potassium concentration of 500 µmol/g of catalyst showed decreased catalytic activity compared to that of the fresh catalysts in the order: K-Fe-MOR (780 cm^3/g.s) > K-Fe-ZSM5 (680 cm^3/g.s) > K-Fe-BEA (300 cm^3/g.s) at 500-525^{o}C.

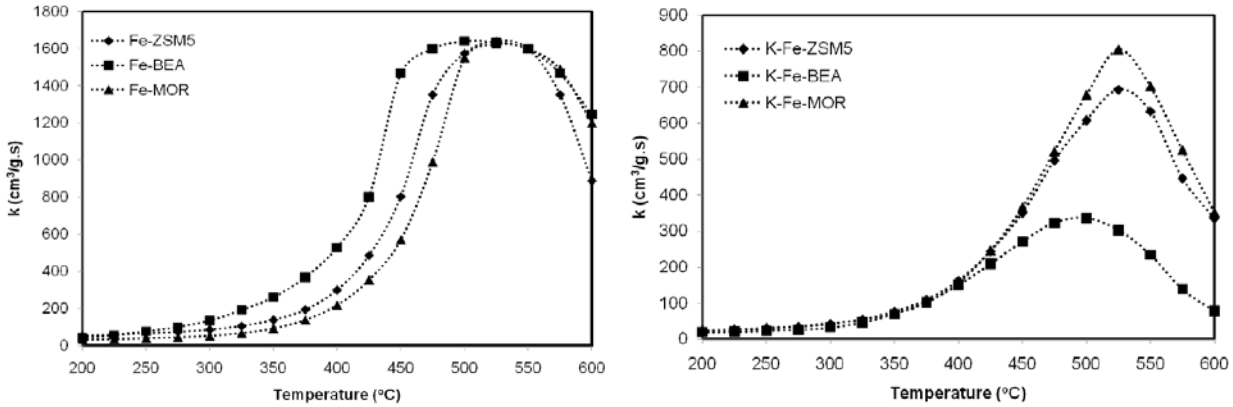

Figure 5.2 Catalytic activity profiles of fresh Fe-zeolite and K-Fe-zeolite catalysts.

Fig. 5.3 shows the relative activity of potassium-doped Fe-zeolite catalysts and commercial vanadium catalyst with different potassium loadings at 400^{o}C, which is a normal operation temperature in commercial stationary SCR units. It was observed that with increase of potassium concentration from 0-500 μmol/g a gradual decrease in the relative activity of Fe-zeolite catalysts occurred, while the commercial VWT catalyst deactivated rapidly even at lower potassium concentration. Hence, with 100 μmol/g of potassium loading the Fe-zeolite catalysts still showed about 90% (or more) of their original activity, whereas the activity of the commercial VWT catalyst had decreased by 60%. Upon further increase in potassium concentration Fe-MOR and Fe-ZSM5 maintained a superior alkali resistivity compared to that of Fe-BEA which, however, still performed significantly better than the commercial VWT catalyst, which only maintained about 10% of its activity under these reaction conditions. Comparing Fe-ZSM5, Fe-BEA and Fe-MOR catalysts at high reaction temperature 500^{o}C showed a relative activity of 39%, 20% and 44%, respectively. Even at 500^{o}C with 500 μmol/g of potassium Fe-MOR and Fe-ZSM5 catalysts performed well. It was reported that the relative activity of the catalysts decreases with increase of reaction temperature [5]. Such a decrease of relative activity with increasing reaction temperature could be due to increased mobility of deactivation species [4]. Supplementary activity studies with SO_2 containing reaction gas were not performed with the Fe-zeolite catalysts since biomass (e.g. straw or wood chips) has very low content of sulfur [11].

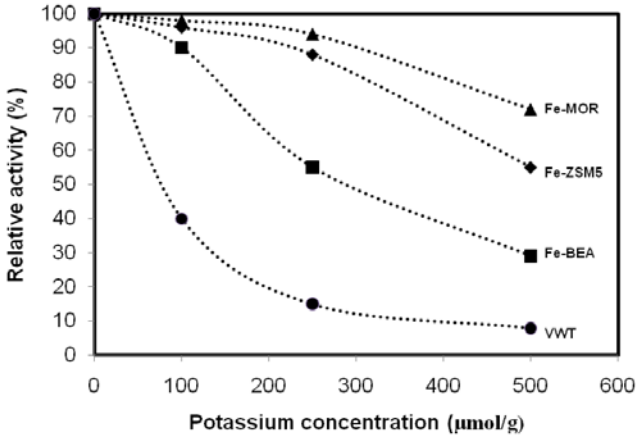

Figure 5.3 Relative catalytic activity of Fe-zeolite and VWT (3wt%V_2O_5-10wt%WO_3/TiO_2) catalysts with different potassium concentrations at 400^{o}C.

SCR of NO with ammonia is a feasible reaction on a catalyst having optimal redox and acidic properties. The difference in acidic and redox properties of the freshly prepared and the potassium poisoned catalysts could give more insight about the observed catalyst deactivation. Surface acidity of the zeolites, the Fe-zeolite catalysts and the potassium doped Fe-zeolites catalysts are reported in Table 5.2. Acidity of the pure zeolites were in the order of MOR > ZSM5 > BEA. This order remained also upon Fe exchange into the zeolites, where the acidity increased even further by around 20%. Due to the pronounced acidity originating from the support these are promising acid scavenging materials for alkali resistant SCR applications. The acidity of the potassium poisoned catalysts were also found to be in the order of K-Fe-MOR > K-Fe-ZSM5 > K-Fe-BEA, as expected. However, after doping with potassium (500 μmol/g of catalyst) Fe-MOR, Fe-ZSM5 and Fe-BEA catalysts lost surface acidic sites of 932, 626 and 605 μmol/g of catalyst, respectively, corresponding to about half their acidic sites. Thus, overall the Fe-zeolite catalysts maintained appreciable surface acidity also at high potassium concentration. In comparison, the commercial vanadium catalyst looses all surface acidic sites even at the low potassium concentration of 100 μmol/g of catalyst [5,6,10]. This superior potassium resistivity is directly related to the high surface area and acidity of the zeolite supports as compared to those of conventional metal oxides like, e.g. ZrO_2 and TiO_2, since these characteristics allow the SCR active metals to be well protected from the potassium poisions by providing dense acidic sites as hosts.

The redox properties of the Fe-zeolite and K-Fe-zeolite catalysts were also characterized by H_2-TPR. The obtained results are shown in Fig. 5.4. The reduction of Fe species on the Fe-zeolites started at 200^{o}C and continued till 900^{o}C with profiles broadly divided into three regions; low temperature reduction region between 200-400^{o}C, medium temperature reduction region between 500-700^{o}C and high temperature reduction region above 800^{o}C. The low temperature reduction peak can be attributed to the reduction of Fe^{3+} to Fe^{2+} species, where Fe^{3+} is located at the Brønsted acid sites of the zeolite, as also reported on Fe-ZSM5 **[**12]. This region had one intense reduction peak and a small shoulder peak on Fe-MOR corresponding to the reduction of iron species at two different sites as also observed on Fe-MOR catalysts prepared from $FeCl_2$ [13]. The medium temperature reduction peak corresponds to reduction of small nanoclusters of Fe_3O_4 to

FeO and the high temperature reduction peak to reduction of Fe^{2+} to Fe^0 along with zeolite framework collapse [14].

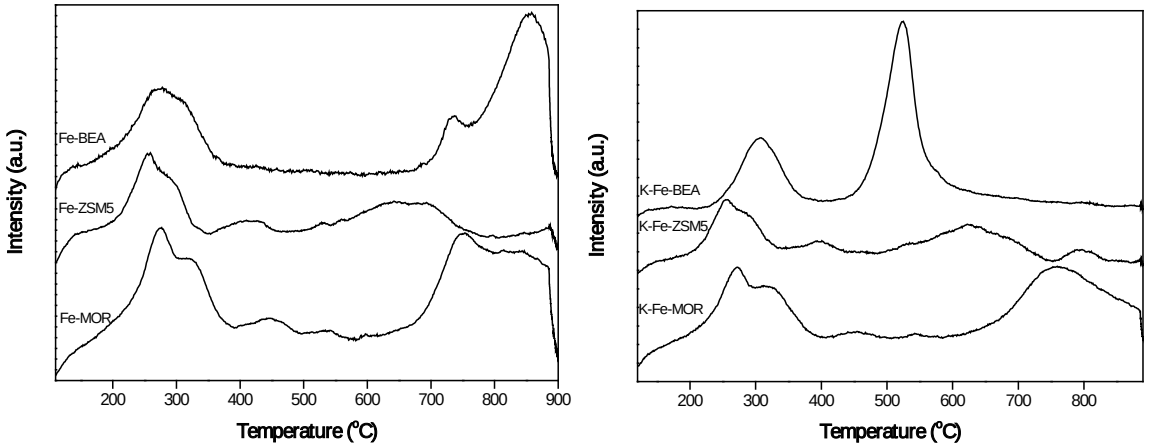

Figure 5.4 H_2-TPR profiles of Fe-zeolites and K-Fe-zeolites.

As evidenced in Fig. 5.4, H_2-TPR profiles of the Fe-zeolite changed slightly with type of support and amount of Fe content. Moreover, the potassium doped catalysts showed similar TPR profiles as that of fresh Fe-zeolite catalysts except a small change of the high temperature reduction peak of the K-Fe-BEA catalyst. Here the peak position was changed from 850^{o}C to 550^{o}C after doping with potassium, possibly due to reduction of formed potassium ferrate or potassium-containing iron. Previously it has been reported that potassium-containing iron substances are reduced between 600-700^{o}C [15]. Potassium ferrate formation was not observed on Fe-MOR and Fe-ZSM5, most likely because the support have sufficient acid sites to host the potassium thus protecting the active Fe.

5.3.3 Copper based catalysts

Activity vs. temperature of 4 wt% Cu-MOR, 5 wt% Cu-ZSM5 and 5 wt% Cu-BEA catalysts are shown in Fig. 5.5 at various potassium loadings. Optimum Cu-MOR, Cu-ZSM5 and Cu-BEA catalysts showed maximum rate constant values of 2542, 2315 and 2646 at their T_{max} of 425, 450 and 500 ^{o}C, respectively. All the catalysts showed high rate constants at the different T_{max}. The different T_{max}, exhibited during the SCR of NO seems to be a function of ease of reduction of copper oxide during the reduction cycle Irrespective of the T_{max} obtained the rate constants observed on these Cu/zeolites are much higher than for commercial vanadium based catalysts. The plots of activity vs. temperature are characteristic of NO conversion occurring on both CuO aggregates and cationic Cu species [16].

The potassium poisoned catalysts showed decreased SCR activity with increasing K/Cu molar ratios. At low K/Cu molar ratio up to 0.20 essentially no influence on the SCR activity was observed and only upon further increase of potassium concentration a slight decrease in activity was observed. The superior performance of these catalysts can be observed even at high potassium concentrations, whereas conventional catalysts like, e.g. V_2O_5/WO_3-TiO_2, V_2O_5/Sulphated-ZrO_2 and V_2O_5/WO_3-ZrO_2 are poisoned severely at a K/V molar ratio of 0.3 where the active hydroxy vanadates are transferred to potassium vanadates [5,10,17,18]. The relative activity of Cu/zeolites

and VWT catalysts with different potassium loadings is shown in Fig. 2.5 at 400^{o}C. All Cu/zeolite catalysts showed a similar relative activity of 90% at a loading of 100 µmol/g of potassium, while the VWT catalyst was performing only at 40%. Upon further increase of the potassium concentration Cu-zeolites experienced a slight drop in relative activity in the order of Cu-MOR<Cu-BEA<Cu-ZSM5 while the VWT catalyst was deactivated severely.

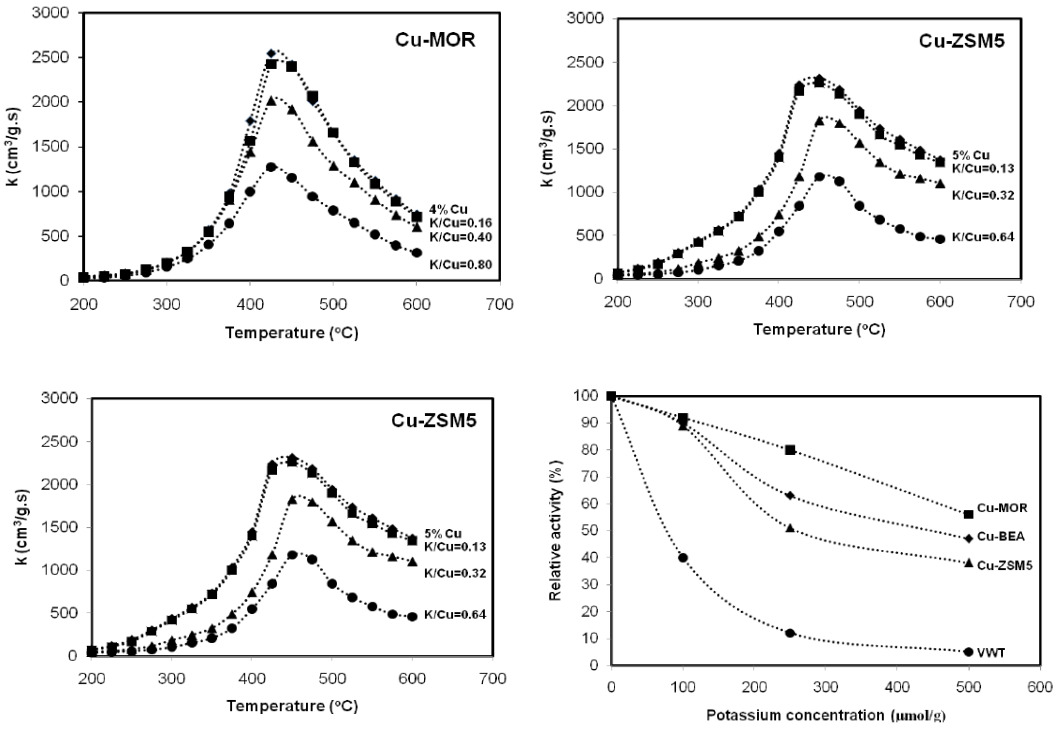

Figure 5.5 SCR activity of Cu/zeolites at various K/Cu molar ratios and relative activity of Cu/zeolite and VWT (3wt%V_2O_5-10wt%WO_3/TiO_2) catalysts at various potassium concentrations.

Table 5.3 catalyst composition and NH_3-TPD results of Cu/zeolite catalysts.

Catalyst	Si/Al ratio	Cu wt%	K/Cu ratio	Cu/Al ratio	Surface acidity (µmol/g)		
					Support	catalyst	K-doped[a]
Cu-MOR	10	4.0	0.80	0.44	1418	1908	1064
Cu-ZSM5	15	5.0	0.64	0.78	1062	1408	823
Cu-BEA	25	5.0	0.64	1.26	1008	1702	1028

[a] K-doped catalysts containing 500 µmol/g of potassium.

Table 5.3 shows NH_3-TPD results of fresh and potassium doped Cu/zeolite catalysts. The total acidity of the pure zeolites follow the order MOR>ZSM5>BEA. The acidity of the fresh and potassium poisoned catalysts were:Cu-MOR>Cu-BEA>Cu-ZSM5. Even at high potassium loadings (K/Cu 0.80 or 0.64) the catalysts showed significant surface acidity, while V_2O_5 supported metal oxide catalysts losses the surface acidic sites at a K/V ratio of 0.3 [5,10,17,18]. This two-fold increased potassium resistivity is most probably due to the unique support properties of zeolites with high surface area and acidity compared to conventional metal oxide carriers. Doping all the

catalysts with similar amount of potassium (500 µmol/g) a loss of 844, 674 and 585 µmol/g of acid sites were found on Cu-MOR, Cu-BEA and Cu-ZSM5 catalysts, respectively. This loss of more than one mole of acid sites, estimated from the uptake of NH_3, per mole of potassium added might be due to partly coordination of K_2O to Cu^{2+} hindering the formation of $Cu^{2+}(NH_3)_2$ complexes. SCR active metals on zeolites might thus be well protected from potassium poisoning by the partly bonding to numerous acidic sites on the carrier attracting the potassium salts.

5.3.4 Copper based monolith catalysts

SCR activity of fresh and potassium chloride aerosol exposed 4 wt% Cu-MOR, 4 wt% Cu-ZSM5 and VWT catalysts are shown in Fig. 5.6. 4 wt% Cu-MOR, 4 wt% Cu-ZSM5 and VWT catalysts showed rate constant values of 94.3, 132.7 and 47.8 $cm^3/g.s$ at 350^{o}C, respectively. The rate constants observed on these Cu/zeolites are much higher than commercial VWT catalyst. It was also know from the powder based catalysts that the Cu/zeolite catalysts are highly active when compared to commercial vanadium based catalysts.

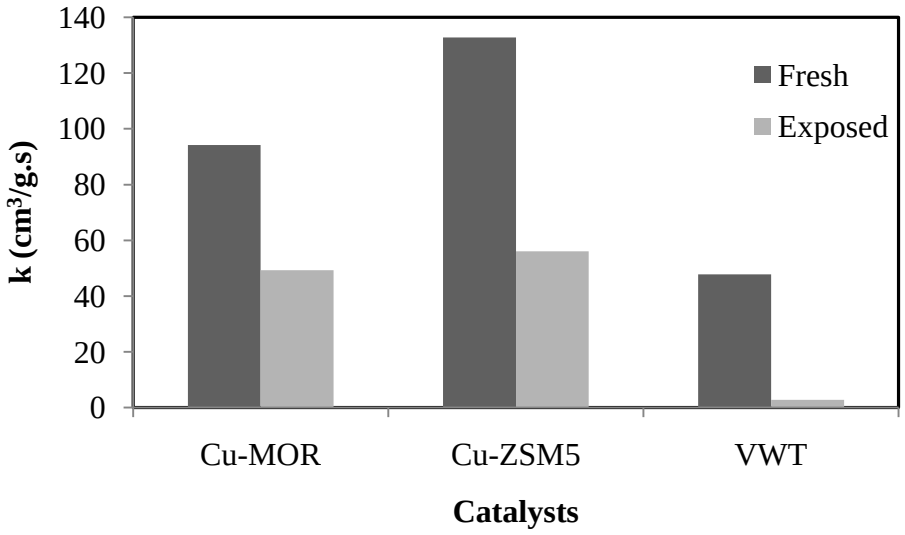

Figure 5.6 SCR activity of fresh and potassium chloride aerosol exposed 4 wt% Cu-MOR, 4 wt% Cu-ZSM5 and VWT (3wt%V_2O_5-10wt%WO_3/TiO_2) catalysts.

Potassium chloride aerosol exposed catalysts after 50 days showed decrease in activity. Aerosol exposure measurements are more realistic and give in depth knowledge about the deactivation phenomena. Aerosol exposed Cu-MOR, Cu-ZSM5 and VWT catalysts showed rate constant values of 49.3, 56.0 and 2.3 $cm^3/g.s$ at 350^{o}C, respectively. Aerosol exposed commercial VWT catalyst showed no activity and that of Cu/zeolites showed appreciable activity. Cu-MOR, Cu-ZSM5 and VWT catalysts showed relative activity (k_{expo}/k_{fresh}) of 0.523, 0.422 and 0.057, respectively. Aerosol exposure deactivation measurements are similar to the fractionized powder based deactivation measurements. However, the activity of aerosol exposed plate shaped catalysts is globally lower since the synthesized plates contain binder material which dilutes the active components and since the pressed plates results in less exposed catalyst surface compared to a

catalyst material consisting of the much smaller individual particles found in the fractionized powders measured in e.g. the previous selections of this chapter and elsewhere in the report.

5.4 Conclusions

In summary, V_2O_5/zeolite, Cu/zeolite and Fe/zeolite catalysts are highly active for the SCR of NO with NH_3 and exhibit high resistance to alkali poisoning. Acidic properties of Cu/zeolites are well preserved after poisoning with potassium unlike that of commercial V_2O_5/TiO_2 catalysts. Unique support properties like high surface area and surface acidity seems to be essential properties for the high alkali resistance. Zeolite based catalysts could therefore be attractive alternatives to conventional SCR catalysts for biomass fired power plant flue gas treatment.

5.4 References

[1] M.E. Davis. Acc. Chem. Res. 26(1993) 111.
[2] D.W. Breck. Zeolite Molecular Sieves. Wiley: New York, 1974.
[3] W.M. Meier, D.H. Olson, Ch. Baerlocher, Atlas of Zeolite Structure Types, 4th Edition. Elsevier: London, 1996.
[4] Y. Zheng, A.D. Jensen, J.E. Johnsson, J.R. Thøgersen, Appl. Catal. B 83 (2008) 186.
[5] J. Due-Hansen, S. Boghosian, A. Kustov, P. Fristrup, G. Tsilomelekis, K. Ståhl, C.H. Christensen, R. Fehrmann, J. Catal. 251 (2007) 459.
[6] J. Due-Hansen, A.L. Kustov, S.B. Rasmussen, R. Fehrmann, C.H. Christensen, Appl. Catal. B 66 (2006) 161.
[7] G.T. Went, L.-J. Leu, R.R. Rosin, A.T. Bell, J. Catal. 134 (1992) 492.
[8] H. Tian, E.I. Ross, I.E. Wachs, J. Phys. Chem. B 110 (2006) 9593.
[9] S.S.R. Putluru, A. Riisager, R. Fehrmann, Appl. Catal. B 97 (2010) 333.
[10] A.L. Kustov, M. Yu. Kustova, R. Fehrmann, P. Simonsen, Appl. Catal. B 58 (2005) 97.
[11] N. Afgan, M.G. Carvalho, M. Jovanovic, Int. J. Sustain. Energy. 26 (2007) 179.
[12] R.Q. Long, R.T. Yang, J. Catal. 207 (2002) 274.
[13] I. Melián-Cabrera, S. Espinosa, J.C. Groen, B. v/d Linden, F. Kapteijn, J.A. Moulijn, J. Catal. 238 (2006) 250.
[14] A. Guzmán-Vargas. G. Delahay, B. Coq, Appl. Catal. B 42 (2003) 369.
[15] S.C. Ndlela, B.H. Shanks, Ind. Eng. Chem. Res. 42 (2003) 2122.
[16] S. Kieger, G. Delahay, B. Coq, B. Neveu, J. Catal. 183 (1999) 267.
[17] J.P. Chen, R.T. Yang, J. Catal. 125 (1990) 411.
[18] Y. Zheng, A.D. Jensen, I.E. Johnsson, Ind. Eng. Chem. Res. 43 (2004) 941.

6. Structural characterization of bis(1,1,3,3 tetramethylguanidine) dichromate

6.1 Introduction

The traditional SCR catalyst is operating at temperatures around 300-400º C [1]. Due to this relative high temperature, the SCR unit is often placed upstream of flue gas cleaning units (e.g. desulfurizer, electrostatic particle remover) to avoid costly reheating of the gas. However, the environment contains high concentrations of dust promoting accelerated deactivation of the catalyst. Placement the unit in the downstream position of the cleaning units would thus solve the deactivation of the catalyst, but also lower the temperature of the flue gas and consequently the activity of the catalyst, since the low-temperature activity of the traditional SCR catalysts is negligible. Accordingly, efforts have been made to develop catalysts operating in the range 80-280°C [2-8], which would render placement of the SCR unit possible in the tail end after the desulfurizer and particulate control installations.

Recent studies have shown that chromium and/or manganese oxides exhibit good low-temperature SCR potential [9,10], but their N_2-selectivity and sulfur resistance need to be improved. Schneider et al. [11] reported higher selectivity to N_2 (>90%) for a range of titania-supported chromia catalysts (i.e. CrO_2 Cr_2O_3, CrOOH), but the catalytic performance, such as N_2O selectivity, was very sensitive to the phase of the chromium oxide. The low-temperature SCR activity of a newly characterized compound of chromium, tetramethylguanidinium dichromate is here examined, which was first reported by Kim et al. [12] for oxidation of alcohols.

6.2 Experimental

6.2.1 Catalyst preparation

$[TMGH]_2Cr_2O_7$ was synthesized by mixing 1,1,3,3-tetramethylguanidine, TMG (Aldrich, 99%) with absolute ethanol in the molar ratio 1:5 according to the following reaction:

$$2TMG + 2(NH_4)_2CrO_4 \rightarrow [TMGH]_2Cr_2O_7 + 4NH_3(g) + H_2O$$

The slurry was stirred overnight before the ethanol and water were subsequently removed under reduced pressure with a rotary evaporator. Finally the residue was dried in a vacuum oven at 60°C.
The preparation of 20 wt% $[TMGH]_2Cr_2O_7$ supported on titania (8.2 mol% Cr/TiO_2) was performed by initial mixing of TMG, $(NH_4)_2CrO_4$ and absolute ethanol in a molar ratio of 1:1:35. To the resulting slurry, TiO_2 (Aldrich, nanopowder, 99.7% anatase) was then added and the mixture stirred overnight before solvent and water were removed under reduced pressure in a rotary evaporator.

6.2.2 Characterization

Powder diffraction data was collected on a Huber G670 Guinier camera using $CuK\alpha_1$ radiation. The samples were placed in a thin layer on scotch tape and rotated during data collection. Data were

collected for 4h in the range 3–100° in steps of 0.005° in 2θ. The patterns were indexed by the program ITO [13] and the crystal structure solved by EXPO [14,15]. The structure was refined by WINPOW (a local variation of LHMP) [16]. Moreover, as the dichromate part was found to be disordered the bridging O4 was split over in two positions (the average position would give a 180° Cr-O4-Cr angle). The individual disordered positions of O1, O2 and O3 could not be resolved, but showed increased thermal parameters. The methyl groups were found rotated out of the central plane to minimize the H–H interactions in agreement with related tetramethylguanidinium structures [17].

SCR activities were measured with a Thermo Environmental chemiluminescence NO_x and NH_3-analyzer, model 17C. About 40 mg of catalyst (pressed at 2 tons, Ø = 13mm, fractionated to 180-300 μm) were fixed in a quartz plug flow reactor with a total ambient flow of 300 ml/min containing 1000 ppm NO, 1100 ppm NH_3, 3.5% O_2, 2.3% H_2O in He. The gas hourly space velocity (GHSV) was 70,000 h^{-1}. The catalytic activity was reported as the first-order rate constant k, in the first order removal of NO using the definition reported previously [18].

6.3 Results and Discussion

The results of the Rietveld refinement of the powder diffraction data of $[TMGH]_2Cr_2O_7$ are displayed in Figure 6.1 (2θ = 10-50º). Here a good agreement between the experimental and fitted data was found for the monoclinic cell. The unit cell of the system (space group $P2_1/n$) was determined to a = 10.79714 (15) Å, b = 11.75844 (16) Å, c = 8.15097 (11) Å, β = 109.5248 (6)º. The structure consists of dichromate anions ($Cr_2O_7^{2-}$) stabilized by tetramethylguanidinium cations ($[H_2NC(N(CH_3)_2)_2]^+$ or $[TMGH]^+$).

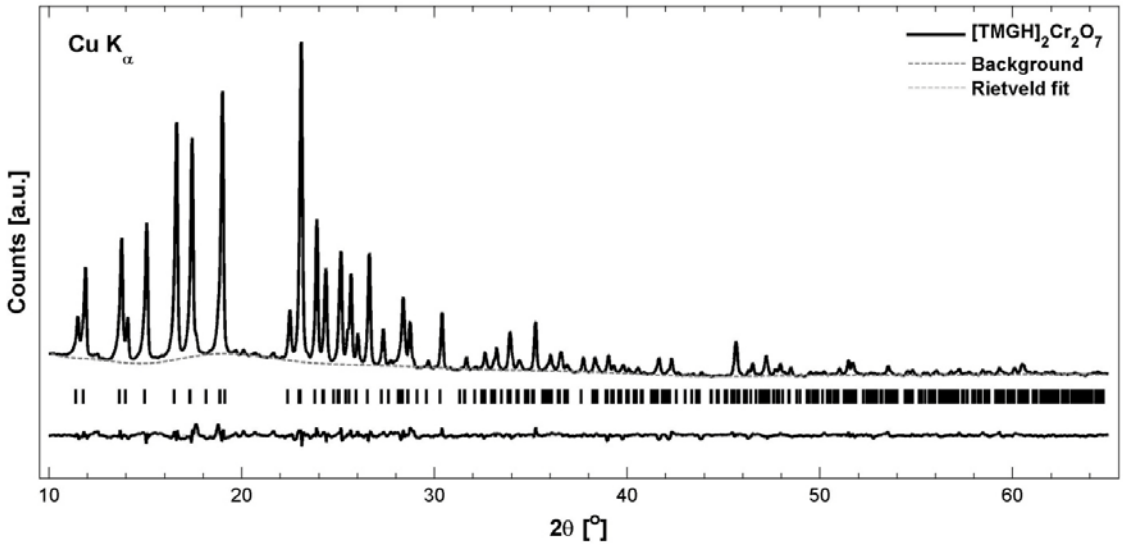

Figure 6.1 XRD diffractogram of $[TMGH]_2Cr_2O_7$ and the difference pattern from the Rietveld refinement. Markers indicate $K\alpha_1$ Bragg positions.

The determined crystal structure of $[TMGH]_2Cr_2O_7$ is presented in Figure 6.2 with both of the two possible O4 positions depicted. Note that the anion therefore is not depicted correctly from a stoichiometric point of view, but should be viewed as two different configurations, presented

simultaneously. Thus, the average position of the bridging oxygen in the Cr1-O4-Cr1 is the 180º configuration. The guanidine part of the tetramethylguanidinium cation group has a planar configuration due to the C1=N3 double bond. The C-N bond distances for the guanidinium molecule are all in agreement with those reported by Bujak and Zaleski [17].

For the $Cr_2O_7^{2-}$ group, the length of the Cr-O bond with the bridging O4 atom was 1.746-1.782 Å and the terminal Cr-O bonds were in the range 1.404-1.585 Å. The slightly shorter bond lengths of the terminal Cr-O bonds observed here than reported for the guanidinium dichromate [19], consistent with the disorder of the dichromate ion due to the alternative O4 sites.

The hydrogen bonds H1···O2 and H2···O3 cross-links the iminium-part of $[TMGH]^+$ with dichromate ions in the (101) plane, thus forming layers connected by ionic and van der Waal's bonds (Figure 6.2b). A similar cation-anion linkage was previously reported for $[TMGH]_3Sb_2Br_9$ [17].

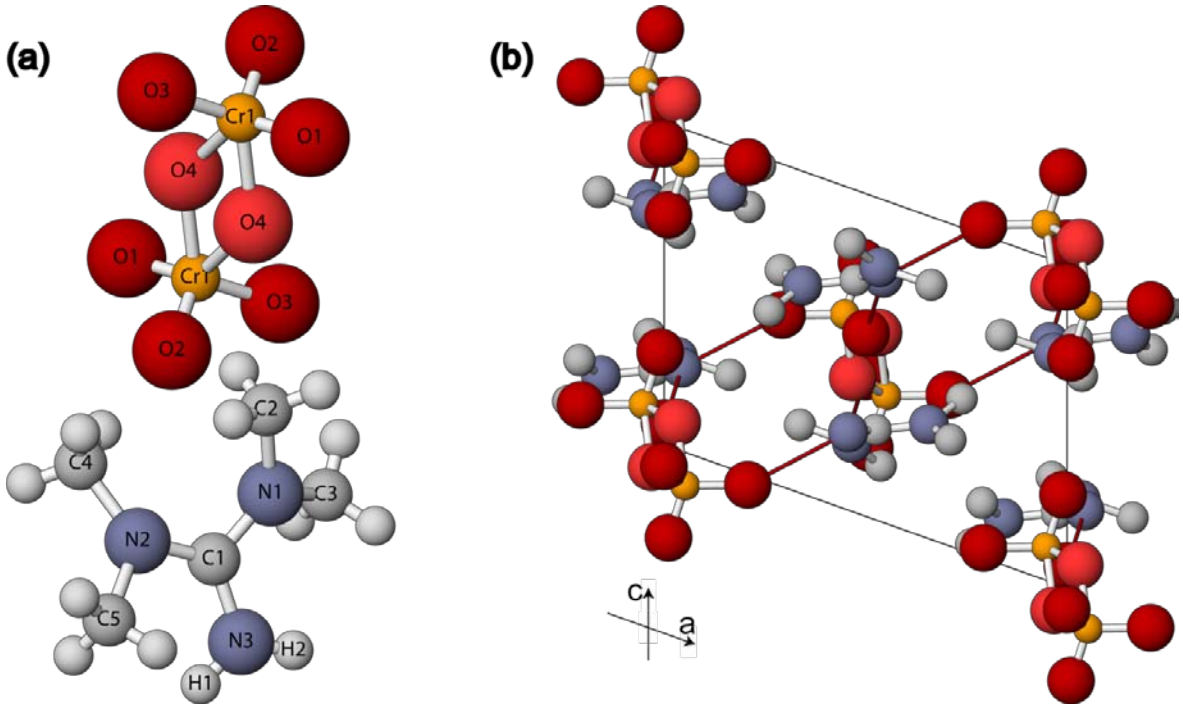

Figure 6.2 (a) The atom labels of $Cr_2O_7^{2-}$ anion displayed with the bridging O4 atom in two possible positions and the 1,1,3,3-tetramethylguanidinium cation with calculated hydrogen atoms. (b) Crystal structure and hydrogen bonds of $[TMGH]_2Cr_2O_7$ (without hydrogen atoms) viewed along the b-axis projection

The performance of $[TMGH]_2Cr_2O_7/TiO_2$ (8.2 mol% Cr/TiO_2) in conversion of NO by reduction with ammonia is depicted in Figure 53 (left) along with a CrO_3/TiO_2 (4.3 mol% Cr/TiO_2) reference catalyst. Above 200°C both samples exhibited increased NO conversion until 300°C, whereas the degree of conversion decreased at temperatures from about 325°C. The achieved low-temperature activity was considerably higher than reported by Schneider et al. [11] for various chromium oxides

on titania (10 wt% chromium oxide content), where no conversion of NO were detected below 350°C, even with a relatively low GHSV at 28,000 h^{-1}.

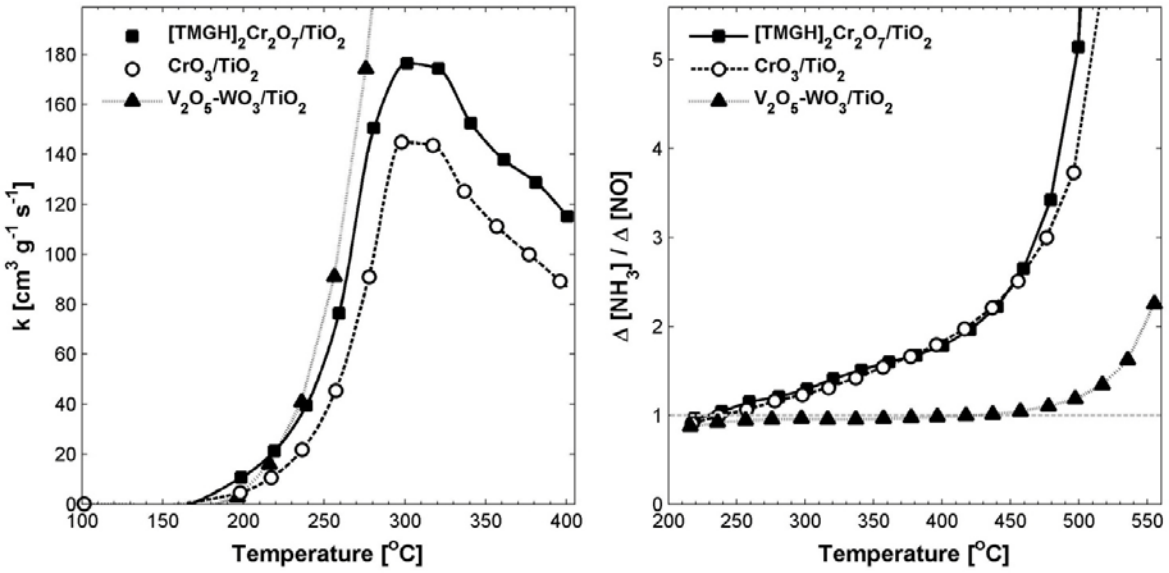

Figure 6.3 Left: SCR activity profile of TiO_2-supported $[TMGH]_2Cr_2O_7$ and two reference catalysts; Right: Relative consumption of ammonia to NO.

At all temperatures $[TMGH]_2Cr_2O_7/TiO_2$ displayed higher SCR activity than CrO_3/TiO_2, this partly can be explained by the higher loading of chromium. Furthermore, it is noteworthy that no SCR activity of $[TMGH]_2Cr_2O_7/TiO_2$ was detected at temperatures below the decomposition temperature at 171°C, thereby making the $[TMGH]_2Cr_2O_7/TiO_2$ unsuitable for SCR catalysis, although a dispersive effect of the chromium species due to the $[TMGH]_2Cr_2O_7$ can be imagined. However, after decomposition the sample exhibited activity in the reduction of NO with fairly high selectivity, resulting in formation of less than 2% NO_2 at temperatures below 325°C. At higher temperatures the chromium-based catalysts exhibited considerable oxidation of both NO and NH_3 (Figure 6.3, right), and seems thus to be more promising candidates for oxidation reactions under normal SCR operation conditions.

6.4 Conclusion

The activity in the SCR process was investigated by supporting 20 wt% of $[TMGH]_2Cr_2O_7$ on TiO_2. Minor conversion of NO was found only at temperatures above ≈170ºC (after decomposition of the salt) and thus attributed to the activity of formed chromium oxides. Furthermore, above ≈325ºC the $[TMGH]_2Cr_2O_7/TiO_2$ functioned as an oxidation catalyst which oxidized the NH_3 to nitrogen oxides, thus making it unsuited as SCR catalyst at normal operation conditions.

6.5 References

[1] G. Busca, L. Lietti, G. Ramis, F. Berti, Appl. Catal. B: Environ. 18 (1998) 1-36
[2] M. Inomata, A. Miyamoto, Y. Murikami, J. Catal. 62 (1980) 140-148
[3] F.J.J.G. Janssen, F.M.G. van den Kerkhof, H. Bosch, J.R.H. Roos, J. Phys, Chem. 91 (1987) 5921-5927
[4] L. Singoredjo, R. Korver, F. Kapeijn, J. Moulijn, Appl. Catal. B: Environ. 1 (1992) 297-316
[5] S.C. Wood, Chem. Eng. Prog. 90 (1994) 32-38
[6] J.A. Dumesic, N.-Y. Topsøe, H. Topsøe, Y. Chen, T. Slabiak, J. Catal. 163 (1996) 409-417
[7] Z. Zhu, Z. Liu, S. Liu, H. Niu, Appl. Catal. B: Environ. 23 (1999) L229-L233
[8] F. Liu, H. He, Y. Ding, C. Zhang, Appl. Catal. B: Environ. 93 (2009) 194-204
[9] J. Li, J. Chen, R. Ke, C. Luo, J. Hao, Catal. Commun. 8 (2007) 1896-1900
[10] M. Casapu, O. Kröcher , M. Elsener, Appl. Catal. B: Environ. 88 (2009) 413-419
[11] H. Schneider, M. Maciejewski, K. Köhler, A. Wokaun, A. Baiker, J. Catal. 157 (1995) 312-320
[12] S. Kim, D.C. Lhim, P.H. Lee, Bull. Korean Chem. Soc. 7 (1986) 86-87
[13] J.W. Visser, J. Appl. Cryst. 2 (1969) 89-95
[14] A. Altomare, G. Cascarano, C. Giacovazzo, M.C. Burla, G. Polodori, G. Camalli, J. Appl. Crystallogr. 27 (1994) 435-436
[15] A. Altomare, M.C. Burla, G. Cascarano, C. Giacovazzo, A. Guagliardi, A.G.G. Moliterni, G. Polodori, J. Appl. Crystallogr. 28 (1995) 842-846
[16] C.J. Howard, R.J. Hill, A computer program for Rietveld analysis of fixed wavelength X-ray and neutron powder diffraction patterns, AAEC (now ANSTO) Report M112, Lucas Heights Research Laboratory, Australia (1986)
[17] M. Bujak, J. Zaleski, J. Acta Crystallogr. E63 (2007) m102-m104
[18] J. Due-Hansen, S. Boghosian, A. Kustov , P. Fristrup, G. Tsilomelekis, K. Ståhl, C.H. Christensen, R. Fehrmann, J. Catal. 251 (2007) 459-473
[19] E. Wajsman, M. Cygler, M.J. Grabowsko, A. Stepien, Roczniki Chemii, Ann. Soc. Chim. Polonorum 50 (1976) 1587-1592

7. NO absorption in ionic liquids

7.1 Introduction

Although the catalytic removal of NO_X from the flue gas is a very effective process, the overall high operating expenses of the SCR process and possibility of ammonia slip, have motivated a search for other methods to abate emissions of nitrogen oxides [1,2]. Although technologies to remove NO and SO_2 exist, such as SO_2 scrubber, the simultaneous NO and SO_2 removal in a $Co(NH_3)_6^{2+}$ solution [3,4], or the complexation of NO with Fe^{2+}-chelates based on ethylenediaminetetraacetic acid (EDTA) or nitrilotriacetate (NTA) [2,5], they are all based on liquids with vapor pressures , which means that the solvent, to some extent, vaporizes.

Thus, the ILs can be utilized to separate gas mixtures. Recently, a promising solid ionic cation (1,1,3,3-tetramethylguanidinium) have been identified [6] for the absorption of SO_2. So far, only little information regarding the gas solubilities in ILs is reported. Besides the reports regarding CO_2 capture [7] the focus of most works evolve around the reactions taking place in the IL with the gas already absorbed. Only few reports exist on gas solubilities [8-10], but especially Brennecke et al. have contributed with a number of seminal studies on absorption of a number of gases in imidazolium-based ILs [9-12].

The focus of this chapter is to study the absorption and desorption behavior of NO in ILs based on the cation 1-ethyl-3-methylimidazolium ($[EMIM]^+$) and 1-butyl-3-methylimidazolium ($[BMIM]^+$) with some common anions, listen in Figure 7.1.

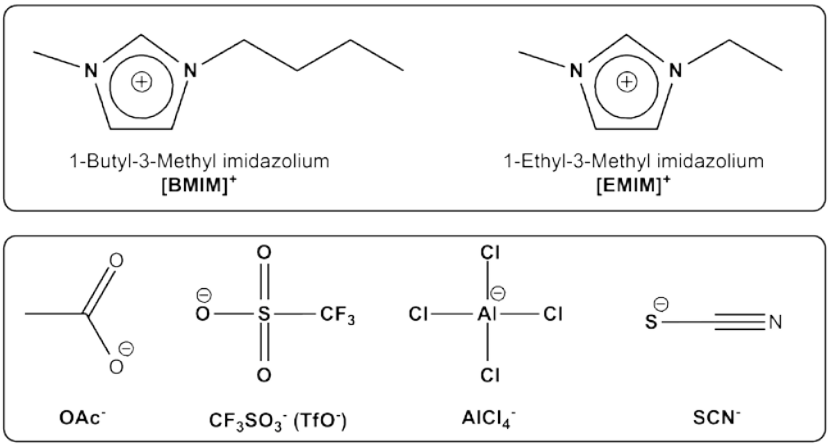

Figure 7.1 The cations and anions used for the NO absorption screening study.

7.2 Experimental

The absorption of 10% NO/N_2 were carried out at 1 bar at varying temperature, by passing the gas stream (ca. 10 ml/min) via a glass frit (Ø = 6 mm) through 100 µl of IL. The IL was loaded in cylindrical glass tubes with inlet and outlet valves. The exit of the glass frit was located in the bottom of the cylinder, as schematically outlined in Figure 7.2. The reactor was placed in a temperature controlled oven. The ionic liquids were gas saturated at room temperature before the

temperature was increased in a stepwise manner, where the solubility of NO was determined at each step. The mass increase of the IL was determined by weighing the reactors on a regular basis.

7.3 Results and discussion

A screening study of the NO absorption capacity if the ILs were carried out to determine suitable ILs. The ILs based on $AlCl_4^-$ and SCN^- all formed precipitate upon contact with the 10% NO/N_2 gas mixture, and was thus not studied further here. On the other hand, the [BMIM]OTf and the acetate-based (OAc^-) ILs exhibited promising NO absorption capacity, and were therefore selected for further studies.

The absorption of NO into [BMIM]OAc and [BMIM]OTf was measured at various temperatures at 1 bar. The absorption results presented here are all based on equilibrium measurements. The NO solubilities in [BMIM]OAc and [BMIM]OTf as a function of temperature are presented in Figure 7.3. Based on the data, it is evident that large amounts of NO can be stored in the present ILs. Especially the [BMIM]OAc exhibited an unprecedented ability to host the gas, being able to retain 4 mol of NO per mol of IL at room temperature. The absorbed NO is possible to remove subsequently by increasing the temperature. In the case of [BMIM]OTf, the NO has been completely already at 60ºC, suggesting a weak interaction between solute and the IL. In contrast, the solute-solvent interaction between NO and [BMIM]OAc is stronger and a temperature above 90ºC is required to desorb the NO.

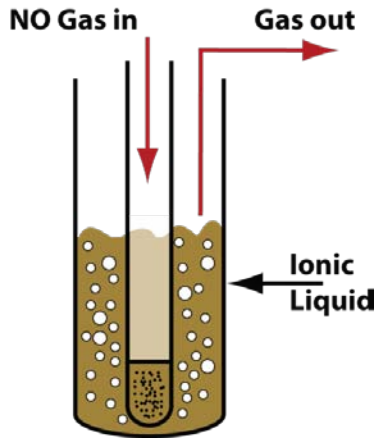

Figure 7.2 Illustration of sorption reactor.

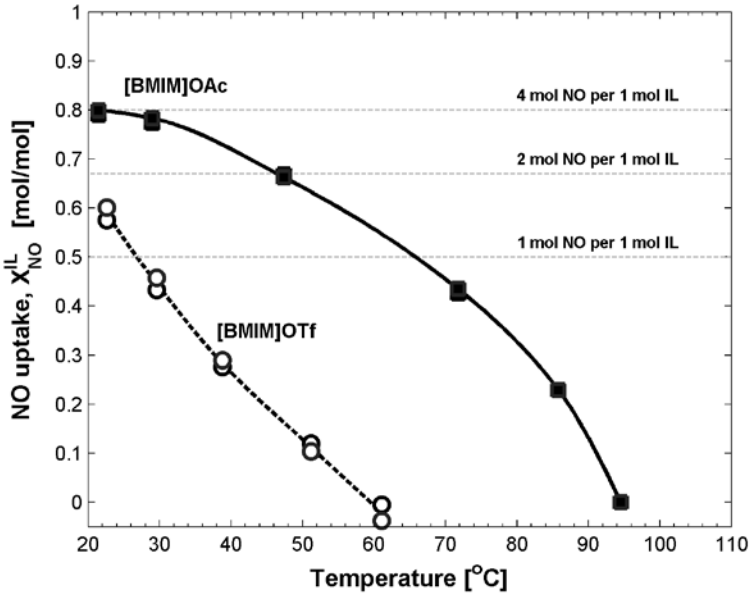

Figure 7.3 NO absorption profile of [BMIM]OAc and [BMIM]OTf.

Comparing the solubilities of NO obtained here (room temperature and 0.1 bar) with e.g. CO_2 absorbed in [BMIM]BF_4 (X_{CO2} = 0.0012, 0.1 bar) reported by Anthony et al. [12] reveal

that NO sorption capacities of [BMIM]OAc and [BMIM]OTf are several magnitudes higher. A more suitable comparison with literature data could not be performed due to the absence of NO sorption data on in the published literature.

The dissolution of NO in the ionic liquids resulted in a number of changes in the physical properties. The viscosity of the fresh and NO-saturated ILs was evaluated and the results presented in Figure 7.4. Saturating [BMIM]OAc with NO results in a dramatic decrease in viscosity from 517±5.2 mPa·s to 29.2±0.2 mPa·s, a 94% reduction. Meanwhile, the density increased from 1.053 g/cm^3 to 1.134 g/cm^3. A similar trend was observed upon saturation of the [BMIM]OTf, although the initial viscosity was somewhat lower than [BMIM]OAc. The fresh [BMIM]OTf revealed a viscosity of 84±2.5 g/cm^3, which decreased about 70% to 25.1±0.1 g/cm^3, together with a small density increase from 1.298 g/cm^3 to 1.315 g/cm^3.

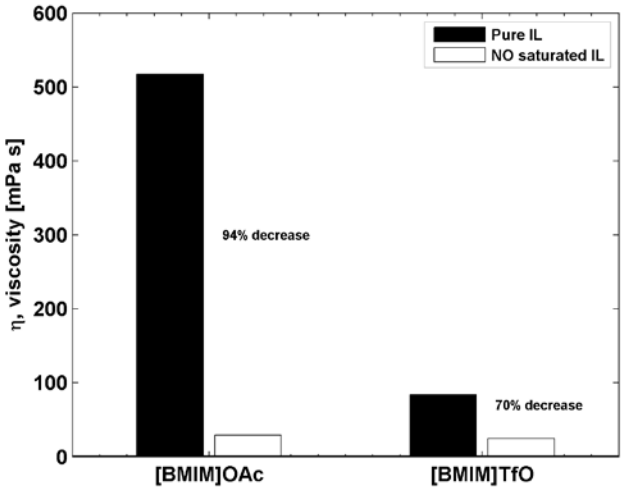

Figure 7.4 Viscosity before and after NO saturation.

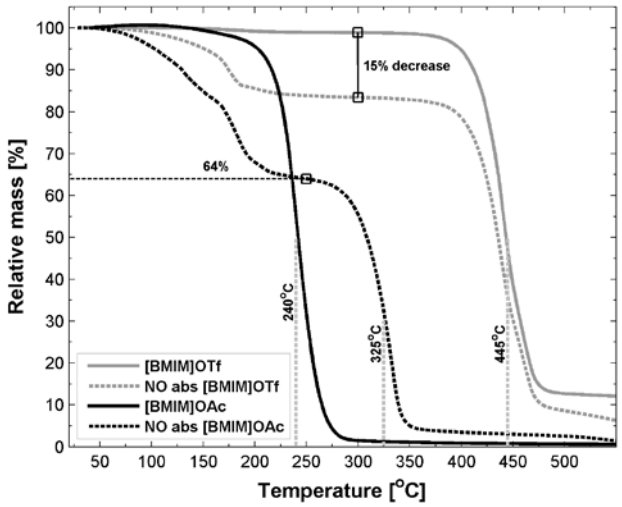

Figure 7.5 TGA of fresh and NO-saturated [BMIM]OTf and [BMIM]OAc.

The viscosities of the ILs presented here are several tens to hundred times higher than that of water at room temperature. Bonhote et al. [13] pointed out that the high IL-viscosities are largely governed by the anion-cation hydrogen bonding and van der Waals forces[2].

The significant decrease in viscosity observed upon gas sorption suggests that NO acts as a dispersive agent, decreasing the van der Waals interaction or by suppressing the CH3COO$^-$···H bonding, known to exist in [BMIM]OAc [13]. This would be in agreement with the significant reduction in viscosity observed in Figure 7.4. Although the density of the ILs increased upon saturation with NO, i.e. higher compactness, an inflation of the volume (about 20-30% increase) could be observed, confirming the presence of a large fraction of solute in the IL.

[2] The attractive or repulsive interaction between closed-shell molecules, such as permanent and induced dipole forces, dipole-dipole interactions

The thermal profile of the fresh and NO-dissolved ILs were examined with TGA. The results are presented in Figure 6.5. Considering the [BMIM]OTf, a decrease in mass of 15 wt% was observed at about 200ºC, implying the desorption of NO taking place. This is in agreement with the absorption results (cf. Figure 7.3) where a weight increase of 15 wt% was observed at room temperature for [BMIM]OTf. It can thus be concluded that the NO absorbed in the IL desorbs readily. Furthermore, the high degree of sorption-reversibility observed previously for [BMIM]OTf, was confirmed by the almost identical temperature of decomposition around 445ºC. In other words, the molecular configuration of NO-saturated [BMIM]OTf after NO desorption is roughly identical to the fresh sample, thus decomposing at similar temperature.

The TGA-profile of the NO-absorbed [BMIM]OAc in Figure 7.5 is composed of two apparent NO desorption steps around 125ºC and 180ºC. Around 250ºC the desorption stagnate, at which point the weight had decreased 36 wt%. This agrees well with the absorption results (cf. Figure 6.3) where the weight of the IL increased 40% upon saturation. Thus, about 4 wt% NO is still trapped in the [BMIM]OAc at 250ºC. The residual NO bound in the IL is likely to be responsible for the increase in decomposition temperature from about 240ºC of the commercial [BMIM]OAc to ca. 325ºC. A small fraction of the NO thus remain bound in the IL, suggesting formation of stronger bonds of covalent character between the solute and solvent, which confirms the irreversibility of the NO absorption in [BMIM]OAc observed.

7.4 Conclusion

Although some “dots” still need to be connected regarding the understanding of the exact nature of the NO absorption in [BMIM]OAc and [BMIM]OTf, the system shows promising behavior.

The absorption capacities of NO in IL reported here reveal a promising system for NO-scrubbing of dust-free tail-end gases, not requiring the addition of reductant such as ammonia or urea. Since no additive is needed to reduce the NO in the gas stream, the complexity of the NO removal system is somewhat reduced compared to the NH_3-SCR process.

Assuming that the selectivity toward NO sorption is sufficiently high, it opens new possibilities of NO removal. The captured NO could easily be removed by increasing the temperature (temperature swing), as observed previously, where only a small increase in temperature was required to remove the NO from [BMIM]OTf. Transport of the NO-saturated IL (i.e. by exploiting the differences in viscosity) or the SILP particles to another container or location followed by desorption of NO would render possible to concentrate the NO gas. Thereby the NO could subsequently be used in e.g. the Ostwald process for the production of HNO_3 in a *waste to value* concept.

For comparison of solubilities, the absorption capacities of CO_2 in ILs are considered. CO_2 capture is an area which has attracted a considerable interest over the latest years. The best IL-candidates present solubilities which are in the range of 0.5-1 mol CO_2 per mol ionic liquid (although a high partial pressure typically is required). A challenge concerning the ILs typically used is that CO_2 is strongly bound in the IL (typically $\Delta H_{sol} \approx$ -80 kJ/mol), requiring a significant amount of energy to release the CO_2 [7,14,15]. Thus, the absorption capacities of the two ILs presented here, [BMIM]OAc and [BMIM]OTf, represent considerably higher absorption capacities, being able to retain 1.5 and 4 NO molecules per IL molecule at room temperature, respectively.

Particularly the high sorption reversibility of [BMIM]OTf (and to some extent also [BMIM]OAc) represents a novel technology for the stripping of NO. Although the results presented here are slightly fragmented, and the nature of NO absorption still somewhat unknown, the first steps in the potential use of ILs for NO_x-sorption have been taken.

7.5 References

[1] Y. Mao, H. Chen, X. Long, W. Xiao, W. Li,W. Yuan, Journal of Hazardous Materials 162 (2009) 99–102

[2] F. Gambardella, M.S. Alberts, J.G.M. Winkelman, E.J. Heeres, Ind. Eng. Chem. Res. 44 (2005) 4234-4242

[3] X. Long, Z. Xin, M. Chen, W. Li, W. Xiao, W. Yuan, Separation and Purification Technology 58 (2008) 328–334

[4] X. Long, W. Xiao, W. Yuan, Ind. Eng. Chem. Res. 43 (2004) 4048-4053

[5] F. Roncaroli, M. Videla, L.D. Slep, José A. Olabe, Coordination Chemistry Reviews 251 (2007) 1903–1930

[6] J. Huang, A. Riisager, R.W. Berg, R. Fehrmann, J. Mol. Catal. A: Chem. 279 (2008) 170–176

[7] J.E. Bara, D.E. Camper, DD.L. Gin, R.D. Noble, Accounts of Chemical Research 43 (2010) 152-159

[8] A. Berger, R.F. de Souza, M.R. Delgado, J. Dupont, Tetrahedron: Asymmetry 12 (2001) 1825–1828

[9] J.L. Anthony, E.J. Maginn, J.F. Brennecke, J. Phys. Chem. B 106 (2002), 7315-7320

[10] J.L. Anderson, J.K. Dixon, J.F. Brennecke, Accounts of Chemical Research 40 (2007) 1208–1216

[11] J.L. Anthony, E.J. Maginn, J.F. Brennecke, J. Phys. Chem. B 105 (2001), 10942-10949

[12] J.L. Anthony, J.L. Anderson, E.J. Maginn, J.F. Brennecke, J. Phys. Chem. B 109 (2005) 6366-6374

[13] P. Bonhôte, A.-P. Dias, N. Papageorgiou, K. Kalyanasundaram, and Michael Grä1tzel, Inorg. Chem. 35 (1996) 1168-1178

[14] Y. Zhang, S. Zhang, X. Lu, Q. Zhou, W. Fan, X. Zhang, Chem. Eur. J. 15 (2009) 3003 – 3011

[15] D. Wappel, G. Gronald, R. Kalb, J. Draxler, International Journal of Greenhouse Gas Control 4 (2010) 486–49

8. Protective coating materials for alkali resistant SCR catalysts

8.1 Introduction

Despite extensive contributions to the literature since 1975 regarding selective catalytic reduction (SCR) catalysis with ammonia for NO_x removal from combustion gases, there is still on-going, controversial discussion in academia concerning both catalytically active sites in the SCR catalyst and deactivation phenomena with regard to practical SCR applications. There are several strategies to limit the alkali deactivation [1], e.g. 10-20% biomass co-firing with coal, fly ash recirculation to capture the potassium and modified super acidic supports to host the alkali poisons are some of the promising strategies. Biomass co-firing and modified super acidic support approaches were part of our previous efforts to decrease the intensity of deactivation. Protective coating technique to counteract the alkali deactivation is a novel and untried approach. The objective of the present work has been to contribute to the knowledge about alternative alkali-resistant technologies for the removal of NO, with focus on protective coating technique. The attention has been on various coating materials like metal oxides and zeolites. Coated vanadia-based commercial SCR catalysts were exposed to potassium aerosols under realistic conditions. Fresh commercial and coated catalysts were exposed to alkali aerosols and their SCR activity tested.

Coating of vanadium supported TiO_2 catalyst to counteract the deactivation due to poisoning is an untried approach. The ultimate success criterion for the coating is minimal loss of activity. Since the coating must bind to the catalyst material loss of activity cannot be avoided unless the coating itself is SCR active. Two possible solutions could be interesting for selecting coating materials.

1. One would be to create a coating which acts as a physical barrier for aerosols and only allows reactant gases to reach the catalyst surface.
2. The second would be to create a coating that may be included in a neutralizing reaction towards potassium poison.

Table 8.1 shows some of the process parameters to be considered while selecting the coating materials.

Table 8.1 Coating materials parameters which influence activity.

Parameter	Effects
1. Optimum thickness	Eliminates the diffusion problems.
2. Adherence	A strong pairing prevents the coating falls off.
3. Durability	Should withstand at 300-400°C for long time in the presence of fly ash.
4. Pressure drop	Should be minimum for high efficiency of power plant.
5. Reactivity to potassium	These materials can interact with potassium forming non-poisonous neutral product, thereby protecting active vanadium.
6. Pore structure	For higher effective diffusion coefficient, improved poison resistance, etc.
7. Relative activity	Drop in initial activity after coating is expected, due to additional coating layer which acts as a resistant layer or blocks the some of the active site.

Coating materials based on physical blocking: A linear correlation between the alkali content in the ultra fine particles and the alkali accumulation on the catalyst samples has been reported [2]. The linear correlation between the accumulation of alkali on the samples and the amount of alkali in the flue gas decreases with increased particles sizes. The results clearly imply that large amounts of alkali in ultra fine particles (<100 nm) in the flue gas increased the alkali accumulation on the catalyst. Based on the above evidence, if the catalyst is protected or covered by fine particles which are less than (<100 nm) the potassium particles will deposit and accumulate on the surface, but not further penetrate into the catalyst. The promising coating materials are nano-metal oxides, zeolites, micoporous and mesoporous materials.

Use of slightly basic materials can also prevent the alkali poisons to reach the active vanadium species. The slightly basic nature of the coating expels the alkali poisons because of the basic nature of both substances. The promising materials are Mg and Mn containing materials.

Coating materials based on chemically reactive compounds toward potassium: Instead of using super acidic support materials for SCR to resist the poisoning effect, it might be used as a coating layer on the surface of vanadium supported on TiO_2. The alkali metal has to cross the coating layer before it reaches the active vanadium species there by the direct alkali attack can be minimized. The promising super acid materials are sulphated ZrO_2, WO_3-ZrO_2 and zeolites with optimum Si/Al ratio.

8.2 Experimental

8.2.1 Commercial catalyst composition

Vanadium based catalyst plates were supplied by Haldor Topsøe A/S. The composition of the catalyst mass base is approx. 1.2-3% V_2O_5, 7% WO_3 dispersed on a fibre reinforced TiO_2 carrier. The fibre material consists of primarily SiO_2 and alumina and calcium to a lesser extent. The monoliths had a size of 75 mm x 75 mm x 500 mm. The hydraulic diameter of the channels was about 6.5mm and the wall thickness was 1.0 mm.

8.2.2 Catalyst coating

To find a suitable method for the coating on the catalyst plates, trail experiments were conducted with various coating techniques and densities of aqueous suspensions. Possible coating techniques were dip coating, spray coating and paint brush or roller coating. Dip-coating technique causes water to penetrate into the catalyst plate and leaches the water-soluble catalytically active components like V_2O_5 and WO_3. Brush and paint roller has shown promising coating features but, requires high viscosity of the suspension. Through this technique well distributed coating can be obtained but, the thickness of coating is very hard to control. Best results were obtained with an air spray gun (1.5 bar) with a nozzle of diameter of 0.5 mm. This technique requires a lower viscosity. High viscosity can easily clog up the small nozzle. The technique provides very thin layer coating without changing the original structure of the catalyst plate.

V_2O_5/WO_3-TiO_2 catalyst plates were coated by spray coating technique with 5-30 wt% of the coating material in water solution. The particle size of the suspension was measured by HYDRO2000G (laser sensor). Average particle size of the coating materials were adjusted (less than 15 μm) by shaking the solution with 3-4 mm glass beads for 5-10 min. Finally coated catalysts plates were dried in the oven for 10 h and calcined at 450°C for 5 h at a heating rate of 5°C/min.

8.2.3 SCR catalyst deactivation

To expose the catalyst to alkali poisons under more realistic conditions plate type catalysts were placed in a pilot plant reactor shown in Figure 8.1 and exposed to well-defined aerosols of KCl. Hot flue gas was produced by a natural gas burner and a solution of the salt in distilled water (7.4 g/l KCl) was prepared and mixed several days before being added to the system. An aerosol of the salt was then generated by injecting the solution through a fluid nozzle into the flue gas close to the burner where the temperature was 1050–1100°C. A bayonet heat exchanger was inserted into the main duct downstream the formation of the desired aerosol particles to cool down the flue gas to avoid accelerated corrosion caused by the potassium compounds.

The catalyst box was well insulated and heated by an electrical heating wire. The exposure temperature was kept at 350°C and the temperature difference over the cross section of the catalyst box at the catalyst inlet was within 4°C and the temperature difference between the catalyst inlet and outlet was kept less than 5°C. A soot blower and a steel grid were installed 20 cm and 5 cm, respectively, above the catalyst to minimize plugging problems. The soot blower consists of a steel pipe with a diameter of 16 mm and a hole of 10 mm, a time controller and connects to compressed air at a pressure of 5 bar. Two additional soot blowers were placed just above the steel grid to blow away the particles deposited on the mesh. Soot blowing was carried out by 3–5 s of blowing with compressed air at an interval of 30 min. The total flow rate at the outlet of the burner was about 60 Nm^3/h and the flow rate through the catalyst was kept at 40-45 Nm^3/h by adjusting the bypass valve, which corresponds to a channel velocity of 6 m/s at 350°C. The experiment was conducted for 650-1200 h continuously. After exposure the catalyst monolith plates were removed immediately to avoid further deactivation.

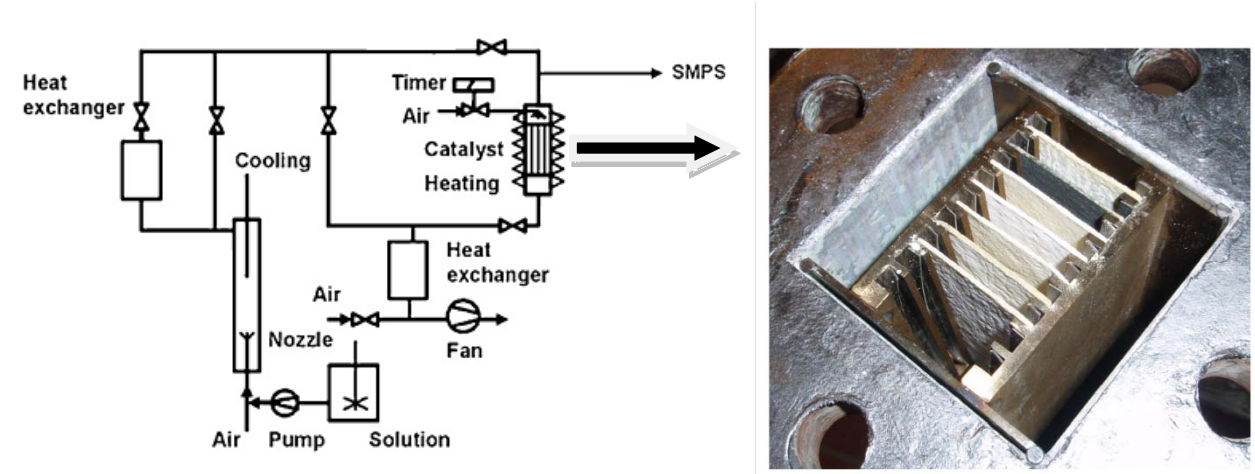

Figure 8.1 Potassium chloride aerosol exposure pilot plant experimental setup.

8.2.4 SCR activity measurements

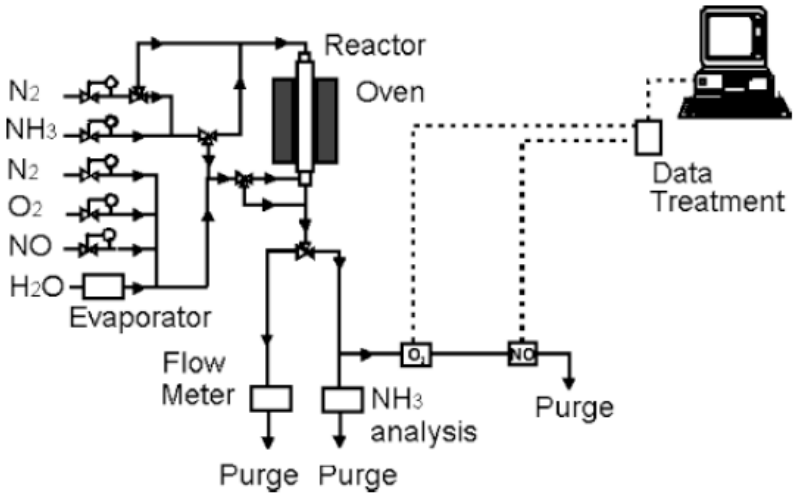

Figure 8.2 The catalyst test setup.

In the laboratory, the activities of the catalysts were measured by means of the setup shown in Figure 8.2. This mainly consists of three sections: a gas metering and mixing section, a reactor, and an analyzer section. The flow rates of the individual gases were controlled by mass flow controllers providing a constant flow, and measured by a bubble flow meter. Mixing was then performed with a flow panel. Normally, two different gas streams were made and directed to the reactor. Water was added by passing part of the nitrogen gas through an evaporator consisting of a Permapure tube placed in a thermostated water bath.

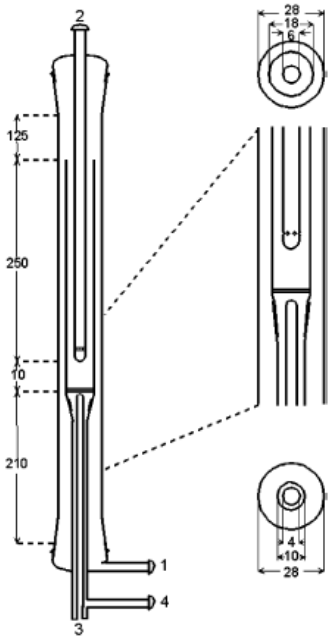

Figure 8.3 Sketch of the laboratory reactor. All shown measures are in millimeters. (1) Bottom gas inlet. (2) Top gas inlet. (3) Thermocouple. (4) Gas outlet.

The fixed-bed reactor made of quartz is shown in Figure 8.3. The inner and bottom tubes of the reactor were removable. Ammonia, O_2, H_2O, and half of the N_2 were added through the bottom (1 in Figure 8.3), which functions as a preheating section, whereas NO and the other half of N_2 were added from the top of the reactor inlet (2 in Figure 8.3). With this arrangement, reactive gases could be kept separated until they were mixed, just above the catalyst placed on the porous quartz plate. This minimizes homogeneous and wall catalyzed reactions in the pre-heating section, which, in any case, were negligible at the temperatures used here. The reactor temperature was measured below the porous quartz plate by a thermocouple shielded in a quartz tube. The reactor was placed in a three-zone oven for effective temperature control. Nitric oxide was analyzed by a conventional UV analyzer. No NH_3 measurements have been performed.

The activity was measured on catalyst plates (1.7 x 1.7 cm^2) with a total flow rate of 3 l / min. The composition of the feed gas was 400 ppm NO, 500 ppm NH_3, 5 vol% O_2 and 1.4 vol% H_2O. Activities of the catalysts were typically measured in situ at 350°C after attaining steady state values of temperature and conversion values. Steady state conversion values of NO and NH_3 gases were measured from online analyzers. As NH_3 is in excess, the observed reaction rate can be regarded as pseudo first order with respect to NO and zero order with respect to NH_3. The observed catalyst activity can be approximated by an observed rate constant K (m/s) with first order in NO as [3]:

$$K=-SV*ln\ (1-X)/A_p \tag{8.1}$$

where SV is the space velocity which represents the flow rate of the flue gas per unit volume of the catalyst element, A_p is the geometric surface area per unit volume, and X is the fractional NO conversion. To compare the deactivation levels of different catalysts, the relative activity were used (Equation 8.2), which was defined stage wise as shown in Figure 8.4.

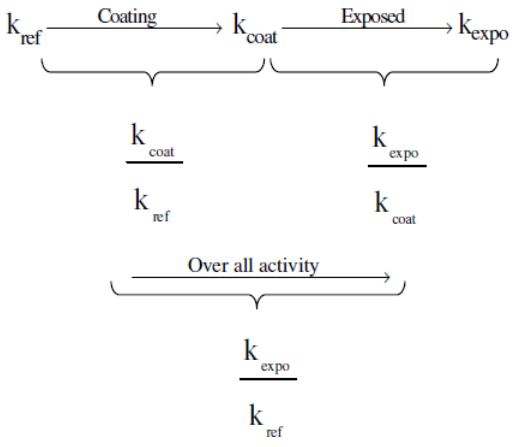

Figure 8.4 Relative activity determined for reference, coated and aerosol exposed catalyst plates.

$$\text{Relative activity} = K_{expo}/K_{ref} \text{ or } K_{coat}/K_{ref} \text{ or } K_{expo}/K_{coat} \tag{8.2}$$

8.2.5 SEM and EDX analysis

The distribution of potassium in the exposed catalysts were investigated at the Centre for Microstructure and Surface Analysis, Danish Technological Institute by SEM-EDX on a LEO 440 microscope and at Haldor Topsøe A/S. The samples were analyzed on the surface and on the cross section. To analyze the surfaces, the samples were attached on Al-stubs with carbon tape. The sample surfaces were analyzed in wet mode with water vapor in the microscope chamber. The samples were not coated. To analyze the cross sections, the samples were embedded and then polished (without water present) with SiC paper. To conduct the embeddings, they were coated with a thin layer of carbon. The embedded samples were operated in high vacuum. To improve the detection limit of the peaks in the X-ray analysis, WDX analysis is used in the microprobe.

Used instruments:

- Light Optical Microscope (LOM) for structure analysis.
- Quanta-SEM for structure analysis of the surface (operated at 20kV, 0.8mbar (wet mode)).
- Quanta-SEM for standard Energy Dispersive X-ray Spectrometry (EDX)-analysis (chemical analysis, operated at 20kV).
- Microprobe-SEM for Wavelength Dispersive X-ray Spectrometry (WDX)-analysis (chemical analysis, operated at 20kV).

8.3 Results and Discussion

8.3.1 Initial screening tests

Possible coating materials are metal oxides like Al_2O_3, MnO_x, MgO, TiO_2, $Zr(SO_4)_2$ as they show good corrosion resistance to alkali substances [4]. Studies have shown that acidic carrier material has a beneficial influence on resistance to alkali poisons [5]. It must therefore be presumed that an acidic coating can increase deactivation resistance. In the present work various coating materials like manganese oxide, sulphated-ZrO_2, silica gel, titanium dioxide, aluminum oxide and magnesium oxide were tested, as discussed below.

Catalytic activity of the reference, coated and exposed catalysts are presented in Figure 8.5. From figure it is clear that the coated catalysts are showing less relative activity compared to that of reference catalyst. By coating the catalyst plates it seems reasonable to expect a decrease in activity because an additional film resistance is added. In some cases the coating material may also be responsible for the NO reduction. Compared to the high activity of V_2O_5-WO_3/TiO_2 catalyst, coating contribution for enhancing the reaction can be neglected. Except for Al and Mg, all the coated catalysts showed relative activity values (K_{coat}/K_{ref}) around 0.85 impaling that there is a thin coating on the catalyst which is responsible for the slight decrease in activity. That of Al and Mg catalysts showed relative values of 0.68 and 0.78 implying that the coating layer thickness is comparatively high.

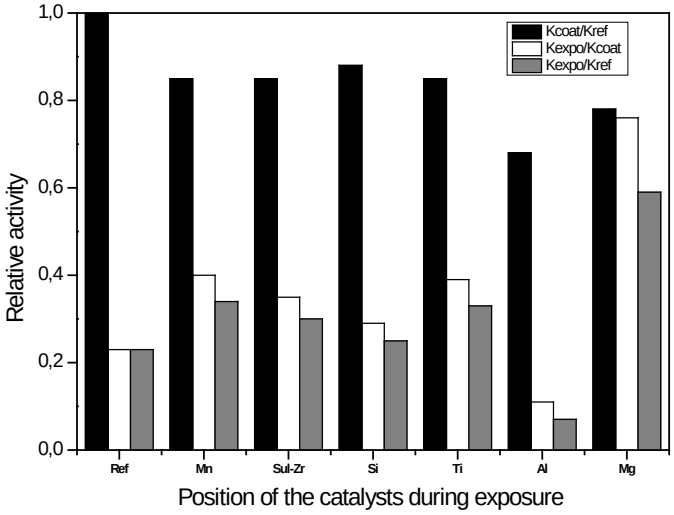

Figure 8.5 Relative activity of reference, coated and aerosol exposed catalysts for 650 h at 350°C.

The relative activity (K_{expo}/K_{coat}) of the aerosol exposed catalysts to the corresponding fresh coated catalyst is shown in Figure 8.5. The reference catalyst showed a relative activity of 0.23 indicating severe deactivation of the catalyst. Similar deactivation patterns were also reported on reference catalysts by Zheng et al. [6, 7]. Among the coated catalysts Mg containing catalyst showed high alkali resistivity as compared to uncoated reference catalyst. Relative activity (K_{expo}/K_{coat}) of Mg coated catalyst is 0.75. Rest of the coated catalysts like Mn (0.40), Sul-Zr (0.35), Si (0.29) and Ti (0.39) catalysts showed less alkali resistivity compared to the Mg coated catalyst. The Al coated catalyst showed a relative value of 0.10 only, when compared to the uncoated reference catalyst, i.e. the level of deactivation is very high. All the measurements are taken based on the average of 2 or 3 experimental runs to minimize the experimental errors. There are no reports available in the literature to compare the SCR activity for protective coated DeNOx catalysts in alkali containing flue gases.

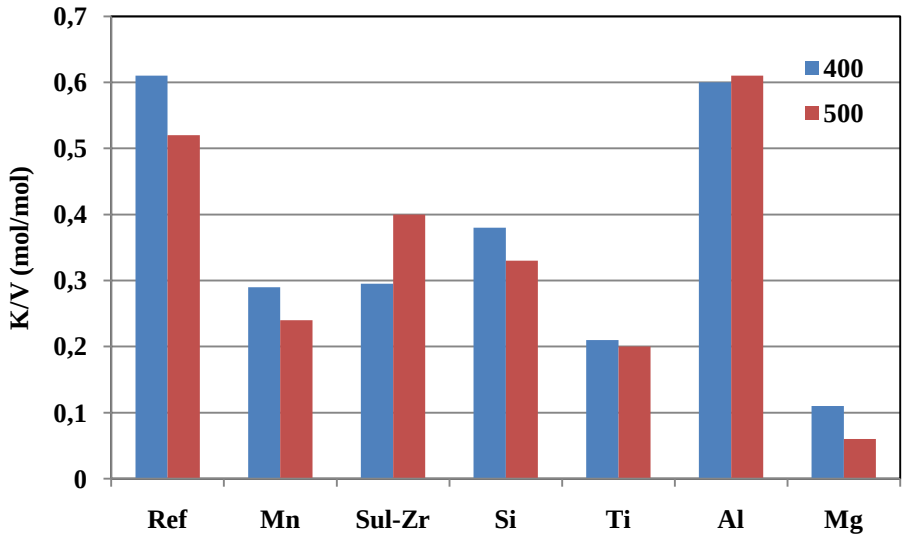

Figure 8.6 K/V molar ratio of catalysts at 400 and 500 µm from the catalyst surface.

Overall relative activity (k_{expo}/k_{ref}) of aerosol exposed catalysts to that of fresh or coated catalyst are also shown in Figure 8.5. Irrespective of type of coating and nature of material overall relative activity is a typical comparison to see the alkali resistivity. Among all the catalysts Mg coated catalyst (0.59) is performing better compared to that of the uncoated reference catalyst (0.23). Other coated catalysts with overall relative value less than 0.5 are not considered as commercially interesting.

On the basis of EDX analysis the K/V molar ratios found for all the exposed plates at 400 and 500 µm from the catalyst surface is shown in Figure 8.6. As mentioned earlier, the ratio between potassium and vanadium on a molar basis vs. cross section is considered, to know how many active vanadium sites are occupied by potassium. For the reference catalyst the K/V ratio at 400 and 500 µm from the catalyst surface is approx. 0.5-0.6. Previous studies have shown a K/V ratio of about 0.7 in the equivalent distance from the catalyst surfaces performed and reported by Zheng et al. [6, 7], with a longer exposure time of around 1800 hours, which may explain the somewhat higher K/V ratio. Mg coated catalysts show very low K/V ratio at 400 and 500 µm from the catalyst surface i.e. approx. 0.11 and 0.06, respectively. For other coated catalysts (Mn, Zr, Si and Ti) the catalysts showed K/V ratios of 0.2-0.4. It can be concluded that all the coated catalysts provide a protection against potassium up to certain extent. Coating with Al has not been successful. Overall there is a good relation between the SCR alkali resistivity and low K/V ratio across the cross section for all the catalysts mentioned in this batch of the catalysts.

8.3.2 Zeolite coated catalysts

In this section the Mg coating adhesion property is improved by using dilute aqueous suspensions for single and double coating to control the thickness. Furthermore, additional possible coating materials considered are: Sulphated –ZrO_2, HBETA-150, HBETA-25 and Montmorillonite. It has

been reported that zeolites (HBETA) are considered to be highly alkali resistant support materials [8, 9-11].

Catalytic activity of the reference, coated and aerosol exposed catalysts are presented in Figure 8.7. From the figure it is clear that the coated catalysts are showing less relative activity compared to that of reference catalyst as already seen in Section 8.3.1. Mg-1 and Mg-2 represent Mg coating with single and double coating, respectively. All the coated catalysts showed relative activity (K_{coat}/K_{ref}) values of 0.7 to 0.9 impaling that the coating is very thin. Mg-2 coated catalyst showed less relative value compared to Mg-1 because of the double coating. HBEA-150, HBEA-25 and K-10 coated catalysts showed relative activity around 0.9 even though they were coated with similar concentration and coating method. The relative activity of the aerosol exposed catalysts to the corresponding fresh coated catalyst is shown in Figure 8.7. The reference catalyst showed a relative activity (K_{expo}/K_{coat}) of 0.25 showing severe deactivation of the catalyst and in good agreement with the result of section 8.3.1 for the reference catalyst. Among coated catalysts Mg-1 and HBEA-25 catalysts showed alkali resistivity as compared to the uncoated reference catalyst. The relative activity of Mg-1 and HBEA-25 are 0.34 and 0.48, respectively. The remaining coated catalysts like Mg-2 and Sul-Zr, HBEA-150 and K-10 catalysts did not show any alkali resistance; instead they further deactivated the catalysts when compared to uncoated reference catalyst. The reason is not clear, but may involve changes in the coating layer thickness and concentration of the aqueous suspension. In this series Mg coated catalysts did not show superior performance, a disappointing result. This will be investigated further.

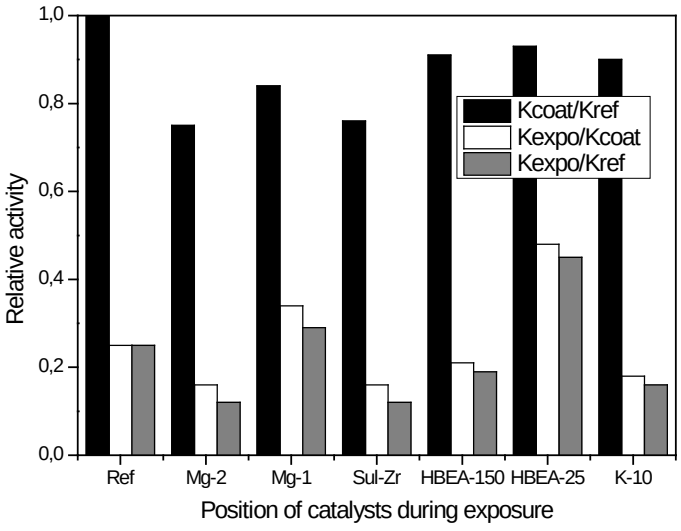

Figure 8.7 Relative activity of reference, coated and aerosol exposed catalysts for 850 h at 350°C.

The Overall relative activity of aerosol exposed catalysts to that of the fresh reference (K_{expo}/K_{ref}) is shown in Figure 8.7. Among all the catalysts Mg-1 and HBEA-25 catalysts are performing better compared to that of the uncoated reference catalyst. Mg-1 and HBEA-25 catalysts showed a relative decrease of 0.29 and 0.45, respectively. HBEA zeolite with Si/Al ratio around 20-25 is reported active for NH_3-SCR, and is especially preferable for alkali containing flue gases [8, 9, 11].

Cu-Zeolite and Fe-Zeolite catalysts showed high poison resistance when compared to commercial vanadium catalysts [8, 9]. Such a high alkali resistivity is due to high surface area and acidity of the zeolite supports compared to simple metal oxides like TiO_2. The superior activity of HBEA-25 can be well discussed from the surface composition the catalysts obtained by SEM and EDX analysis. Coating acts as an alkali barrier and thereby the active vanadium sites can be protected.

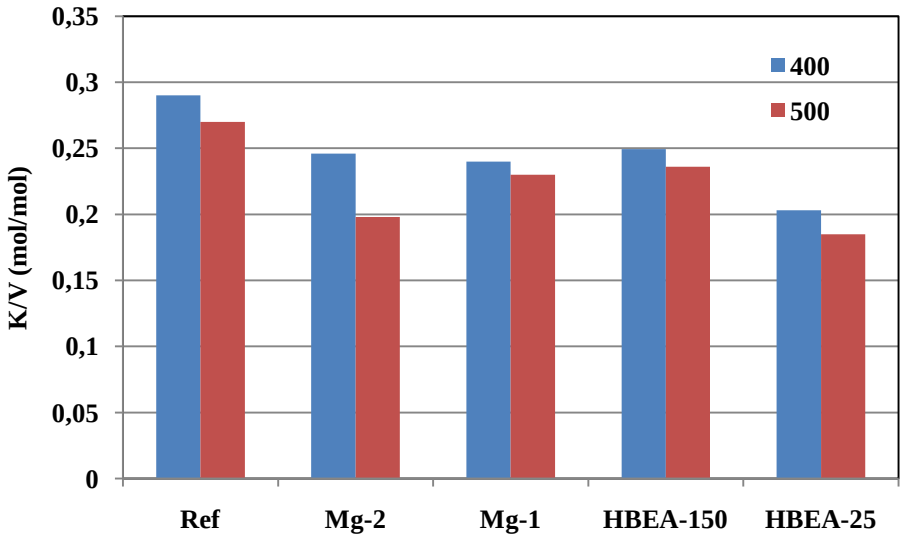

Figure 8.8 Potassium concentration of catalysts at 400 and 500 µm from the catalyst surface.

On the basis of elemental analysis potassium concentrations found for all the exposed plates over 400 and 500 µm from the catalyst surface are shown in Figure 8.8. For the reference catalyst, the potassium concentration at 400 and 500 µm from the catalyst surface is approx. 0.29 and 0.27 wt%, respectively. HBEA-25 catalyst showed a potassium concentration of 0.12 and 0.17 wt% at 400 and 500 µm, respectively from the surface. That of Mg-1, Mg-2 and HBEA-150 catalysts showed potassium concentration around 0.25 wt% i.e. almost the same as on the reference catalyst. Mg coated catalysts did not performed well in the present batch. After examining SEM images of the exposed catalysts there was very thin coating or film on the surface, performing like a reference catalyst without any protection. Sul-Zr and K-10 were not considered for surface analysis due to poor SCR alkali resistivity.

8.3.3. Improved Mg coatings with Si binder

In section 8.3.1 and 8.3.2 it was concluded that the Mg and zeolite containing coatings were promising for SCR of alkali containing flue gases. In section 8.3.2 the adhesion property of Mg coated catalysts was very poor and resulted in low alkali resistivity. In this section the Mg coating properties were improved by adding silicagel as binder. In this section the possible coating materials considered are Mg, Mg with Si gel, HZSM5-15, HZSM5-140 and HMOR-10.

The catalytic activity of the reference, coated and aerosol exposed catalysts are presented in Figure 8.9. From the figure it is clear that the coated catalysts are showing less relative

activity compared to that of the reference catalyst. 5% Mg and 15% Mg represent Mg coatings with 5 wt% and 15 wt% aqueous solution, respectively. All the coated catalysts showed relative activity (K_{coat}/K_{ref}) values around 0.9 showing that the coating is providing a low additional resistance to diffusion of the reactants. The relative activity of the aerosol exposed catalysts to the corresponding fresh coated catalyst is shown in Figure 8.9. The reference catalyst showed a relative activity (K_{expo}/K_{ref}) of 0.192 which indicates that there is severe deactivation of the catalyst once again. All the coated catalysts were performing better than the uncoated reference catalyst. Relative activity of 5% Mg and 15% Mg was 0.377, 0.319, respectively. Mg coating with Si binder showed improved alkali resistivity of 0.474 and 0.397 for 5% Mg-5% Si, 5% Mg-1% Si, respectively. Zeolite based HZSM5-140, HZSM5-15 and HMOR-10 coated catalysts showed relative activity of 0.32, 0.495, and 0.494, respectively. Again it proved that zeolites with Si/Al ratio around 10-25 are promising alkali resistant barriers as also observed in section 8.3.2 with HBEA-25 coating. Overall relative activity (K_{expo}/K_{ref}) of aerosol exposed catalyst to that of fresh reference is shown in Figure 8.9. Coated catalysts showed an activity trend of HZSM5-15 (0.495) > HMOR-10 (0.49) > 5% Mg-5% Si > 5%Mg-1% Si (0.374) > 5% Mg (0.361) > 15% Mg (0.316) > HZSM5-140 (0.28) > Ref (0.192).

Irrespective of the surface concentration of potassium, the best coating can be correlated with potassium accumulation across the plate. The uncoated reference catalyst showed comparatively high potassium (0.725 wt%) across the cross section of the plate. Among all the catalysts 5 wt% Mg - 5 wt% Si coated catalyst showed the lowest potassium concentration (≈0.2 wt%) across the plate, while that of HMOR-10 showed 0.25 wt%. The HZSM5-15 coated catalyst showed potassium concentration of 0.35 wt%. The cross section results indicate that coatings (5% Mg–5% Si, zeolites) significantly prevent potassium to reach the catalyst surface, by up to a factor of three or more.

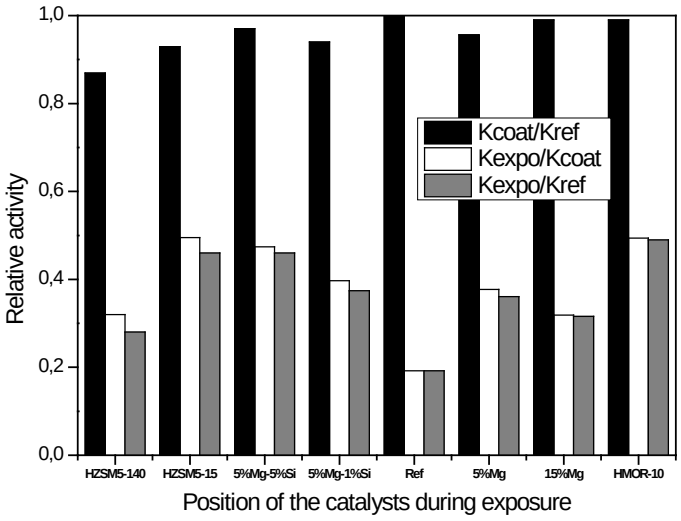

Figure 8.9 Relative activity of reference, coated and aerosol exposed catalysts for 850 h at 350°C.

8.3.4 Metal oxide and zeolite coatings

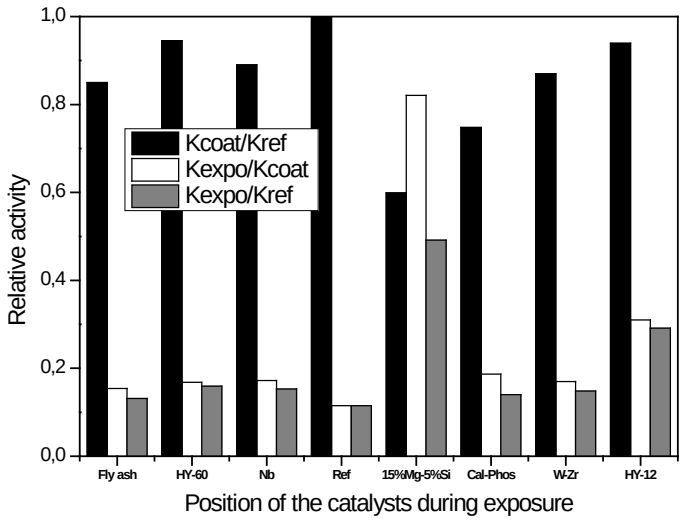

Figure 8.10 Relative activity of reference, coated and aerosol exposed catalysts for 850 h at 350°C.

Possible coating materials considered are 15%Mg-5%Si, HY-12, HY-60, Fly ash, Nb_2O_5, calcium phosphate and WO_3-ZrO_2. Catalytic activity of reference, coated and aerosol exposed catalysts are presented in Figure 8.10. From the figure it is clear that the coated catalysts are showing large deviation in relative activity (K_{coat}/K_{ref}). HY-12 and HY-60 are showing around 0.94. Fly ash, Nb, and WO_3-ZrO_2 are showing a relative activity of 0.83-0.89. Calcium phosphate and 15%Mg-5%Si are showing a relative activity of 0.748 and 0.60, respectively. The relative activity of the aerosol exposed catalysts to the corresponding fresh coated catalysts is shown in Figure 8.10. The reference catalyst showed a relative activity (K_{expo}/K_{ref}) of 0.115. Among all the coated catalysts 15%Mg-5%Si and HY-12 are performing well with relative activity (K_{expo}/K_{coat}) of 0.821 and 0.31, respectively. As reported in the previous sections Mg coated catalysts are always superior. The HY-12 zeolite activity cannot be compared with other zeolites like HZSM5-15 and HMOR-10. The rate of deactivation can also depend on zeolite pore size/structure other than acidity as also reported by Reddy et al. [8, 11]. Irrespective of the pore size and structure, zeolites with Si/Al around 10-20 are showing high alkali resistivity compared to other zeolite formulations. The rest of the coatings showed relative activity around 0.2. 15%Mg-5%Si and HY-12 coated catalysts showed overall activity (K_{expo}/K_{ref}) of 0.4918 and 0.29145, respectively. Again it shows that Mg coated catalysts are the most promising candidates for the alkali resistant SCR process.

A comparison is made in Table 8.2 in section 8.3.1 to 8.3.4 with the 3 best performing catalysts from each batch. Among all the catalysts the Mg coated catalysts are generally working well, though it is not the case for the batch related to section 8.3.2. Such a variation is due to a very thin film of Mg coating. 2nd best candidates are the zeolite family materials like HZSM5-15, HMOR-10 and HBEA-25. All these materials fall under the broad classification mentioned in the introduction.

Table 8.2 Comparison of overall relative activity (K_{expo}/K_{ref}) of the coating materials.

	1st choice	2nd choice	3rd choice
Section 8.3.1	Mg (0.59)	Mn (0.34)	Ti (0.32)
Section 8.3.2	HBEA-25 (0.45)	Mg (0.29)	-----
Section 8.3.3	HZSM5-15 (0.49)	HMOR-10 (0.49)	Mg (0.46)
Section 8.3.4	Mg (0.4918)	HY-12 (0.2914)	Cal-Phos (0.24)

1. Coating materials based on physical blocking (Ti and Mn)
a. Slightly basic substances to block the potassium (Mg)
2. Coating materials based on chemically reactive compounds to potassium
a. Acidic substances for hosting the potassium on surface (zeolites)

From the broad classification with materials it can further be concluded that Mg coated compounds are the ultimate choice. Even if we imagine a long life of the second best choice coated materials like zeolites they lose the surface acidic sites and become like a physical blocking materials. Then the potassium can easily penetrate through the wall of the catalyst. Ultimate success of the coating technique lies in the slightly basic substances since, they are the only materials which are not depending on acidic nature and effectively avoid that the basic potassium poisons penetrate the wall. The lack of acidic Brønsted sites makes it difficult for the potassium to diffuse into the catalyst wall. With this typical comparison and coating strategy to counter the potassium poisons Mg coating is chosen for the long term exposure in comparison with the reference catalyst.

8.4 Long term testing of Mg-coated catalysts

A set of experiments were planned for long term aerosol exposure as shown in the matrix (Table 8.3). Total exposure time was 50 days with 10 days of interval for each exposure. After every 10 days of exposure one reference and one coated catalyst was removed and replaced with 2 fresh catalysts. X represent first batch of exposed catalyst and # represent 2nd batch of replaced catalyst. In this way repeatability of the experiments can be done along with long exposure time. With 10 days interval the rate of deactivation can also be measure for both reference and coated catalysts. After the exposure the catalysts were stored in a desiccator to avoid further deactivation by atmospheric moisture.

Table 8.3 Design of experiments for long term aerosol exposure.

Days	Ref -1	Ref -2	Ref -3	Ref -4	Ref- 5	Mg-1	Mg-2	Mg-3	Mg-4	Mg-5
10	X	X	X	X	X	X	X	X	X	X
20	#	X	X	X	X	#	X	X	X	X
30	#	#	X	X	X	#	#	X	X	X
40	#	#	#	X	X	#	#	#	X	X
50	#	#	#	#	X	#	#	#	#	X
	Ref-6	Ref-7	Ref-8	Ref-9	Ref-5	Mg-6	Mg-7	Mg-8	Mg-9	Mg-5

The relative activity (K_{expo}/K_{ref}) of the aerosol exposed catalyst to corresponding fresh reference catalyst is shown in Figure 8.11. The reference catalysts showed a decrease in activity with exposure time. These reported values are average measurements along the length of the exposed plates. After 10 days of exposure the reference catalysts showed a relative value of 0.71 in both batches. 10-40 days of exposure of the catalysts in both batches showed a maximum deviation of 5% indicating that the experimental data can be validated. Almost complete loss of activity can be seen after 50 days of exposure. In the previous sections the reference catalyst showed a relative value of 0.20-0.25 after 850 hours of operation, that data is fitting well into the observed deactivation trend line in these long term experiments. From Figure 8.11 an average deactivation rate of 20%/every10 days can be observed. Such a high rate of deactivation reveals that the potassium aerosol exposure is very intense.

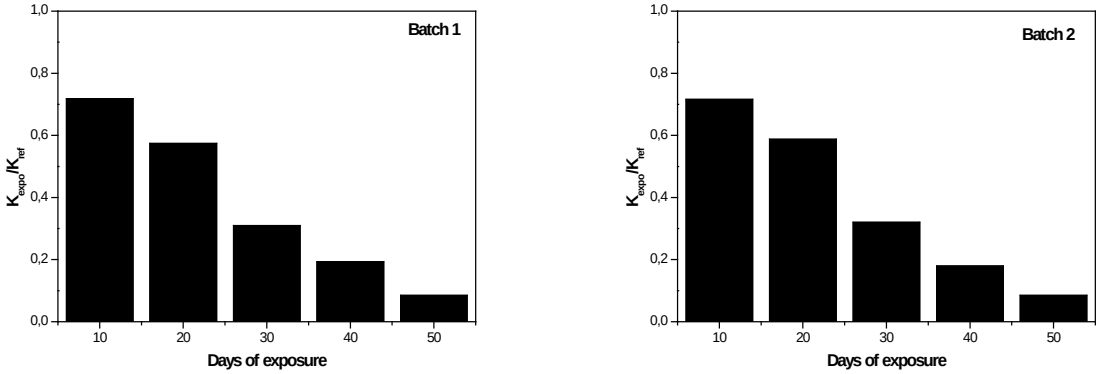

Figure 8.11 Relative activity (K_{expo}/K_{ref}) of reference catalysts with aerosol exposure time at 350°C.

The relative activity (K_{coat}/K_{ref}) of Mg coated catalysts is shown in Figure 8.12. From the figure it is clear that the coated catalysts are showing large deviation in relative activity, ranging from 0.75 to 0.55. This could be due to slight variation in coating time from plate to plate. After measuring the relative activity, the position of the catalysts was arranged for aerosol exposure by decreasing relative of K_{expo}/K_{ref} value with increasing days of exposure. It was expected that Mg with thicker coating can withstand the potassium aerosols in an effective manner for long term exposure, which was also observed.

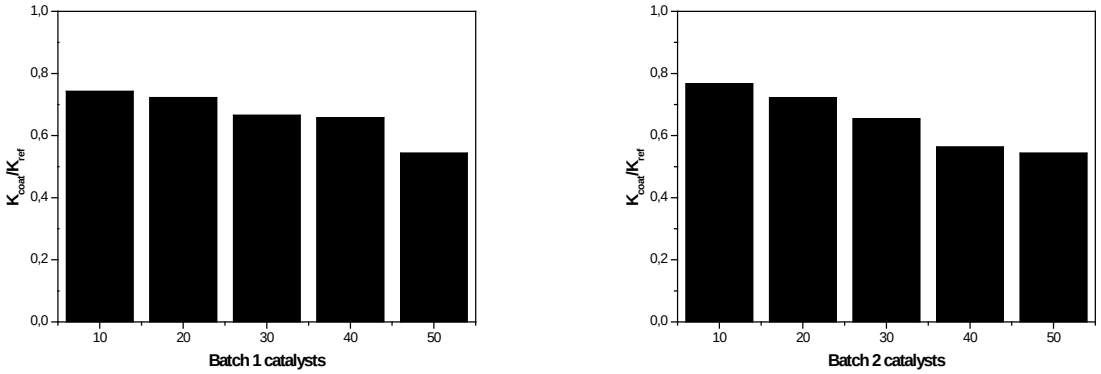

Figure 8.12 Relative activity (K_{coat}/K_{ref}) of Mg coated catalysts at 350°C.

The relative activity (K_{expo}/K_{coat}) of Mg coated catalysts along with exposure time is shown in Figure 8.13. The Mg coated catalysts showed decrease in activity with exposure time. After 10 days of exposure the Mg coated catalysts showed a relative value of ≈0.84 in both batches. After 10-40 days of exposure the catalysts in both batches showed maximum deviation of 5-7% indicating that the Mg coated catalysts are slightly deviating in repeatability compared to the reference catalyst. Mg coated catalysts showed a relative value of 0.60 after 50 days of exposure while that of reference catalyst almost completely deactivated. From Figure 8.13 an average deactivation rate of 5%/every10 days can be observed. The slow rate of deactivation under similar conditions could reveal Mg is acting as a protecting layer to prevent alkali aerosols to reach the vanadium catalyst interior.

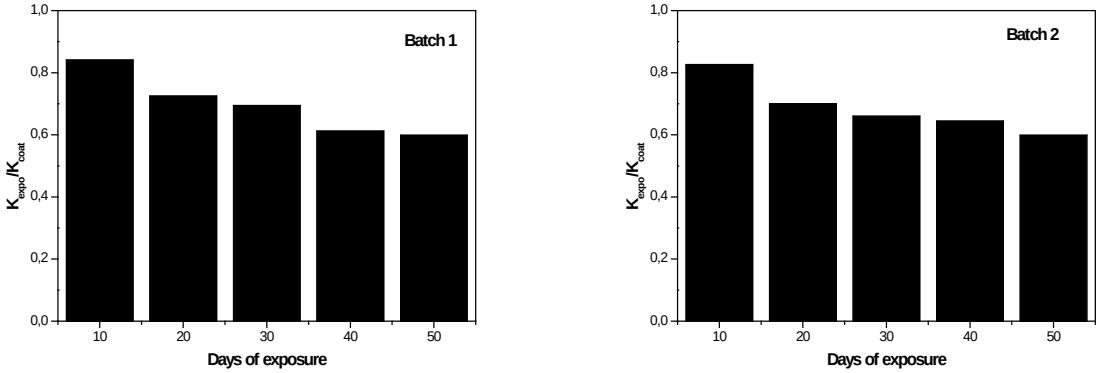

Figure 8.13 Relative activity (K_{expo}/K_{coat}) of Mg coated catalysts with aerosol exposure time at 350°C.

The overall relative activity (K_{expo}/K_{ref}) of the Mg exposed catalysts to the fresh reference catalyst is shown in Figure 8.14. The overall relative activity includes loss of activity due to coating barrier and potassium aerosol deactivation. Overall relative values can give more information and direct comparison can be possible with the reference catalyst. The Mg coated catalysts showed a rate of deactivation of 6-7% every 10 days. The Mg coated catalysts showed a relative value of 0.32 and that of the reference catalyst showed 0.08 after 50 days of aerosol exposure. The 50 days exposed Mg catalyst showed 40% loss of activity due to coating (actually changing with the thickness of coating) and 28% due to alkali aerosol exposure. The uncoated reference catalyst showed loss of 92%, only due to alkali aerosol exposure. Thus, Mg appears to be a good choice of coating material to protect the commercial vanadium catalyst from alkali poisons in biomass fired SCR applications.

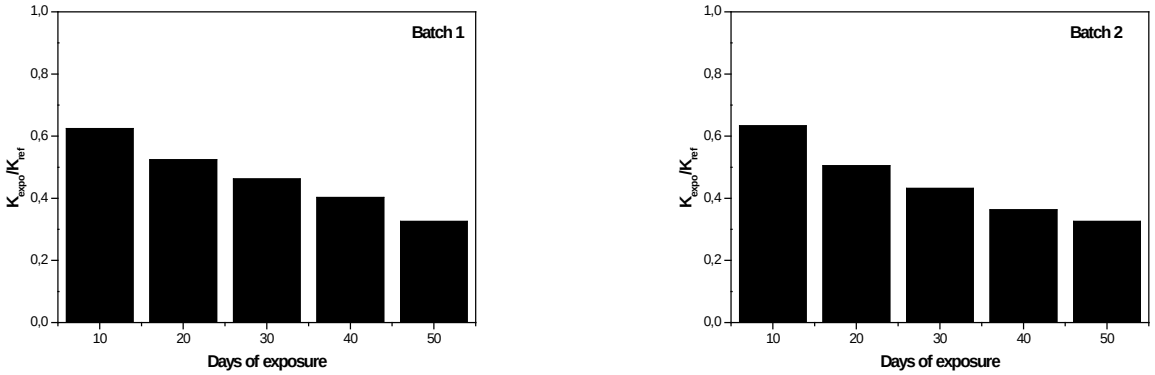

Figure 8.14 Overall relative activity (K_{expo}/K_{ref}) of Mg coated catalysts with aerosol exposure time at 350°C.

8.5 Conclusions

To limit the high rate of alkali deactivation, a novel protective coating technique has been developed and tested using a range of different candidate materials. Among all the tested catalysts the slightly basic nature of Mg coated catalysts are generally working well. Mg is acting like a barrier repelling the potassium with basic-basic nature on the surface. Further design of experiments on reference and Mg coated catalysts for long term exposure gave more insight into the rate of deactivation and consistency of results. 50 days of alkali aerosol exposure reveals that the reference catalyst is losing 92% of the initial activity only due to alkali and that of the Mg coated catalyst is losing 40% due to coating barrier and only 28% due to alkali. Thus, severe rate of deactivation due to alkali poisons can be avoided by coating the vanadium catalyst with Mg. Overall the protective coating of SCR catalysts developed in the project seems promising. Further research and industrial prototype tests are recommended. Intellectual protection of the investigation has been initiated through a patent application entitled 'Deactivation-resistant catalyst for selective catalytic reduction of NO_x' and the innovation is transferred to Haldor Topsøe A/S. The results of the present research have not been published because of the patent issues; once the patent is issued publications can be initiated in the near future.

8.6 References

[1] Jensen-Holm, J. R. Thøgersen, P. Lindenhoff, Presented at Power-Gen Europe, Germany (2009).
[2] Å. Kling, C. Andersson, Å. Myringer, D. Eskilsson, S. G. Järås, Appl. Catal. B, 69 (2007) 240.
[3] Y. Zheng, A. D. Jensen, J. E. Johnsson, Ind. Eng. Chem. Res., 43 (2004) 941.
[4] T.K. Li, D.A. Hirschfeld, J.L. Brown, J Mater Sci 32 (1997) 4455.
[5] P. Gabrielsson, H. Guldberg Pedersen, Volume 5, Handbook of Heterogeneous catalysis.
[6] Y. Zheng, A. D. Jensen, J. E. Johnsson, Appl. Catal. B. 60 (2005) 253.
[7] Y. Zheng, A.D. Jensen, J.E. Johnsson, J.R. Thøgersen, Appl. Catal. B 83 (2008) 186.
[8] S.S.R. Putluru, A. Riisager, R. Fehrmann, Appl. Catal. B (Press).
[9] P. Kern, M. Klimczak, T. Heinzelmann, M. Lucas, P. Claus, Appl. Catal. B 95 (2010) 48.
[10] S.B. Rasmussen, J. Due-Hansen, M. Yates, M. Villaroel, F. Llambias, R. Fehrmann, P. Avila, Stud. Surf. Sci. Catal. 175 (2010) 739.
[11] S.S.R. Putluru, A. Riisager, R. Fehrmann, Appl. Catal. B 97 (2010) 333.

9. Summary and recommendations

The overall evaluation of the prepared and tested potential SCR deNOx catalysts is condensed in Table 9.1 and 9.2:

Table 9.1 Summary of potential value of investigated catalysts; promising"+", not promising "-", and not investigated "?"

	TiO_2	SO_4^{2-}-Nano-TiO_2	Nano-TiO_2	SO_4^{2-}-ZrO_2-	Zeolites	ZrO_2/CeO_2
V	-	+	+	+	+	+
Fe	?	+	+	-	+	?
Cu	?	+	+	-	+	?
[TMGH]Cr_2O_7	-	?	?	?	?	?

Table 9.2 Summary of potential value of investigated heteropoly acid promoted catalysts; promising"+", not promising "-", and not investigated "?"

Heteropoly acid	Fe-TiO_2	V-TiO_2	Cu-TiO_2
TPA	+	+	+
MPA	+	+	+
TSiA	+	+	+

Several are promising alternatives to the state-of-the-art industrial reference catalyst employed in the present work also illustrated through the 5 patent applications filed during the project period. Of those the very best catalysts are compared in Figure 9.1.

As can be seen all catalysts prepared in the present project and displayed in the figure exhibit higher to much higher alkali resistance compared to the commercial reference. Furthermore, two catalysts, i.e. 20 wt% V_2O_5-TiO_2 nano-catalyst (a last minute discovered optimization of the nano-catalyst compared to the 15 wt% described in chapter 4) and the 4 wt% CuO-Mordenite zeolite based catalyst have also a higher initial SCR activity compared to the commercial one before alkali poisoning. Thus, those two catalysts might be attractive for SCR deNOx purposes even under “normal” fuel conditions in power plants and elsewhere making them strong candidates for further development towards industrial commercialization. These efforts regarding all the promising catalysts will be pursued after this project has expired through a one year Proof of Concept (PoC) project just granted to us from the Danish Agency for Science, Technology and Innovation.

Also the severe rate of deactivation due to alkali poisons can be avoided by coating the vanadium catalyst with Mg. Overall the protective coating of SCR catalysts developed in the project seems promising and another patent application has been filed as a result of the PSO-project regarding this technology. Further research and industrial prototype tests are recommended. The intellectual protection of the investigation has been initiated through the patent application entitled ‘Deactivation-resistant catalyst for selective catalytic reduction of NO_x’ and the innovation is transferred to Haldor Topsøe A/S.

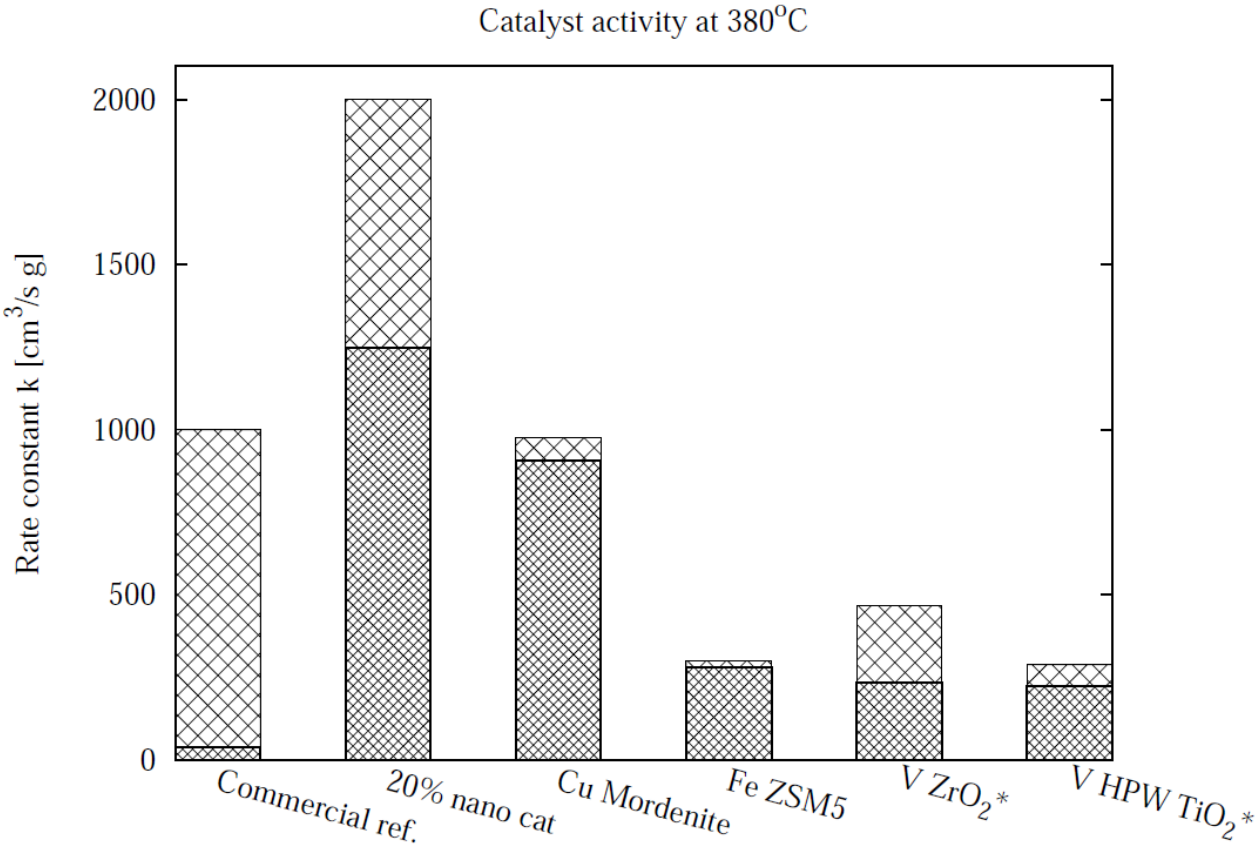

Figure 9.1 Activity measurements of four different deNO$_x$ catalysts fresh (whole bar) and potassium doped with 280 µmole/g KNO_3 (bottom part of bar), a commercial reference (3wt%V_2O_5-10wt%WO_3/TiO_2), a 20 wt% V_2O_5 on TiO_2–SO_4^{2-} nano catalyst, a 4 wt% CuO on Mordenite and a 3 wt% Fe_2O_3 on ZSM5, 3.0 wt% V_2O_5 on sulfated ZrO_2, 3.0 wt%V_2O_5 + 15 wt% H_3PO_4.12(WO_3) on TiO_2. * = 100µmole/g KNO_3.

Finally a completely different approach to alkali resistant deNOx technologies has been developed in the present PSO project, i.e. selective gas absorption of NO by ionic liquids. Also in this case a patent application has been filed and further development e.g. in the form of SILP materials for convenient installation in industrial units will be investigated in another "spin-off" project supported directly by DONG Energy and Vattenfall A/S.

The results of the project PSO 7318 "Alternative deNO$_x$ catalysts and technologies" has led to 45 international publications, patents or conference contributions as listed in the following chapter.

10. Project publications

Journal articles

1. The Effect of Acidic and Redox Properties of $V_2O_5/CeO_2–ZrO_2$ catalysts in Selective Catalytic Reduction of NO by NH_3. P. Siva Sankar Reddy, Anders Riisager, Rasmus Fehrmann. Catalysis Letters 133 (2009) 370.
2. Vanadia supported on zeolites for SCR of NO by ammonia P. Siva Sankar Reddy, Anders Riisager, Rasmus Fehrmann. Applied Catalysis B 97 (2010) 333.
3. Alkali resistant Cu/Zeolite De-NO_x catalysts for flue gas cleaning in biomass fired applications P. Siva Sankar Reddy, Anders Riisager, Rasmus Fehrmann. Applied Catalysis B 101 (2011) 183
4. Alkali resistant Fe-zeolite catalysts for SCR of NO with NH_3. P. Siva Sankar Reddy, Anders Riisager, Rasmus Fehrmann. Topics in catalysis (Communicated).
5. Heteropoly acid promoted Cu and Fe catalysts for the selective catalytic reduction of NO with ammonia. P. Siva Sankar Reddy, Anders Riisager, Rasmus Fehrmann. Catalysis Today (accepted)
6. Fe-BEA Zeolite Catalysts for NH_3-SCR of NO_x, Frey, A. M., Mert, S., Due-Hansen, J., Fehrmann, R., Christensen, C.H., Catal. Lett. 130 (1-2) (2009) 1-8
7. Impact of Support and Potassium-Poisoning on the V_2O_5-WO_3/ZrO2 Catalyst Performance in Ammonia Oxidation, Due-Hansen, J., Kustov, A. K., Christensen, C. H., Fehrmann, R., Catal. Comm. 10 (2009) 803-806
8. SCR activity of conformed CuO_x/ZrO_2-SO_4 catalysts, Rasmussen, S.B., M. Yates, Due-Hansen, J., Ávila, P., Fehrmann, R, Stud. Surf. Sci. Catal. 175 (2010) 735-738.
9. Pore design of pelletised VO_x/ZrO_2-SO_4/Sepiolite composite catalysts, Rasmussen, S.B., Due-Hansen, Yates, M., Villaroel, M., Gil Llambías, F.J., Fehrmann, R., Ávila, P., Stud. Surf. Sci. Catal. 175 (2010) 739-742.
10. Redox behavior of vanadium during hydrogen-oxygen exposure to the V_2O_5-WO_3/TiO_2 SCR catalyst at 250°C , Due-Hansen, J., Rasmussen, S.B., Mikolajska, E., Bañares, M.A., Ávila, P., Fehrmann, R, (manuscript)
11. Structural characterization and catalytic properties of bis(1,1,3,3-tetramethylguanidinium) dichromate, Due-Hansen, J., Ståhl, K., Boghosian, S., Riisager, A., Fehrmann, R., Polyhedron, 2011, (accepted)
12. Seed-assisted sol–gel synthesis and characterization of nanoparticular V_2O_5/anatase, A.J. Kruse, S.B. Kristensen, A.Riisager, S.B. Rasmussen and R. Fehrmann, J. Mater. Sci. 44 (2009) 323.
13. Highly active vanadia-anatase nanoparticle SCR deNO_x catalysts, S.B. Kristensen, A. J. Kunov-Kruse, A.Riisager, S.B. Rasmussen and R. Fehrmann, J. Catal., (submitted).
14. Multidisciplinary Determination of the Phase Distribution for VO_X-ZrO_2-SO_4^{2-}-Sepiolite Catalysts for NH_3-SCR, S.B. Rasmussen, J. Due-Hansen, M. Villaroel, F.J. Gil-Llambías, R. Fehrmann, P. Ávila, manuscript.

Patents

1. Alkali Resistant Catalyst, Rasmussen, S.B., Kustov, A., Fehrmann, R., Due-Hansen, J., (WO/2008/037255), September 2007.
2. Nano deNOx catalysts, R. Fehrmann, A. Riisager, S.B. Rasmussen, S.B. Kristensen and A.J. Kunov-Kruse, Patent application 08169238.6-2104, 2008 (DTU).
3. Vanadia-supported on zeolites for SCR of NO by ammonia or urea. Putluru Siva Sankar Reddy, Anders Riisager, Rasmus Fehrmann, patent application, filed 4. May 2010 (DTU).
4. Zeolite SCR catalysts with iron or copper. Putluru Siva Sankar Reddy, Anders Riisager, Rasmus Fehrmann, patent application, filed 27. August 2010 (DTU).
5. Heteropoly acid promoted catalyst for SCR of NOx with ammonia. Putluru Siva Sankar Reddy, Anders Riisager, Rasmus Fehrmann, patent application, filed 3. September 2010 (DTU).
6. NO sorption by ionic liquids, Due-Hansen, J., Riisager, A., Fehrmann, R., Patent pending 2010.
7. Deactivation-resistant catalyst for selective catalytic reduction of NOx, Per Donskov Rams, Jannik Blaabjerg Pedersen, Anker Degn Jensen, Siva Sankar Reddy Putluru, Francesco Castellino, patent application, field 10th February 2010 (Topsøe).

Conference – Oral contributions

1. Reversible gas absorption by ionic liquids, Riisager, A., Due-Hansen, J., Berg, R. W., Fehrmann, R., 34. Edition des Journées d'Etudes des Equilibres entre Phases (JEEP), Marrakech, Marocco, March 26–28, 2008.
2. Improved NO_x removal with novel iron-based zeolite catalysts, Frey, A. M., Mert, S., Due-Hansen, J., Fehrmann, R., Christensen, C.H., 2nd EuCheMS Chemistry Congress, Turin, Italy, September 16-20, 2008.
3. Nano-particle SCR deNOx catalysts, Steffen B. Kristensen, Andreas J. Kunov-kruse, Søren B. Rasmussen, Anders Riisager and Rasmus Fehrmann, 21th North American Catalysis Society Meeting, 7th-12th June 2009, San Francisco, USA
4. Mechanism of deactivation and alternative alkali-resistant catalysts, Due-Hansen, J., Rasmussen, S. B., Riisager, A., Kustov, A., Fristrup, P. Fehrmann, R., DeNO$_x$ SCR catalysts VIII International Conference - Mechanisms of catalytic reactions, Novosibirsk, June 29-July 2, 2009.
5. Nano-sized metaloxides as highly active SCR deNOx catalysts, Steffen B. Kristensen, Andreas J. Kunov-kruse, Søren B. Rasmussen, Anders Riisager and Rasmus Fehrmann, Europacat IX 30th aug - 4th sep 2009, Salamanca, Spain.
6. On the importance of the phase distribution and acidity of VO_x-ZrO_2-SO_4^{2-}-sepiolite catalysts for the NH_3-SCR process in relation to biomass-fueled power plants, Due-Hansen, J., Rasmussen, S.B, Riisager, A., Ávila, P., Fehrmann, R., Dansk Kemiingeniørkonference - DK2, Lyngby, Denmark, June 16-17, 2010.

7. New applications with an industrially proven concept, Riisager, A., Supported Ionic Liquid-Phase (SILP) catalysis, EAM Young Researchers' Day, Universität Erlangen-Nürnberg, July 19, 2010.
8. In-situ & Operando spectroscopic methods for studying industrial applications and deactivation phenomena of modified vanadium oxide catalysts for the NH_3-SCR reaction, Rasmussen, S.B., Due-Hansen, J., Mikolajska, E., Bañares, M.A., Ávila, P., Fehrmann, R., 14th Nordic Symposium on Catalysis, Helsingør, Denmark, August 29-31, 2010.
9. Ionic liquid gas absorption of NO_x, CO_x and SO_x, Ionic Liquids in Sustainable Energy and Fuels , Saravanamurugan, S., Due-Hansen, J., Kegnæs, S., Grétarsdóttir, T., Riisager A., Fehrmann, R., 240th ACS National Meeting, Boston, USA, August 22-26, 2010.
10. Alkali resistant Fe-zeolite catalysts for SCR of NO with NH_3, 14th Nordic symposium on catalysis, 29.-31. August 2010, Helsingør, Denmark. P. Siva Sankar Reddy, Anker Degn Jensen, Anders Riisager, Rasmus Fehrmann.
11. Heteropoly acid promoted Cu and Fe catalysts for the selective catalytic reduction of NO with ammonia, 2nd international symposium on air pollution abatement catalysis, 8.-11. September 2010, Krakow, Poland. P. Siva Sankar Reddy, Anders Riisager, Rasmus Fehrmann.
12. Alternative deNOx katalysatorer, Steffen B. Kristensen, Andreas J. Kunov-kruse, Søren B. Rasmussen, Anders Riisager and Rasmus Fehrmann, DK2, 16th-17th, 2010, Danmarks Tekniske Universitet, DK-2800 Kgs. Lyngby

Conference – Poster contributions

1. Novel Fe-based Zeolites with Improved NH_3-SCR Activity, Frey, A. M., Mert, S., Due-Hansen, J., Fehrmann, R., Christensen, C.H., 9th Netherlands' Catalysis and Chemistry Conference, Noordwijkerhout, The Netherlands, March 3-5, 2008
2. V_2O_5-based NH_3-SCR Catalysts Doped with Potassium, Due-Hansen, J., Rasmussen, S. B., Riisager, A., Kustov, A., Christensen, C. H., Fehrmann, R., 6th International Symposium on GROUP FIVE ELEMENTS, Poznań, Poland, May 7-10, 2008.
3. A study of Fe-based zeolites as NH_3-SCR catalysts, Frey, A. M., Mert, S., Due-Hansen, J., Fehrmann, R., Christensen, C.H, Kemisk Forenings Årmøde, Odense, June 13, 2008.
4. Development of new and improved Fe-zeolite NH_3-SCR catalysts for automotive applications, Frey, A.M., Mert, S., Due-Hansen, J., Fehrmann, R., and Christensen, C.H., 14th Int. Congress on Catalysis, Seoul, Korea, July 13 - 18, 2008
5. Alternative SILP-SCR Catalysts based on Guanidinium Chromates, Due-Hansen, J., Riisager, A., Ståhl, K., Fehrmann, R., EUCHEM 2008 Conference on Molten Salts and Ionic Liquids, Copenhagen, Denmark, August 24–29, 2008.
6. Supported ionic liquids: New versatile catalysts and absorber materials, Riisager, A., Fehrmann, R., Due-Hansen, J., Van Buu, O. N., Haumann, M., Wasserscheid. P., 2nd EuCheMS Chemistry Congress, Torino, Italy, September 16–20, 2008.
7. Sulfated zirconia as support for alkali-resistant SCR catalysts, Due-Hansen, J., Rasmussen,

S. B., Riisager, A., Kustov, A., Fehrmann, R., EuropaCat-IX, Salamanca, August 30-September 4, 2009

8. Influence of metal oxide promoters on V_2O_5/TiO_2 catalysts for selective reduction of NO by NH_3: Minimization of N_2O formation, Europacat IX, 30.- 4. September 2009, Salamanca, Spain. P. Siva Sankar Reddy, Anders Riisager, Rasmus Fehrmann.
9. Selective flue gas cleaning with ionic liquids, Kegnæs, S., Due-Hansen, J., Berg, R.W., Riisager, A., Fehrmann, R., EUCHEM Conference on Molten Salts and Ionic Liquids 2010, Bamberg, Germany, March 14-19, 2010.
10. SCR activity of conformed CuO_x/ZrO_2-SO_4 catalysts, Rasmussen, S.B., M. Yates, Due-Hansen, J., Ávila, P., Fehrmann, Scientific Bases for the Preparation of Heterogeneous Catalysts, PREPA10, Louvain-La-Neuve, Belgium, July 11-15, 2010.
11. Pore design of pelletised VO_x/ZrO_2-SO_4/Sepiolite composite catalysts, Rasmussen, S.B., Due-Hansen, Yates, M., Villaroel, M., Gil Llambías, F.J., Fehrmann, R., Ávila, P., Scientific Bases for the Preparation of Heterogeneous Catalysts, PREPA10, Louvain-La-Neuve, Belgium, July 11-15, 2010.

Ph.D. Theses

1. Alternative deNO_x catalysts and technologies, J. Due-Hansen, DTU Chemistry, June 2010.